Collaborative source-seeking control

Ruggero Fabbiano

UNIVERSITÉ DE GRENOBLE

THÈSE

pour obtenir le grade de

DOCTEUR DE L'UNIVERSITÉ DE GRENOBLE

spécialité : **automatique-productique**

arrêté ministériel : 7 août 2006

Présentée par

Ruggero FABBIANO

Thèse dirigée par **Carlos CANUDAS DE WIT**
et codirigée par **Federica GARIN**

Préparée au sein de l'institut de recherche **Inria - Grenoble Rhône-Alpes**, du laboratoire **GIPSA-lab** et de l'école doctorale **EEATS**

Collaborative Source-Seeking Control

Thèse soutenue publiquement le **28 mai 2015**
devant le jury composé de :

M. Christophe PRIEUR, président
directeur de recherche CNRS - GIPSA-lab (Saint-Martin-d'Hères)

M. Jamal DAAFOUZ, rapporteur
professeur - Institut national polytechnique de Lorraine (Vandœuvre-lès-Nancy)

M. Wilfrid PERRUQUETTI, rapporteur
professeur - École centrale de Lille (Villeneuve-d'Ascq)

M. Claudio ALTAFINI, examinateur
professeur - *Linköping universitet* (Linköping - SUÈDE)

M. Alexandre SEURET, examinateur
chargé de recherche CNRS - LAAS (Toulouse)

M^lle^ Federica GARIN, encadrante
chargée de recherche - Inria (Montbonnot-Saint-Martin)

Bjartar vonir rætast
er við göngum bæinn
brosum og hlæjum glaðir

Vinátta og þreyta mætast
höldum upp á daginn
og fögnum tveggja ára bið

Borðum og drekkum saðir
og borgum fyrir okkur
með því sem við eigum í dag

Við vorum sammála um það
sammála um flesta hluti
við munum gera betur næst

Þetta er ágætis byrjun

Sigur Rós

Résumé de la thèse

Cette dissertation fait face au problème de la localisation de sources, un sujet qui a été largement étudié dans la littérature récente au vu de son grand nombre d'applications. En particulier, ce travail se concentre sur le pilotage de multiples capteurs, capables de prendre des mesures ponctuelles de la quantité émise, vers la source sans faire usage d'aucune information de position, qui se trouve être indisponible dans de nombreux cas pratiques (par exemple, sous l'eau ou dans l'exploration souterraine).

En faisant quelques hypothèses sur le processus de diffusion, nous développons un modèle qui permet d'utiliser des outils mathématiques (l'intégrale de Poisson et ses dérivées) pour obtenir une simple approximation du gradient de la fonction décrivant le processus de diffusion, dont la source représente le maximum, ce qui permet d'utiliser l'algorithme du gradient et trouver l'emplacement de la source.

Les contributions sont de trois ordres : d'abord, nous utilisons ces outils pour résoudre le problème de la recherche d'une source en deux dimensions à travers d'un contrôle centralisé, où un seul véhicule, équipé de multiples capteurs et sans information de position, se déplace dans un environnement planaire où se trouve une source. Ensuite, nous étendons cette recherche à un cadre en trois dimensions, en considérant un engin volant équipé de capteurs qui se déplace dans l'espace ; pour ce cas plus général, outre la validation par simulations, nous fournissons également une étude théorique des propriétés de convergence de la loi de commande proposée. Enfin, nous abordons le problème de la localisation de source de façon distribuée, compte tenu de plusieurs capteurs autonomes mobiles (en deux dimensions) ; outre le

problème de mettre en œuvre l'algorithme de localisation de source de manière distribuée, nous devons garantir un contrôle de la formation approprié pour assurer l'exactitude de l'estimation du gradient, et donc atteindre la source.

Preface

Abstract

The dissertation faces the problem of source localisation, a topic which has been extensively studied in recent literature due to its large number of applications. In particular, it focuses on steering multiple sensors, able to take point-wise measurements of the emitted quantity, towards the source without making use of any position information, which happens to be unavailable in many practical cases (for example, underwater or underground exploration).

By making some assumptions on the diffusion process, we develop a model which allows us to use some mathematical tools (the Poisson integral and its derivatives) for a simple approximation of the gradient of the function describing the diffusion process, whose source represents its maximum, making it possible to perform a gradient ascent to find the source location.

The contributions are threefold: first, we use such tools to solve a 2-dimensional centralised source-seeking problem, where a single vehicle, equipped with multiple sensors and without position information, is moving in a planar environment where a source is supposed to emit. Then, we extend it to a 3-dimensional framework, considering a flying vehicle equipped with sensors moving in the space; for this more general case, in addition to simulation validation, we provide a theoretical study of the convergence properties of the proposed control law. Finally, we tackle the distributed source-localisation problem, considering several autonomous

moving sensors (in two dimensions); in addition to the problem of implementing the source-localisation algorithm in a distributed manner, in this latter case we have also to guarantee a suitable formation control, to ensure the correctness of the gradient estimation and hence reach the source.

Dissertation Outline

1. Introduction

This chapter introduces and defines the main topics faced throughout the dissertation, *i.e.*: *source localisation*, *multi-agent systems* and *formation control*. In particular it focuses on the first one, where a summary of the state of the art is provided to give an overview of the main approaches to the source-seeking problem. We state also the main contributions given in this work.

2. Poisson Integral and Gradient Computation

In this chapter we introduce the first contribution of the thesis: the computation of the gradient of the function describing the diffusion process via the *Poisson integral*. We will start by describing the model for the source that we will be using throughout all the dissertation. Roughly speaking, we will make several assumptions about the measured scalar field, *i.e.*, that the signal distribution representing the scalar field is continuous, that the signal is emitted by a single source and is assumed to decay away from the position of the source, such that the source is the only maximum of the scalar field. Such model, ideal yet applicable in many cases of practical interest, will allow to develop a way to compute the gradient of f, the function describing the diffusion process, avoiding a direct derivative computation, and thus making it easy to implement it in different control laws. This is the key-point of our source-seeking strategy, as we aim at computing a gradient approximation to reach the source via a gradient-based optimisation technique, where the source loc-

ation represents the point which maximises the value of the distribution function.

3. Source Localisation on the Plane

We apply here the theory explained in the previous chapter to a problem of source localisation in two dimensions. We start by describing the planar sensing vehicle we intend to use, and then show how it is possible to get a discrete approximation of the gradient of the function describing the diffusion process by approximating the previous developed formulæ with the measurements from the sensing device endowed on the vehicle. Finally, we propose a simple control law, involving both the approximate gradient and Hessian, and show by some simulations the effectiveness of the proposed method.

The second part of the chapter is dedicated to a short presentation of a practical experimental implementation of such algorithm (with a slightly modified control law) on a real robot prototype, developed in the framework of a master internship project of a M.Sc. student from the University of Bristol (England, UK). The robot operated in a scenario in which the assumptions under which we elaborate our method do not hold anymore, yet it demonstrated a satisfying behaviour, as shown in the final tests.

4. Tridimensional Source-Seeking

Here we extend the results of the previous chapter to a tridimensional framework. After introducing the vehicle dynamics and its proposed feedback, we consider the problem of how to dispose the set of sensors on a sphere, which is not obvious as for the bi-dimensional case. Then we formally prove the convergence the proposed source-seeking control law, and show some wider simulation results, analysing by this mean the sensitivity of the algorithm to the variation of the number of sensors, of the radius and of the measurement noise.

5. Distributed Source-Seeking

We present here a distributed control law to steer a group of autonomous communicating sensors towards the source of a diffusion process. We assume to have a set of autonomous moving sensors which are able to measure, in addition to the diffusing quantity of interest, only the relative bearing angle with respect to its neighbour; they have no absolute position information and do not know any relative distance; the sensors can communicate to each other, and the graph describing the communication links has a time-invariant ring-topology.

We propose a distributed algorithm to estimate the gradient of a function describing a diffusion process, and use this information to drive a set of moving sensors towards the source; our approach is based on a twofold control law, which is able to bring and keep the set of sensors on a circular equispaced formation, and to steer the circular formation towards the source via a gradient-ascent technique. The effectiveness of the proposed algorithm is both theoretically proven and supported by simulation results.

6. Conclusions

The purpose of this chapter is to summarise the contributions presented in the dissertation, and introduce some perspectives of future research to complete and improve this work.

List of Publications

Journal Papers

R. Fabbiano, C. Canudas de Wit, F. Garin, "Source Localization by Gradient Estimation Based on Poisson Integral", *Automatica*, vol. 50 Nº 6, pp. 1715-1724; June 2014.

R. Fabbiano, F. Garin, C. Canudas de Wit, "Distributed Source Seeking without Global Position Information", *IEEE Transactions on Control of*

Network Systems (under review).

Proceedings of Peer-Reviewed International Conferences

C. Canudas de Wit, F. Garin, R. Fabbiano, P. Rouchon, A. Rousseau, "Source Localization Using Poisson Integrals", *Proceedings of the 3rd IFAC Workshop on Distributed Estimation and Control in Networked Systems (Necsys)*, pp. 127-132; Santa Barbara (USA), September 2012.

R. Fabbiano, C. Canudas de Wit, F. Garin, "Distributed Source Localisation with no Position Information", *Proceedings of the 13th EUCA European Control Conference (ECC)*, pp. 569-574; Strasbourg (France), June 2014.

Contents

List of Floatings

Figures

Tables

Algorithms

List of Acronyms

ABS antilock braking system

ACC American Control Conference

AP access point

AUV autonomous underwater vehicle

CCC Chinese Control Conference

CDC Conference on Decision and Control

CNRS *Centre National de la Recherche Scientifique*
National Center for Scientific Research

DC direct current

ECC European Control Conference

EEATS *Électronique, Électrotechnique, Automatique et Traitement du Signal*
Doctoral school of Electronics, Electrotechnics, Automation and Signal Processing

ETNA Electronic Transactions on Numerical Analysis

EUCA European Control Association

GIPSA-lab *Grenoble Images Parole Signal Automatique - Laboratoire*
Grenoble laboratory of Images, Speech, Signal Processing and Automation

GPS	global positioning system
HIP	hardware-in-the-loop
ICASSP	International Conference on Acoustic, Speech and Signal Processing
ICRA	International Conference on Robotics and Automation
ICTAI	International Conference on Tools with Artificial Intelligence
IEEE	Institute of Electrical and Electronics Engineers
Ifac	International Federation of Automatic Control
Inria	*Institut National de Recherche en Informatique et Automatique* National Research Institute in Computer Science and Automation
KAM	Knowledge Acquisition and Modeling
Laas	Laboratory for Analysis and Architecture of Systems
led	light-emitting diode
MMSE	minimum mean-squared error
Nasa	National Aeronautics and Space Administration
NeCS	Networked Controlled Systems
PDE	partial differential equation
PID	proportional-integral-derivative widely-used industrial controller
SEOS	Science Education through Earth Observation for High Schools European high-school project
UAV	unmanned aerial vehicle
USB	universal serial bus

Chapter 1

Introduction

The problem of *source localisation* consists in finding, by one or several agents, which can be fixed or autonomously moving, the source of a substance — chemical, light, sound, pollutant, heat, and so on — that is being produced at one particular location but spreads over a region through a diffusion process. Solving such task is not only relevant to many human applications, but is crucial as well in nature: animals developed a huge variety of complex source-localisation strategies in order to reach a wide variety of objectives. Sound-source localisation is crucial to survive for both hunters and preys; simpler forms of life (*e.g.*, bacteria or insects) follow chemical signals to find food or partners for reproduction, while more complex species perform odour-source localisation to reach the same goals.

Scientists have been investing a huge effort in studying and trying to fully understand these complex mechanisms, with the aim of reproducing such behaviours in what is known as *bio-inspired* source localisation. For example, blue crabs (*Callinectes Sapidus*, figure 1.1) use input from two sets of chemosensors to regulate food tracking behaviour in water plumes: chemosensors on the antennules, which are elevated on the blue crab's body, control the forward movement to induce upstream motion towards the odourant source, while chemosensors on the crab's legs, which are spatially separated and near the substrate, are believed to mediate cross-stream motion relative to the water plume structure. The combination of

Figure 1.1. Blue crabs use chemosensors on the antennules and on the legs to regulate their tracking behavior [75], being able in this way to quickly find food moving in water plume spikes (source: Wikipedia).

sensors at different heights in the water column means that blue crabs are acquiring time-varying, three-dimensional information about their environment [75]. Again, male moths (figure 1.2) are capable to detect and localise female moths over up to several hundred meters while the latter secrete only minute quantities of pheromones dispersed in turbulent plumes; they solve this task by combining highly specialised olfactory, anemotactic, and visual sensors with specific information processing and behavioral control strategies [61]. Finally, flagellate bacteria, *e.g.*, *Escherichia Coli* (figure 1.3), have a characteristic movement called "run and tumble" which consists of two phases that allow them undergo random walks: they can use their flagella to swim straight (the "run" phase), or to tumble so that when they start swimming again they move in a random direction; in its turn, the probability of a change of direction increase as the sensed concentration of their chemical target decrease.

In research and engineering, the problem of localising the source of a signal received growing interest over the last decades, in particular in applications where the agents have to physically reach the source position and have limited or no position information. This is relevant in many applications of heat or vapor-emitting [60] sources, such as ocean sampling, surveillance, mapping and space exploration (see [25, 42, 72, 82] and references therein), explosive detection, drug detection, sensing leaking or hazardous chemicals, pollution sensing and environmental studies, vent

sources in underwater field. We recall here that there exist also many fields in which it is relevant to localise the direction, and possibly the distance, a source is emitting from, and this is done via different techniques (*e.g.*, using differences in the arrival time of the signal) by static sensors that do not move towards the source; examples are sound-source localisation, which is pertinent in many applications (for example in intelligent conference call systems that identify the speakers to improve sound and video quality [80]), or medical studies, for example using surface sensors to explore internal brain activity.

In the next sections we will shortly introduce the two main topics covered by this thesis: we will first give a (non-exhaustive) overview of the literature about source localisation, and then recall the concept of *multi-agent systems* and its application in the field of source seeking.

1.1 Survey on Source Localisation

The source-seeking task can be performed statically, with a network of sensors that collect and exchange information on the surrounding environment and try to identify where a signal of interest is coming from, or by autonomous vehicles, equipped with sensors, which physically reach the source. The first setting is particularly suitable for sound-source localisation or localisation of electromagnetic signals, that can make use of methods that require different measurements than the signal strength, such as triangularisation and the difference in the arrival time of the wave at different sensors. As we already mentioned we are interested in this second field (*i.e.*, source localisation by moving sensors reaching the source), so we will focus the survey on such topics.

From a mathematical point of view, the signal distribution is a scalar field described by a spacial function $f(\boldsymbol{x})$, whose maximum is in correspondence to the position of the source $\boldsymbol{x}^{\mathrm{s}}$. There exists in the literature a huge variety of methods to treat the problem of source localisation and related issues, that make an exhaustive exposition impossible, but the com-

mon line is that in all these missions we have vehicles without crew, that need to move and take measurements of such unknown scalar field, with the objective of using such measurements to calculate the position of the signal source. For example, we can be interested in localising a heating source, and in this case the signal of interest is given by the temperature at given points; or we may want to find the source of a chemical substance polluting the environment, and thence we will be interested in the concentration of such chemical.

Inverse Problems

Many techniques deal with formulations associated with isotropic diffusion processes described by diffusion equations for which a closed-form solution is known; as the explicit solution depends (among other parameters) on the source location, several identification methods have been devised to estimate the source position: in [49] it is proposed a two-step identification procedure, dealing with the inhomogeneous case and a fixed sensor array; in [60] it is formulated a similar problem but with moving sensors, using a maximum-likelihood approach to estimate the source position, and considering moving sensors which update their position so as to approximately minimise the estimation error, by following the gradient of the Cramér-Rao bound to error variance. More fundamental problems, such as source identifiability and optimal sensor placement, are discussed in depth by [39] using concepts and ideas of control system theory. The above mentioned approaches can be viewed as inverse problems for partial differential equations, with the goal of finding the initial conditions or a forcing term. Because of their nature, all such methods share the common drawbacks of heavy computations, and of high sensitivity to the explicit knowledge of the closed-form solution of the partial differential equation (PDE) describing the diffusion process.

Gradient-Based Source Localisation

A different line of research consists in computing or approximating the gradient field of the measured quantity, and moving towards the source along the gradient direction; this can be done either directly, via an *ad hoc* method developed for the particular problem at hand, or implicitly, by estimating the gradient via different techniques. One of the first contributions making use of an explicit gradient computation can be found in [14], where the agent obtains different measurements of a hydrothermal plume and performs a least-square gradient estimation of the overall slope to move towards the source. In [6] unicycle vehicles are driven towards a source by a control law related to the geometry of the diffusion process. A least-square gradient estimation combined with a gradient-descent method is also used in [4] to steer a single vehicle to the maximum/minimum of a scalar field. In [23] a gradient method which converges in finite time is developed; in this work the author present the bases of gradient search methods.

In addition to that, recent results dealing with odour-source localisation [24, 37, 78] tried to deal with source plumes, and have to be able to measure also the wind or flow that creates this plume, since in this case a direct gradient estimation is not possible. In this framework worth noting are some recent works from Zhang *et al.* [15, 76], where the authors developed a strategy to map the discontinuous field given by the plume in a continuous one in which the signal of interest is the plume duration, and thus were able to apply their previous method [77] to perform a normal gradient search on this last quantity.

These methods share the advantage to be in general simpler than the following ones, but are generally based on stronger assumptions, as some regularity of the signal profile (or the possibility to directly measure the gradient), and might require a long convergence time if carried out by a single agent.

Figure 1.2. A moth is able to localise a female by her pheromones dispersed in turbulent air plumes [61] (source: Wikipedia).

Extremum Seeking

Another related but quite different approach for source localisation is based on *extremum seeking* techniques, a seminal contribution in the field of adaptive control [2]. This method can still be considered as a gradient-based optimisation technique, as it relies on the idea of collecting rich enough information to approximate the gradient through the use of a periodic probing signal; however, in contrast to the methods mentioned previously, this approach is not based on any particular structure or knowledge of the diffusion solution, and for this reason it only applies for moving sensors. In extremum seeking, the steady-state input-output characteristic is optimised without requiring any explicit knowledge about the characteristic itself, other than that it exists and that it has an extremum; such situation arises in a wide range of engineering applications: biochemical reactors, ABS control in automotive brakes, electromechanical valves, axial compressors, mobile robots, mobile sensor networks, PID tuning, optical-fibre amplifiers and so on [27, 74, 81, 83]. Although this method dates back to the half of last century, the first local stability analysis of this class of controllers was reported in 2000 by Krstić and Wang [41], and later extended to semi-global stability analysis in [69, 70]; for other theoretical studies on extremum seeking, see [58, 71]: in the first, Nešić demonstrates that the simplified scheme presented therein operates on average in its

slow time scale as the steepest-descent optimisation scheme, while in the last some conditions that ensure global extremum-seeking in the presence of local extrema are shown. A rigorous formalisation of its theory is given in [1], while a good survey on the literature on extremum-seeking can be found in [68].

Contributions about extremum-seeking-based source localisation are represented by [18, 36, 79], where a nonholonomic unicycle is controlled respectively on the forward velocity, then on the angular one, and finally on the two together; in all these papers the setting is given by sources with unknown spatial distributions and nonholonomic unicycle vehicles without position measurement. In the first case the vehicle employs a constant positive forward speed, and steering of the vehicle in the plane is performed using only the variation of the angular velocity, while in the second the opposite setting is studied; as Ghods points out in the last one, where the forward velocity is regulated as well as the angular one, neither of the first two strategies are ideal, since the first sacrifices the transients, whereas the second, even if it is a reasonable strategy motivated by implementation with aerial vehicles, leads to complexities in the asymptotic behavior of the vehicle, since it can at best converge to a small-size attractor around the source, but cannot settle.

In [51, 52], a hybrid controller is implemented to improve extremum-seeking performances for source-localisation purposes; in these works, the authors develop an optimisation method with successive heading changes based on conjugate vectors, and the resulting system is shown to be practically stable under perturbations for a certain class of signal strength distributions. A stability analysis for the source-localisation problem with a nonholonomic unicycle has been previously reported in [19], and in [22] this is applied to several scenarios. Contributions on 3D source localisation are given by [17, 20, 21]. A slightly different approach is proposed in [50], where they use a strategy with sliding-mode control laws where the single vehicle does not need to compute the gradient of the signal distribution to reach its source.

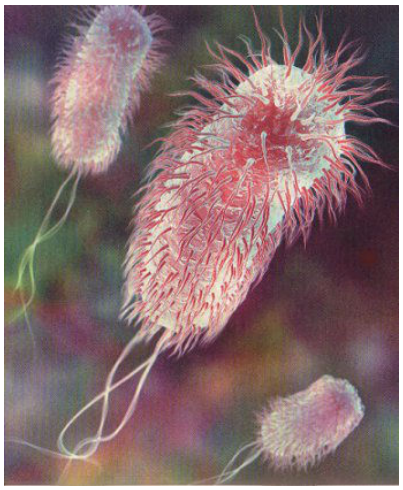

Figure 1.3. *Escherichia Coli* rotate their flagella counter-clockwise to swim and clockwise to tumble, performing stochastic source localisation.

Stochastic Source-Seeking

Another technique worth mentioning is given by stochastic methods, which try to reproduce some biological behaviours, like fish shoals or bacteria movements, and model the agent's motion via a probability function that describes the rate of a change of direction. Worth mentioning is *Optimotaxis* [54]: in this work, the agents move in a way that mimics *Escherichia Coli*'s movement, *i.e.*, they perform a random motion where the probability of a direction change increases as the food sensed concentration decreases; this method can be also used with nonquadratic-like signal profiles, including the ones with multiple maxima. Another contribution is given by [53], where the authors localise a source of polluting substance and track the boundary of the contaminated region. Finally, in [44, 66] a novel method is introduced, that combines a stochastic approach with the previously mentioned extremum-seeking algorithm.

1.2 Multi-Agent Systems

As well as for source localisation, in large groups of individuals nature shows often examples of cooperative behaviours too: we can just think

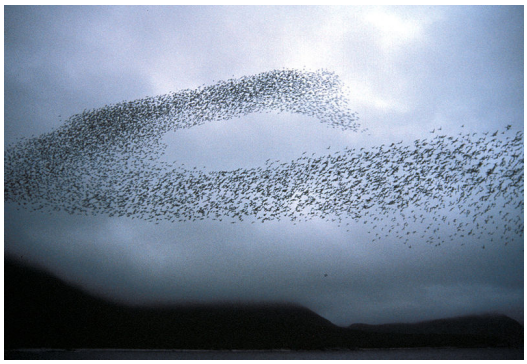

Figure 1.4. Flocking birds are an example of self-organization in biology (source: Wikipedia).

about collective food-gathering in ant colonies, and migrations of birds in flocks and fish shoals [67]. The fundamental property of this cooperation is that the group behaviour is not dictated by one of the individuals, but it comes implicitly as a result of the local interactions between the individuals [11].

In engineering, a multi-agent system is a group of agents (which can be sensors, vehicles, or even humans), usually represented by a network of nodes interconnected via a communication topology, which are able to exchange information in order to reach a common goal; the interest that such systems have received in engineering lie on the property that, as in nature, they can solve problems that are difficult, or even impossible, for an individual agent or a monolithic system [11].

Multi-agent systems are studied in relation to many research topics, as computer science [29, 73], distributed computation [7, 9], game theory [10] and social science [26]; the interest in automatic control is particularly relevant for the large number of applications, in many different areas, where one has to face with systems consisting of multiple vehicles, equipped with several sensors and actuators, which are intended to perform a coordinated task; examples are surveillance, collaborative search and rescue, environmental monitoring, exploration and distributed reconfigurable sensor networks [11].

There is a huge literature on control of autonomous systems, multi-

agent systems and distributed control in general; we do not aim to give here an exhaustive overview of the main contributions, and we refer to the seminal books [5, 13, 32, 48, 63]. We will expose in the next subsection the main contributions on distributed source localisation, and the define the problem of *formation control* and specifically of the *cyclic pursuit*, that we will face in our thesis to solve the distributed source-localisation task.

1.2.1 Distributed Source-Localisation

In order to avoid the large distances covered by the vehicle, and the oscillations needed by extremum-seeking techniques, some collaborative strategies can be devised. Such a goal is obtained by a group of vehicles gathering — and possibly sharing — enough information about the signal's field to carry out the source-seeking problem; this opens up new challenges, such as efficient optimisation algorithms to estimate the gradient in a distributed way (in general with only local informations known by each agent) and communication constraints.

One of the first contributions in this direction, that uses a gradient-based approach, is [56], where it is assumed that each vehicle, modeled with simple integrator dynamics, can measure the full gradient, and the authors develop a twofold algorithm with a gradient-descent term and inter-vehicle forcing terms. Another relevant gradient-based contribution is [59], where a group of gliders equipped with sensors estimate the model parameters of the scalar field via collecting concentration measurements at different locations, reconstruct an approximate value of the signal's gradient by applying a least-square approximation, and use this information to reach the source. A real-life application of such approach is presented in [30]. Collaborative control laws to steer a fleet of autonomous underwater vehicles (AUVs) to the source of a signal distribution using only direct signal measurements by a circular formation of agents are presented in [12, 55]. The gradient is estimated in an implicit way in [77], where the authors take inspiration from fish swarms to design an algorithm adapted also for seeking the source of a turbulent flow [76].

Extremum-seeking is applied in a collaborative way in [35], in a 1D framework, where authors considered the problem of deploying a group of autonomous vehicles in a formation which has higher density near the source of a measurable signal, and lower density away from it. In [8], the authors drive a formation of agents to the maximum (or minimum) of a scalar field, using a multi-agent but not collaborative approach: the extremum-seeking algorithm is actually implemented by one single vehicle, the leader of the formation, and the remaining agents follow the leader keeping a particular formation. Finally, a very recent extremum-seeking application in a distributed manner is [40], where a source is localised using a discrete-time algorithm.

Two distributed stochastic source localisations are in [65], where a group of chemical sensors takes measures of a plume concentration values to estimate the source position via a stochastic approximation technique, and in [62], in which the authors use the sensor measurements to estimate the model parameters of the concentration plume. A mixed stochastic/extremum-seeking approach can be found also in a distributed approach, in [34], where a group of autonomous fully-actuated vehicles are deployed in a planar signal field; such contributions are distributed but non *cooperative*, since there is no information exchange: each vehicle employs a stochastic extremum-seeking control law, whose goal is to maximise the value of the measured signal as well as to simultaneously minimise a function of the distances between neighbouring agents; this produces a Nash equilibrium that depends on the agents' control parameters and the unknown signal distribution.

1.2.2 Circular Formation Control

Among all the possible application fields of multi-agent systems, a relevant issue is their motion coordination; in particular, when the objective of such coordination is to make the agents reach a disposition that maintain a particular given shape, we talk about *formation control*. A formation is defined as a group of autonomous agents (vehicles, sensors or robots)

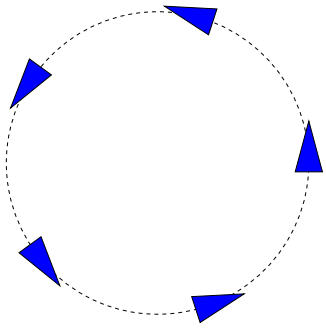

Figure 1.5. A 5-agent formation in cyclic pursuit.

with communication capacities, which form a particular configuration (*i.e.*, desired positions and/or orientations), in which the agents collaborate to achieve a common goal; keeping a group of vehicles in formation presents several advantages, as reducing the system cost, increasing the reconfiguration ability of the system, increasing its robustness and improving the properties of the communication topology [11]. There is an extensive literature about the formation-control problem; we refer the reader to the seminal books [16] for a wide analysis of the possible approaches.

We focus on the concept of circular formation control, also know as *cyclic pursuit*, which will be useful to us to tackle the distributed source-localisation problem. This particular task focuses on finding a distributed control law to bring a group of identical vehicles, which have information about their neighbours (predecessors and/or followers) only, in an ordered circular formations where each agent i pursuits agent $i+1 \bmod n$ (figure 1.5). Among the literature on cyclic pursuit, in particular, we point out the contributions of Moshtagh *et al.* [57] and Marshall *et al.* [45–47], to our knowledge the only approaches that do not make use of global position information; we will make use of the second ones, which, differently from the first one, have also theoretical guarantees.

1.3 Contributions of the Thesis

The originality of the proposed source-localisation solution lies in the computation of the gradient from Poisson integrals: in opposition to other

solutions published in the literature, on the one hand it does not require specific knowledge of the solution of the diffusion process, and it can compute the gradient direction from the point-wise concentration samples with a small computation load; on the other hand it does not make use of a probing signal, and thus avoids the oscillations required by extremum-seeking techniques. Moreover, such method is easily adaptable to any dimension, and the fact that derivatives are computed using integrals makes the methods low sensitive to measurement noise, since such computation is intrinsically high-frequency filtering. Such method represents a theoretical formalisation of previous solutions proposed in the literature [11, 12, 55]; moreover, it allows also for the computation of higher-order derivatives (*i.e.*, the Hessian), making it possible to design more complex control laws.

Such method is applied in a centralised manner both in a 2D and in a 3D framework, giving a theoretical convergence proof, and finally we propose a distributed algorithm, whose effectiveness is also theoretically proven, which differs from previous contributions as we suppose to have no full position information (which may be unavailable in various operating environments such as underwater or indoor vehicles, or in applications where inertial navigation systems are too expensive or not sufficiently accurate), but we only assume that the autonomous sensors are be able to measure the relative angle with respect to their neighbours.

Chapter 2

Poisson Integral and Gradient Computation

In this chapter we introduce the first contribution of the thesis: the computation of the gradient of the function describing the diffusion process via the *Poisson integral*.

We will start by describing the model for the source that we will be using throughout the dissertation. Roughly speaking, we will make several assumptions about the measured scalar field, *e.g.*, that the signal distribution representing the scalar field is continuous, that the signal is emitted by a single source and is assumed to decay away from the position of the source, such that the source is the only maximum of the scalar field. Such model, ideal yet applicable in many cases of practical interest, will allow to develop a way to compute the gradient of f, the function describing the diffusion process, avoiding a direct derivative computation, and thus making it easy to implement it in various control laws. This is the key-point of our source-seeking strategy, as we aim at computing a gradient approximation to reach the source via a gradient-based optimisation technique, where the source's location represents the point which maximises the value of the distribution function f.

2.1 Model of the Diffusion Process

We will consider, throughout our dissertation, a diffusion process where the source is isotropic and the diffusion is homogeneous; this means that the properties of the source, as well as the diffusion process itself, are independent of the spacial direction considered. Such diffusion is described by the well-known linear parabolic PDE with constant coefficients known as "(isotropic) diffusion equation"

$$\frac{\partial f(\boldsymbol{x},t)}{\partial t} - c\nabla^2 f(\boldsymbol{x},t) = 0, \quad \forall \boldsymbol{x} \in D,\ t \geq 0, \tag{2.1}$$

where f is the concentration function, c is the isotropic diffusion coefficient, and D is an open subset of $\mathbb{R}^n$ (see [31]). Such an equation is suitable to describe various diffusion phenomena: for example, f can represent the distribution of temperature in an environment, or the concentration of a chemical (*e.g.*, a pollutant or salinity).

In this work, we assume that the diffusion process is fast enough, so that our interest is in studying the steady-state behaviour resulting from equation (2.1); therefore, we limit our attention to solutions of the following equation, known as *Laplace equation*:

$$\nabla^2 f(\boldsymbol{x}) = 0, \quad \forall \boldsymbol{x} \in D. \tag{2.2}$$

Our interest is in the case where the steady-state has been reached but a source is still emitting somewhere at a constant rate (as it happens in many cases of practical interest, *e.g.*, in a heating process or in the dispersion of a chemical substance), or that possible source variations are slow in the time-scale of interest, and our goal is to find the source location. As a model for such a source, we assume that the source occupies a portion of space not belonging to D, and it affects the values of f in D by imposing a boundary condition. More precisely, we consider an open domain $D = \tilde{D} \setminus D_s$, where $\tilde{D} \subseteq \mathbb{R}^n$ is a connected set representing the region we are interested in studying, and D_s is a small connected subset of

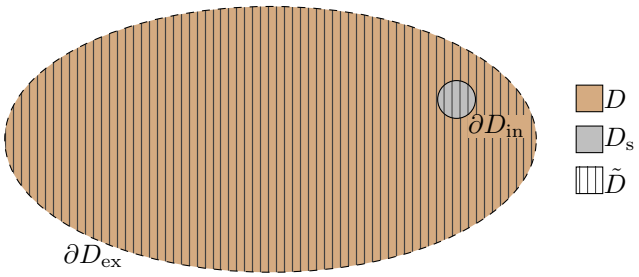

Figure 2.1. Representation of the domains of interest for our source model.

$\tilde{D}$ which represents the area occupied by the source. Thus, the boundary of D is formed by an inner part, equal to the boundary of the source region D_{s} and denoted by ∂D_{in}, and possibly an external part, equal to the boundary of $\tilde{D}$ and denoted by ∂D_{ex} (figure 2.1).

We will consider below some illustrative examples.

Example 2.1 (constant Dirichlet boundary conditions in 2D). Consider a disk whose border is kept at a (low) constant temperature f_{ex}, with a smaller circular heater at its centre $\boldsymbol{x}^{\mathbf{c}}$. Denoting by $B_r(\boldsymbol{x}^{\mathbf{c}})$ the disk $B_r(\boldsymbol{x}^{\mathbf{c}}) = \{\, \boldsymbol{x} \colon \|\boldsymbol{x} - \boldsymbol{x}^{\mathbf{c}}\| < r \,\}$, we have that the disk is $\tilde{D} = B_r(\boldsymbol{x}^{\mathbf{c}})$ and the heater location is $D_{\text{s}} = B_{r_{\text{s}}}(\boldsymbol{x}^{\mathbf{c}})$, where the centre $\boldsymbol{x}^{\mathbf{c}}$ is the same for both disks, but the radius r_{s} is much smaller than r. In this example, we assume that the boundary conditions are a constant temperature f_{ex} on the border and a higher constant temperature f_{s} around the source, so that we are looking for a solution of the Dirichlet problem

$$\begin{aligned} f(\boldsymbol{x}) &= f_{\text{s}} && \text{on } \partial D_{\text{in}} = \partial B_{r_{\text{s}}}(\boldsymbol{x}^{\mathbf{c}}) \\ f(\boldsymbol{x}) &= f_{\text{ex}} && \text{on } \partial D_{\text{ex}} = \partial B_r(\boldsymbol{x}^{\mathbf{c}}) \\ \nabla^2 f(\boldsymbol{x}) &= 0 && \text{in } D = B_r(\boldsymbol{x}^{\mathbf{c}}) \setminus B_{r_{\text{s}}}(\boldsymbol{x}^{\mathbf{c}}). \end{aligned}$$

It is easy to verify that all functions of the form $f(\boldsymbol{x}^{\mathbf{c}}) = a_1 \log\|\boldsymbol{x} - \boldsymbol{x}^{\mathbf{c}}\| + a_2$ satisfy $\nabla^2 f(\boldsymbol{x}) = 0$ for all $\boldsymbol{x} \neq \boldsymbol{x}^{\mathbf{c}}$, so in particular for all $\boldsymbol{x} \in D$; moreover, it is easy to see that such functions are constant along circles centered in $\boldsymbol{x}^{\mathbf{c}}$. Then, by imposing the given boundary conditions, one can find the correct values of a_1 and a_2, and can find the following solution f to the

problem:

$$f(\boldsymbol{x}) = \frac{f_{\text{ex}} \log \frac{\|\boldsymbol{x}-\boldsymbol{x}^{\mathbf{c}}\|}{r_{\text{s}}} - f_{\text{s}} \log \frac{\|\boldsymbol{x}-\boldsymbol{x}^{\mathbf{c}}\|}{r}}{\log \frac{r}{r_{\text{s}}}}.$$

Thanks to the properties of the Laplacian operator, and to the choice of the boundary conditions, this is actually the only solution of the problem.

Example 2.2 (mixed Dirichlet-Neumann boundary conditions). In some cases, a harmonic function cannot be written in closed-form, but it can be expressed as the solution of a PDE problem. As an example, consider a rectangular plane: similarly to example 2.1, a circular heater D_{s} lies in the middle, and imposes a constant boundary condition $f(\boldsymbol{x}) = f_{\text{s}}$ for all $\boldsymbol{x} \in \partial D_{\text{in}}$; on the borders, the boundary condition is imposed not on f, but on the derivative of f in the direction of the outward unit normal $\hat{\boldsymbol{n}}$: we assume that $\nabla f(\boldsymbol{x}) \cdot \hat{\boldsymbol{n}} = 0$ along the borders, which models perfectly isolating borders; in the middle of one of the longer borders there is a large opening, which imposes a constant boundary condition $f(\boldsymbol{x}) = f_{\text{ex}}$ due to the external colder temperature. The temperature profile at the steady state is obtained by the solution of the problem mixed Dirichlet-Neumann boundary conditions

$$\begin{aligned}
f(\boldsymbol{x}) &= f_{\text{s}} && \text{on } \partial D_{\text{in}} = \partial D_{\text{s}} \\
f(\boldsymbol{x}) &= f_{\text{ex}} && \text{on } [a_3, a_1 - a_3] \times a_2 \\
\nabla f(\boldsymbol{x}) \cdot \hat{\boldsymbol{n}} &= 0 && \text{on } \partial D_{\text{ex}} \setminus [a_3, a_1 - a_3] \times a_2 \\
\nabla^2 f(\boldsymbol{x}) &= 0 && \text{in } D = [0, a_1] \times [0, a_2] \setminus B_r(\boldsymbol{x}^{\mathbf{c}}),
\end{aligned}$$

where a_1 is the length of the longer side, a_2 the length of the shorter ones, and the external opening is long $a_1 - 2a_3$; the heater is represented by $B_r(\boldsymbol{x}^{\mathbf{c}})$, with $r \ll \frac{a_2}{2}$. Figure 2.2 shows the temperature obtained by solving the above-described problem via a finite-element method using the FreeFem++ software (see [38]), for a domain 10 m wide and 6 m long; the window is 6 m large and the heater occupies a circle with a radius of 50 cm; the heater's temperature is $f_{\text{s}} = 45$ °C, and the temperature outside is $f_{\text{ex}} = 10$ °C.

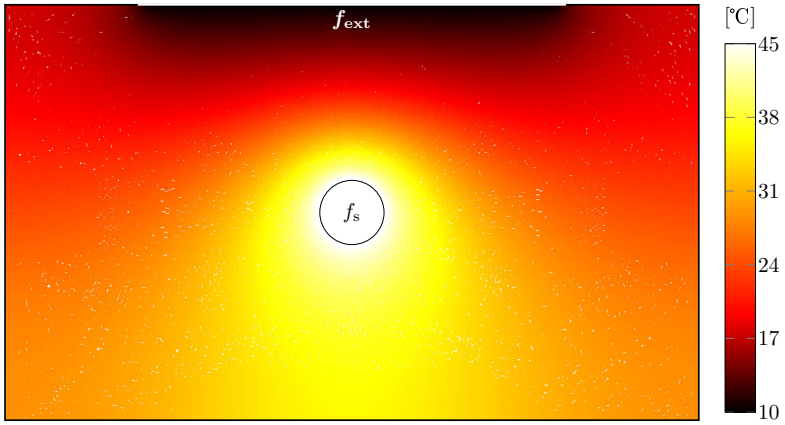

Figure 2.2. Solution of the problem in example 2.2; the white spots are due to the discrete solution obtained via a finite element approximation.

EXAMPLE 2.3 (UNBOUNDED DOMAIN IN 3D). As an example in three dimensions, we can consider the function

$$f(\boldsymbol{x}) = \frac{a}{\|\boldsymbol{x} - \boldsymbol{x}^{\text{s}}\|_2},$$

with $\boldsymbol{x} \in \mathbb{R}^3$. This function is represented by spherical level sets centered at the given point $\boldsymbol{x}^{\text{s}}$; it is easy to verify that, for all $\boldsymbol{x} \neq \boldsymbol{x}^{\text{s}}$,

$$\frac{\partial f(\boldsymbol{x})}{\partial x_i} = -a \frac{x_i - x_i^{\text{s}}}{\|\boldsymbol{x} - \boldsymbol{x}^{\text{s}}\|^3}$$

$$\frac{\partial^2 f(\boldsymbol{x})}{\partial x_i^2} = a \left[3 \frac{(x_i - x_i^{\text{s}})^2}{\|\boldsymbol{x} - \boldsymbol{x}^{\text{s}}\|^5} - \frac{1}{\|\boldsymbol{x} - \boldsymbol{x}^{\text{s}}\|^3} \right]$$

$$\nabla^2 f(\boldsymbol{x}) = \sum_{i=1}^{3} \frac{\partial^2 f(\boldsymbol{x})}{\partial x_i^2} = \frac{3a}{\|\boldsymbol{x} - \boldsymbol{x}^{\text{s}}\|^5} \sum_{i=1}^{3} (x_i - x_i^{\text{s}})^2 - \frac{3a}{\|\boldsymbol{x} - \boldsymbol{x}^{\text{s}}\|^3} = 0.$$

The solutions of the Laplace equation (2.2) are called *harmonic*, and have many interesting properties which we recall below[1].

Definition 2.1 (Harmonic function). Let $D \subseteq \mathbb{R}^n$ be an open set. A

[1]For a more detailed study of the properties of harmonic functions we refer to [3, 31], from where some of the following statements are taken.

function $f\colon D \to \mathbb{R}$ is harmonic in D if $f \in \mathcal{C}^2(D)$ and $\nabla^2 f(\boldsymbol{x}) = 0$ for all $\boldsymbol{x} \in D$. •

The above definition of a harmonic function requires the function to be twice differentiable. Then, it is possible to prove that harmonic functions have a much higher regularity: if f is harmonic on D, then it is analytic [31, corollary 2.11], and in particular $f \in \mathcal{C}^\infty(D)$. Moreover, the assumption that $f \in \mathcal{C}^2(D)$ in the definition of a harmonic function is convenient for having well-defined second-order partial derivatives, but it is not an essential assumption: any distribution $f \in \mathcal{D}(D)$ which satisfies $\nabla^2 f = 0$ in $\mathcal{D}(D)$ is indeed a harmonic function [31, corollary 2.20], and hence belongs to $\mathcal{C}^\infty(D)$.

Harmonic functions satisfy the so-called *maximum principle* (and an analogous property for the minimum), which we state below; such principle imposes strong limitations on the location of extrema of such functions.

Proposition 2.1 (Maximum principle). Let $D \subset \mathbb{R}^n$ be a connected set, and let $f\colon \bar{D} \to \mathbb{R}$ be harmonic in D. If f has a maximum in D, then f is constant. •

Two interesting properties of proposition 2.1 are the following.

Corollary 2.1 (Maximum principle). Let $D \subset \mathbb{R}^n$ be a bounded open set, and let $f\colon \bar{D} \to \mathbb{R}$ be continuous in $\bar{D} = D \cup \partial D$ and harmonic in D. Then, the maximum value of f on $\bar{D}$ is achieved on ∂D. •

Corollary 2.1 implies that on a bounded domain a harmonic function is determined by its boundary values, thus enabling us to solve the Dirichlet problem for the ball, as explained later.

Proposition 2.2 (Local maximum principle). Let $D \subseteq \mathbb{R}^n$ be a connected open set, and let $f\colon D \to \mathbb{R}$ be harmonic on D. If f has a local maximum in D, then f is constant. •

Because in our scenario the inner domain ∂D_s represents the source,

we assume that values of f on ∂D_{in} are higher than values of f on ∂D_{ex} (or at ∞); under this assumption, the maximum principle ensures that the maximum value of f on $\bar{D}$ is attained on ∂D_{in}. Hence, the problem of finding the source can be described as the problem of finding the maximum value of f on $\bar{D}$; more precisely, having assumed a constant value for f along ∂D_{in}, we will consider that the source seeking problem is solved if any point along ∂D_{in} has been reached. Moreover, the local maximum principle ensures we have no local maxima inside D, hence making it is possible to use a gradient-search technique to localise the source without getting trapped into local maxima.

2.2 The Poisson Integral

In this section we will introduce the Poisson integral, a tool which we will use to compute values of the function $f(\boldsymbol{x})$, and of its derivatives of any order, at any point inside a circular region, by using only measurements along a circular path (the circle where the sensors are placed). In particular, we will provide, in the following section, specific formulæ to estimate the gradient $\nabla f(\boldsymbol{x}^{\mathrm{c}})$ at the centre of the sensor array by using only informations from the circular path.

Consider a bounded domain A and the Dirichlet problem with homogeneous boundary condition

$$\begin{aligned} f(\boldsymbol{x}) &= \bar{f}(\boldsymbol{x}) && \text{on } \partial A \\ \nabla^2 f(\boldsymbol{x}) &= 0 && \text{in } A. \end{aligned}$$

Under some regularity assumptions on the border ∂A of the domain and on the function $\bar{f}$ describing the imposed border conditions, there exists a unique solution of such problem which is continuous on $\bar{A}$. For some particular domains, such a solution can be characterised in the form of an integral, involving the values of $\bar{f}$ on ∂A and a function (called *Poisson kernel*) depending on the shape of the domain. When the domain is the unit

ball centered at the origin, *i.e.*, $A = B_1(0) = \{\, \boldsymbol{x} \colon \|\boldsymbol{x}\| < 1 \,\}$, the Poisson kernel is the following.

Definition 2.2 (Poisson kernel for the unit ball). Given a generic point $\boldsymbol{x} \in B_1(0)$ inside the unit ball of dimension n, and $\bar{\boldsymbol{x}} \in \partial B_1(0)$ being a point on the outer boundary, *i.e.*, on the unit ball surface, we call *Poisson kernel for the unit ball* the function

$$P_{B_1(0)}(\boldsymbol{x}, \bar{\boldsymbol{x}}) = \frac{1 - \|\boldsymbol{x}\|^2}{\|\boldsymbol{x} - \bar{\boldsymbol{x}}\|^n}. \qquad \bullet$$

We note that the problem of finding the value of a harmonic function inside a domain, given its values on the border of the domain itself, is well-defined for every shape of the domain border, not only for the ball; however, it is not possible to write the Poisson kernel in a closed-form for domains other than the half-plane and the ball.

Thanks to corollary 2.1 the solution of the Dirichlet problem is unique; for any function f which is harmonic on the unit ball and continuous on its closure, $f(\boldsymbol{x})$ at points inside the ball can be computed with a formula involving only the values of the restriction of f to the border $\partial B_1(0)$ and the Poisson kernel as follows.

Theorem 2.1 (Poisson integral for the unit ball [3, theorem 1.21]). Let $f \colon \bar{B}_1(0) \to \mathbb{R}$ be continuous on the closed unit sphere $\bar{B}_1(0)$, harmonic on $B_1(0)$. Then f is, on $B_1(0)$, the *Poisson integral* of its restriction on $\partial B_1(0)$, namely:

$$f(\boldsymbol{x}) = \frac{1}{\Omega_n} \int_{\partial B_1(0)} P_{B_1(0)}(\boldsymbol{x}, \bar{\boldsymbol{x}}) f(\bar{\boldsymbol{x}}) \, \mathrm{d}S_{B_1(0)}(\bar{\boldsymbol{x}}),$$

for all $\boldsymbol{x} \in B_1(0)$, and where Ω_n is the measure of the unit ball of dimension n. $\bullet$

Then by a simple dilation and translation of coordinates, mapping the point $\boldsymbol{x}$ to the point $\frac{\boldsymbol{x} - \boldsymbol{x}^{\mathbf{c}}}{r}$, it is possible to obtain the analogous formula

for the generic ball $B_r(\boldsymbol{x}^{\mathbf{c}}) = \{\, \boldsymbol{x} \colon \|\boldsymbol{x} - \boldsymbol{x}^{\mathbf{c}}\| < r \,\}$.

Theorem 2.2 (Poisson integral for the generic ball). Let $f \colon \bar{B}_r(\boldsymbol{x}^{\mathbf{c}}) \to \mathbb{R}$ be continuous on $\bar{B}_r(\boldsymbol{x}^{\mathbf{c}})$, harmonic on $B_r(\boldsymbol{x}^{\mathbf{c}})$. Then:

$$f(\boldsymbol{x}) = \frac{1}{\Omega_n r} \int_{\partial B_r(\boldsymbol{x}^{\mathbf{c}})} P_{B_r(\boldsymbol{x}^{\mathbf{c}})}(\boldsymbol{x}, \bar{\boldsymbol{x}}) f(\bar{\boldsymbol{x}}) \, \mathrm{d}S_{B_r(\boldsymbol{x}^{\mathbf{c}})}(\bar{\boldsymbol{x}}), \tag{2.3}$$

where $\boldsymbol{x} \in B_r(\boldsymbol{x}^{\mathbf{c}})$, and $P_{B_r(\boldsymbol{x}^{\mathbf{c}})}$ is the Poisson kernel for the generic ball, defined as

$$P_{B_r(\boldsymbol{x}^{\mathbf{c}})}(\boldsymbol{x}, \bar{\boldsymbol{x}}) = \frac{r^2 - \|\boldsymbol{x} - \boldsymbol{x}^{\mathbf{c}}\|^2}{\|\boldsymbol{x} - \bar{\boldsymbol{x}}\|^n}. \qquad \bullet \tag{2.4}$$

Hence, if we consider an open set $D \subseteq \mathbb{R}^n$ and a function f harmonic on D, we can apply the Poisson integral formula given in theorem 2.2 to any ball $B_r(\boldsymbol{x}^{\mathbf{c}})$ such that its closure $\bar{B}_r(\boldsymbol{x}^{\mathbf{c}})$ is contained in D, because this ensures that f is harmonic and continuous in $\bar{B}_r(\boldsymbol{x}^{\mathbf{c}})$. This allows us to compute the value of $f(\boldsymbol{x})$ at points $\boldsymbol{x}$ inside the ball by using measurements of f along the circle $\partial B_r(\boldsymbol{x}^{\mathbf{c}})$. In particular, when evaluated in the center of the ball on which the integral is computed, the Poisson kernel in (2.4) reduces to

$$P_{B_r(\boldsymbol{x}^{\mathbf{c}})}(\boldsymbol{x}^{\mathbf{c}}, \bar{\boldsymbol{x}}) = \frac{r^2}{r^n} = \frac{1}{r^{n-2}},$$

and the expression for $f(\boldsymbol{x})$ from (2.3) becomes much simpler:

$$f(\boldsymbol{x}^{\mathbf{c}}) = \frac{1}{\Omega_n r^{n-1}} \int_{\partial B_r(\boldsymbol{x}^{\mathbf{c}})} f(\bar{\boldsymbol{x}}) \, \mathrm{d}S_{B_r(\boldsymbol{x}^{\mathbf{c}})}(\bar{\boldsymbol{x}}). \tag{2.5}$$

2.3 Derivative Computation

The Poisson integral formula given in (2.3) also gives a technique to compute derivatives (gradient, Hessian etc.) of f at any point inside the ball $B_r(\boldsymbol{x}^{\mathbf{c}})$ with an integral involving only the values of f along the circle $\partial \bar{B}_r(\boldsymbol{x}^{\mathbf{c}})$, as stated in the next proposition.

Proposition 2.3. Let $D \subseteq \mathbb{R}^n$ be an open set, and $f \colon D \to \mathbb{R}$ be har-

monic on D. For any $\boldsymbol{x}^{\mathbf{c}} \in D$, for any $r > 0$ such that $\bar{B}_r(\boldsymbol{x}^{\mathbf{c}}) \subseteq D$, for any $\boldsymbol{x} \in B_r(\boldsymbol{x}^{\mathbf{c}})$, and for any non-negative integers $g_1, g_2, \ldots, g_n$ such that $\sum_{i=1}^n g_i = g$,

$$\frac{\partial^g f(\boldsymbol{x})}{\prod_{i=1}^n \partial x_i^{g_i}} = \frac{1}{\Omega_n r} \int_{\partial B_r(\boldsymbol{x}^{\mathbf{c}})} \frac{\partial^g P_{B_r(\boldsymbol{x}^{\mathbf{c}})}(\boldsymbol{x}, \bar{\boldsymbol{x}})}{\prod_{i=1}^n \partial x_i^{g_i}} f(\bar{\boldsymbol{x}}) \, \mathrm{d}S_{B_r(\boldsymbol{x}^{\mathbf{c}})}(\bar{\boldsymbol{x}}). \tag{2.6}$$

Proof. The assumptions ensure that f is harmonic and continuous on $\bar{B}_r(\boldsymbol{x}^{\mathbf{c}})$, so that the Poisson integral formula from theorem 2.2 holds true. Then, it is immediate to notice that in the Poisson integral formula the only dependence on $\boldsymbol{x}$ is in the Poisson kernel, so that one can exchange integration (which is with respect to $\bar{\boldsymbol{x}}$) and derivation (which is with respect to $\boldsymbol{x}$). ✓

Applying (2.6) it is easy to obtain the expression of the gradient $\nabla f(\boldsymbol{x}^{\mathbf{c}})$. The gradient of the Poisson kernel can be computed from (2.4) as

$$\begin{aligned}
\nabla P_{B_r(\boldsymbol{x}^{\mathbf{c}})}(\boldsymbol{x}^{\mathbf{c}}, \bar{\boldsymbol{x}}) &= \frac{\partial}{\partial \boldsymbol{x}} \frac{r^2 - \|\boldsymbol{x} - \boldsymbol{x}^{\mathbf{c}}\|^2}{\|\boldsymbol{x} - \bar{\boldsymbol{x}}\|^n}\bigg|_{\boldsymbol{x}=\boldsymbol{x}^{\mathbf{c}}} = \\
&= \left[\frac{2}{\|\boldsymbol{x} - \bar{\boldsymbol{x}}\|^n} (\boldsymbol{x}^{\mathbf{c}} - \boldsymbol{x}) + \frac{n\left(r^2 - \|\boldsymbol{x} - \boldsymbol{x}^{\mathbf{c}}\|^2\right)}{\|\boldsymbol{x} - \bar{\boldsymbol{x}}\|^{n+2}} (\bar{\boldsymbol{x}} - \boldsymbol{x}) \right] \bigg|_{\boldsymbol{x}=\boldsymbol{x}^{\mathbf{c}}} = \\
&= \frac{nr^2}{r^{n+2}} \boldsymbol{r} = \frac{n}{r^{n-1}} \hat{\boldsymbol{r}},
\end{aligned}$$

where $\boldsymbol{r}$ is the outward oriented radius $\boldsymbol{r} = \bar{\boldsymbol{x}} - \boldsymbol{x}^{\mathbf{c}}$, and $\hat{\boldsymbol{r}}$ is its unit vector $\hat{\boldsymbol{r}} = \frac{\boldsymbol{r}}{r}$; this gives the expression for the gradient

$$\begin{aligned}
\nabla f(\boldsymbol{x}^{\mathbf{c}}) &= \frac{1}{\Omega_n r} \int_{\partial B_r(\boldsymbol{x}^{\mathbf{c}})} \nabla P_{B_r(\boldsymbol{x}^{\mathbf{c}})}(\boldsymbol{x}^{\mathbf{c}}, \bar{\boldsymbol{x}}) f(\bar{\boldsymbol{x}}) \, \mathrm{d}S_{B_r(\boldsymbol{x}^{\mathbf{c}})}(\bar{\boldsymbol{x}}) = \\
&= \frac{n}{\Omega_n r^n} \int_{\partial B_r(\boldsymbol{x}^{\mathbf{c}})} \hat{\boldsymbol{r}} f(\bar{\boldsymbol{x}}) \, \mathrm{d}S_{B_r(\boldsymbol{x}^{\mathbf{c}})}(\bar{\boldsymbol{x}}).
\end{aligned} \tag{2.7}$$

Similarly, we can compute the Hessian of f at the centre $\boldsymbol{H}(\boldsymbol{x}^{\mathbf{c}})$. The Hessian of the Poisson kernel $\boldsymbol{H}_P(\boldsymbol{x}^{\mathbf{c}})$ is composed by the diagonal elements

$$\frac{\partial^2}{\partial x_i^2}\left[\frac{2(x_i^{\mathrm{c}}-x_i)}{\|\boldsymbol{x}-\bar{\boldsymbol{x}}\|^n}+\frac{n\left(r^2-\|\boldsymbol{x}-\boldsymbol{x}^{\mathbf{c}}\|^2\right)(\bar{x}_i-x_i)}{\|\boldsymbol{x}-\bar{\boldsymbol{x}}\|^{n+2}}\right]\Bigg|_{\boldsymbol{x}=\boldsymbol{x}^{\mathbf{c}}}=$$

$$=\left\{-2\frac{\|\boldsymbol{x}-\bar{\boldsymbol{x}}\|^n+(x_i^{\mathrm{c}}-x_i)n\|\boldsymbol{x}-\bar{\boldsymbol{x}}\|^{n-2}(x_i-\bar{x}_i)}{\|\boldsymbol{x}-\bar{\boldsymbol{x}}\|^{2n}}+\right.$$

$$-n\frac{\left[2(x_i-x_i^{\mathrm{c}})(\bar{x}_i-x_i)+\left(r^2-\|\boldsymbol{x}-\boldsymbol{x}^{\mathbf{c}}\|^2\right)\right]\|\boldsymbol{x}-\bar{\boldsymbol{x}}\|^{n+2}}{\|\boldsymbol{x}-\bar{\boldsymbol{x}}\|^{2(n+2)}}+$$

$$\left.-n\frac{\left(r^2-\|\boldsymbol{x}-\boldsymbol{x}^{\mathbf{c}}\|^2\right)(\bar{x}_i-x_i)(n+2)\|\boldsymbol{x}-\bar{\boldsymbol{x}}\|^n(x_i-\bar{x}_i)}{\|\boldsymbol{x}-\bar{\boldsymbol{x}}\|^{2(n+2)}}\right\}\Bigg|_{\boldsymbol{x}=\boldsymbol{x}^{\mathbf{c}}}=$$

$$=-\frac{2}{r^n}-n\frac{r^{n+4}-(n+2)r^{n+2}r_i^2}{r^{2(n+2)}}=\frac{n+2}{r^n}\left(\frac{nr_i^2}{r^2}-1\right),\quad (2.8\,\text{A})$$

and by the off-diagonal elements

$$\frac{\partial^2}{\partial x_i\partial x_j}\left[\frac{2(x_i^{\mathrm{c}}-x_i)}{\|\boldsymbol{x}-\bar{\boldsymbol{x}}\|^n}+\frac{n\left(r^2-\|\boldsymbol{x}-\boldsymbol{x}^{\mathbf{c}}\|^2\right)(\bar{x}_i-x_i)}{\|\boldsymbol{x}-\bar{\boldsymbol{x}}\|^{n+2}}\right]\Bigg|_{\boldsymbol{x}=\boldsymbol{x}^{\mathbf{c}}}=$$

$$=\left\{-2(x_i^{\mathrm{c}}-x_i)\frac{n(x_j-\bar{x}_j)}{\|\boldsymbol{x}-\bar{\boldsymbol{x}}\|^{n+2}}-n(\bar{x}_i-x_i)\left[\frac{2(x_j-x_j^{\mathrm{c}})\|\boldsymbol{x}-\bar{\boldsymbol{x}}\|^{n+2}}{\|\boldsymbol{x}-\bar{\boldsymbol{x}}\|^{2(n+2)}}+\right.\right.$$

$$\left.\left.+\frac{\left(r^2-\|\boldsymbol{x}-\boldsymbol{x}^{\mathbf{c}}\|^2\right)(n+2)\|\boldsymbol{x}-\bar{\boldsymbol{x}}\|^n(x_j-\bar{x}_j)}{\|\boldsymbol{x}-\bar{\boldsymbol{x}}\|^{2(n+2)}}\right]\right\}\Bigg|_{\boldsymbol{x}=\boldsymbol{x}^{\mathbf{c}}}=$$

$$=nr_i\frac{(n+2)r^{n+2}r_j}{r^{2(n+2)}}=\frac{(n+2)}{r^n}\frac{nr_ir_j}{r^2},\quad (2.8\,\text{B})$$

where r_i is the ith coordinate of vector $\boldsymbol{r}$; combining (2.8) in a vector form gives the vector form allows to express $\boldsymbol{H}_P(\boldsymbol{x}^{\mathbf{c}})$ as

$$\boldsymbol{H}_P(\boldsymbol{x}^{\mathbf{c}})=\frac{n+2}{r^n}\left(n\hat{\boldsymbol{r}}\hat{\boldsymbol{r}}^{\mathsf{T}}-\mathbf{I}\right),$$

with $\mathbf{I}$ the identity matrix of size n. Hence, the Hessian of $f(\boldsymbol{x}^{\mathbf{c}})$ can be obtained, via the Poisson integral, as

$$\boldsymbol{H}(\boldsymbol{x}^{\mathbf{c}}) = \frac{1}{\Omega_n r} \int_{\partial B_r(\boldsymbol{x}^{\mathbf{c}})} \boldsymbol{H}_P(\boldsymbol{x}^{\mathbf{c}}, \bar{\boldsymbol{x}}) f(\bar{\boldsymbol{x}}) \, \mathrm{d}S_{B_r(\boldsymbol{x}^{\mathbf{c}})}(\bar{\boldsymbol{x}}) = \\ = \frac{n+2}{\Omega_n r^{n+1}} \int_{\partial B_r(\boldsymbol{x}^{\mathbf{c}})} (n\hat{\boldsymbol{r}}\hat{\boldsymbol{r}}^{\mathsf{T}} - \mathbf{I}) f(\bar{\boldsymbol{x}}) \, \mathrm{d}S_{B_r(\boldsymbol{x}^{\mathbf{c}})}(\bar{\boldsymbol{x}}). \quad (2.9)$$

Beyond Harmonic Functions

Equation (2.7) becomes exact for every function $f \in \mathcal{C}^1(\boldsymbol{x}^{\mathbf{c}})$ when the radius tends to zero. Indeed, as already shown in [12, lemma 1] for the gradient approximation in two dimensions, we can write the first-order Taylor expansion

$$f(\bar{\boldsymbol{x}}) = f(\boldsymbol{x}^{\mathbf{c}} + \boldsymbol{r}) = f(\boldsymbol{x}^{\mathbf{c}}) + \nabla f(\boldsymbol{x}^{\mathbf{c}}) \cdot \boldsymbol{r} + o(r),$$

and, multiplying both sides by $\hat{\boldsymbol{r}}$ and integrating over the ball, we get

$$\int_{\partial B_r(\boldsymbol{x}^{\mathbf{c}})} f(\bar{\boldsymbol{x}}) \hat{\boldsymbol{r}} \, \mathrm{d}S_{B_r(\boldsymbol{x}^{\mathbf{c}})}(\bar{\boldsymbol{x}}) = f(\boldsymbol{x}^{\mathbf{c}}) \int_{\partial B_r(\boldsymbol{x}^{\mathbf{c}})} \hat{\boldsymbol{r}} \, \mathrm{d}S_{B_r(\boldsymbol{x}^{\mathbf{c}})}(\bar{\boldsymbol{x}}) + \\ + r \int_{\partial B_r(\boldsymbol{x}^{\mathbf{c}})} \big(\nabla f(\boldsymbol{x}^{\mathbf{c}}) \cdot \hat{\boldsymbol{r}}\big) \hat{\boldsymbol{r}} \, \mathrm{d}S_{B_r(\boldsymbol{x}^{\mathbf{c}})}(\bar{\boldsymbol{x}}) + o(r^n);$$

the first integral on the right-hand side is equal to zero, while the second gives $\frac{\Omega_n r^{n-1}}{n} \nabla f(\boldsymbol{x}^{\mathbf{c}})$, leading us to (2.7) up to an error $o(r^n)$. We presented here a framework in which, under additional assumptions on f, and provided that the ball $B_r(\boldsymbol{x}^{\mathbf{c}})$ is contained in D, the formulæ for the gradient and Hessian computation are exact for any radius.

We note also that the above formulæ are exact also for the class of quadratic functions, although such functions are in general non-harmonic. As an example, let us consider the quadratic function

$$f(\boldsymbol{x}) = \frac{1}{2} \boldsymbol{x}^{\mathsf{T}} \boldsymbol{A} \boldsymbol{x} + \boldsymbol{b}^{\mathsf{T}} \boldsymbol{x},$$

with $\boldsymbol{A}$ symmetric; as we know,

$$\nabla f(\boldsymbol{x}) = \boldsymbol{A}\boldsymbol{x} + \boldsymbol{b}, \qquad \boldsymbol{H}(\boldsymbol{x}) = \boldsymbol{A},$$

so that $\nabla^2 f(\boldsymbol{x}) = \operatorname{tr} \boldsymbol{A} \neq 0$. Focusing for simplicity on the gradient in two dimensions, we can compute the gradient with the Poisson integral formula considering a circle of centre $\boldsymbol{x}^{\mathbf{c}}$ and radius r, such that equation (2.7) becomes

$$\nabla_{\mathrm{P}} f(\boldsymbol{x}^{\mathbf{c}}) = \frac{1}{\pi r} \int_0^{2\pi} \begin{bmatrix} \cos\gamma \\ \sin\gamma \end{bmatrix} f(\gamma)\, \mathrm{d}\gamma,$$

where

$$\begin{aligned} f(\gamma) = f\left(\boldsymbol{x}^{\mathbf{c}} + r \begin{bmatrix} \cos\gamma \\ \sin\gamma \end{bmatrix}\right) = \\ = r(a_1 x_1^{\mathrm{c}} + a_{1,2} x_2^{\mathrm{c}} + b_1)\cos\gamma + \frac{a_1 r^2}{2}\cos^2\gamma + a_{1,2} r^2 \cos\gamma \sin\gamma + \\ + r(a_{1,2} x_1^{\mathrm{c}} + a_2 x_2^{\mathrm{c}} + b_2)\sin\gamma + \frac{a_2 r^2}{2}\sin^2\gamma + \frac{a_1 x_1^{\mathrm{c}\,2}}{2} + a_{1,2} x_1^{\mathrm{c}} x_2^{\mathrm{c}} + \\ + \frac{a_2 x_2^{\mathrm{c}\,2}}{2} + b_1 x_1^{\mathrm{c}} + b_2 x_2^{\mathrm{c}}, \end{aligned} \tag{2.10}$$

so that the two components of the gradient are given by the integral of the multiplication of this function by, respectively, $\cos\gamma$ and $\sin\gamma$. All such combinations of trigonometric functions give a null integral over the circle, except for the square power of $\cos\gamma$ and $\sin\gamma$, for which we have that $\int_0^{2\pi} \cos^2\gamma\, \mathrm{d}\gamma = \int_0^{2\pi} \sin^2\gamma\, \mathrm{d}\gamma = \pi$; therefore, the only contributions to the integral are the multipliers of respectively $\cos\gamma$ and $\sin\gamma$ in (2.10) that get multiplied by a factor π, *i.e.*,

$$\nabla_{\mathrm{P}} f(\boldsymbol{x}^{\mathbf{c}}) = \frac{1}{\pi r} \begin{bmatrix} r(a_1 x_1^{\mathrm{c}} + a_{1,2} x_2^{\mathrm{c}} + b_1)\pi \\ r(a_{1,2} x_1^{\mathrm{c}} + a_2 x_2^{\mathrm{c}} + b_2)\pi \end{bmatrix} = \boldsymbol{A}\boldsymbol{x}^{\mathbf{c}} + \boldsymbol{b} = \nabla f(\boldsymbol{x}^{\mathbf{c}}).$$

Chapter 3

Source Localisation on the Plane

We present here a method for solving the source-seeking problem in two dimensions, without position information. The idea is to steer the vehicle towards the source by performing a gradient-ascent method based on the formulæ derived previously, with the gradient (and possibly the Hessian) being estimated by collecting point-wise measurements of the emitted quantity of interest around a circle. Hence, we need the vehicle to be equipped with a suitable sensing device, as we are going to explain in the next section.

3.1 Planar Mobile Vehicles

We consider mobile robots, each one endowed with one or more sensors providing point-wise concentration measures. In this chapter we consider the problem where each robot is required to perform the source-localisation task *alone*, without any collaboration or information exchange between different vehicles; the presence of multiple robots is useful to ensure redundancy, so as to protect against failures, and also to better describe the source boundary in a scenario where each robot is able to find only one point on ∂D_{s}.

The robots' dynamics can be modeled in various ways, depending on the application at hand: as an example, we consider underactuated vehicles

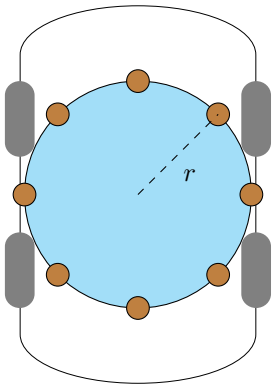

(A) A circular array of sensors with equispaced angles is fixed on the robot (example 3.1).

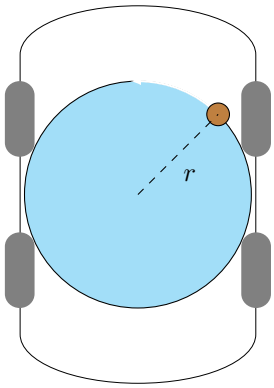

(B) A single sensor is rotating fast around a circle fixed on the robot (example 3.2).

Figure 3.1. Possible sensor deployment over a planar autonomous vehicle.

modeled as nonholonomic unicycles with dynamics

$$\begin{aligned} \dot{\boldsymbol{x}}(t) &= v \begin{bmatrix} \cos\theta(t) \\ \sin\theta(t) \end{bmatrix} \\ \ddot{\theta}(t) &= u(t), \end{aligned} \tag{3.1}$$

controlled by the torsional torque $u(t)$. The position of the vehicle in the plane is described by $\boldsymbol{x}(t)$, and $\theta(t)$ represents its heading angle; the forward velocity v is assumed here to be constant for simplicity, even if different strategies can be alternatively devised.

The central point is how to design the control $u(t)$ using information from the sensors devices to reach the source's location. Ideally, we would like each robot to compute the gradient at its center position $\boldsymbol{x}(t)$ by using the Poisson formula (2.7), with $\boldsymbol{x}^{\mathbf{c}} = \boldsymbol{x}(t)$; to this aim, it needs to collect measurements on a circle $\partial B_r(\boldsymbol{x}^{\mathbf{c}})$ and to compute the Poisson integral. Two practical ways to obtain good approximations are given below.

Example 3.1. A first effective sensing device, depicted in figure 3.1a, consists in N sensors arranged along a circular array of radius r, centered at the robot's central position $\boldsymbol{x}(t)$ with equispaced angles; namely, the ith

sensor is at position

$$\boldsymbol{x}_i(t) = \boldsymbol{x}(t) + r \begin{bmatrix} \cos\gamma_i \\ \sin\gamma_i \end{bmatrix}, \tag{3.2}$$

where $\gamma_i = \frac{2\pi}{N}(i-1)$. The array of sensors is solidly connected to the vehicle, and it rotates with the robot heading angle; therefore, the robot will compute the gradient in the local coordinate system where its heading has a fixed value. Then, the integral is approximated by the Riemann sum using the N measured values.

Example 3.2. A second setup, depicted in figure 3.1b, can obtained by considering only one sensor instead of N, but allowing for a rotation of the sensor around the center of the robot; in this case, either it is supposed that the robot stays still during such a rotation, so that the integrals in equations (2.7) and (2.9) are perfecly computed (apart from the measurement noise), or the robot moves during the rotation but with a speed sufficiently slow with respect to the rotation of the sensor, so that only a small error is introduced due to the deviation from the perfect circle.

Throughout this chapter we will focus on the first setup.

3.2 Derivative Approximation

We can approximate the integrals in (2.7) and (2.9) by the Riemann sum of the N values provided by the sensors arranged along the circle (see figure 3.1a).

Using the polar coordinates $\boldsymbol{r} = r(\cos\gamma,\ \sin\gamma)$, with $\gamma \in [0, 2\pi)$, $\mathrm{d}S = r\,\mathrm{d}\gamma$ and the measure of the unit circle equal to $\Omega_2 = 2\pi$, the Poisson formulæ (2.5), (2.7) and (2.9) in two dimensions become

$$f(\boldsymbol{x}(t)) = \frac{1}{2\pi}\int_0^{2\pi} f(\bar{\boldsymbol{x}}(\gamma))\,\mathrm{d}\gamma \tag{3.3a}$$

$$\nabla f(\boldsymbol{x}(t)) = \frac{1}{\pi r} \int_0^{2\pi} \begin{bmatrix} \cos\gamma \\ \sin\gamma \end{bmatrix} f(\bar{\boldsymbol{x}}(\gamma))\,\mathrm{d}\gamma \tag{3.3 B}$$

$$\boldsymbol{H}(\boldsymbol{x}(t)) = \frac{2}{\pi r^2} \int_0^{2\pi} \begin{bmatrix} 2\cos^2\gamma - 1 & 2\cos\gamma\sin\gamma \\ 2\cos\gamma\sin\gamma & 2\sin^2\gamma - 1 \end{bmatrix} f(\bar{\boldsymbol{x}}(\gamma))\,\mathrm{d}\gamma. \tag{3.3 C}$$

By denoting the measurement of sensor i at time t by

$$\hat{f}_i\big(\boldsymbol{x}(t), t\big) = f\big(\boldsymbol{x}_i(t)\big) + e_i(t),$$

where $\boldsymbol{x}_i$, defined in equation (3.2), is the discretisation of $\bar{\boldsymbol{x}}$ and $e_i(t)$ is the error due to the white Gaussian measurement noise affecting sensor i, we can now compute the approximation of equations (3.3) as

$$\hat{f}\big(\boldsymbol{x}(t), t\big) = \frac{1}{N} \sum_{i=1}^{N} \hat{f}_i\big(\boldsymbol{x}(t), t\big) \tag{3.4 A}$$

$$\widehat{\nabla f}\big(\boldsymbol{x}(t), t\big) = \frac{2}{Nr} \sum_{i=1}^{N} \hat{\boldsymbol{r}}_i \hat{f}_i\big(\boldsymbol{x}(t), t\big) \tag{3.4 B}$$

$$\hat{\boldsymbol{H}}\big(\boldsymbol{x}(t), t\big) = \frac{4}{Nr^2} \sum_{i=1}^{N} \tilde{\boldsymbol{H}}_i \hat{f}_i\big(\boldsymbol{x}(t), t\big), \tag{3.4 C}$$

where $\hat{\boldsymbol{r}}_i = \begin{bmatrix} \cos\gamma_i \\ \sin\gamma_i \end{bmatrix}$ and, after some simple trigonometrics on the matrix in (3.3 C),

$$\tilde{\boldsymbol{H}}_i = \begin{bmatrix} \cos 2\gamma_i & \sin 2\gamma_i \\ \sin 2\gamma_i & -\cos 2\gamma_i \end{bmatrix}.$$

We note that all the integrals and sums of vector- or matrix-valued quantities are intended as entry-wise integrals or sums of the entries of the vectors or matrices.

3.3 Feedback Design

The main idea is to perform a gradient ascent, with the gradient being computed by equation (3.4 B). In general, a harmonic function f might not be convex; however, the local maximum principle (see proposition 2.2) ensures that f does not have any local maximum inside D: hence, search is ensured not to get trapped in any local maximum, except possibly on the outer boundary ∂D_{ex}. The termination of the search on a local maximum on ∂D_{ex} can be avoided by introducing some simple rule that allows to distinguish the external boundary from the internal one; for instance, one might have a knowledge of a rough lower bound on the value of f at the source, which is also an upper bound for values on the external boundary.

The gradient-ascent strategy can be implemented by defining a reference heading $\theta^{\text{r}}(\boldsymbol{x})$ in the direction of the gradient of the diffusion function at the point $\boldsymbol{x}$, using formula (3.4 B). Thanks to the ease of computation of the previous formulæ, we can use a control law involving the Hessian, *e.g.*, including a damping term, useful as the system is second-order, involving the time derivatives of both the heading angle and its reference θ^{r}; such term can be computed from the approximated gradient (3.4 B) and Hessian (3.4 C).

The proposed feedback is

$$u(t) = k_1\Big(\theta^{\text{r}}\big(\boldsymbol{x}(t),t\big) - \theta(t)\Big) + k_2\Big(\dot\theta^{\text{r}}\big(\boldsymbol{x}(t),t\big) - \dot\theta(t)\Big), \tag{3.5}$$

with the reference and its time-derivative given by

$$\begin{aligned}\theta^{\text{r}}\big(\boldsymbol{x}(t),t\big) &= \arg\widehat{\nabla f}\big(\boldsymbol{x}(t),t\big)\\ \dot\theta^{\text{r}}\big(\boldsymbol{x}(t),t\big) &= \frac{\dot{\boldsymbol{x}}^{\mathsf{T}}(t)\hat{\boldsymbol{H}}\big(\boldsymbol{x}(t),t\big)\boldsymbol{R}\widehat{\nabla f}\big(\boldsymbol{x}(t),t\big)}{\|\widehat{\nabla f}\big(\boldsymbol{x}(t),t\big)\|^2},\end{aligned}$$

where $\widehat{\nabla f}\big(\boldsymbol{x}(t),t\big)$ and $\hat{\boldsymbol{H}}\big(\boldsymbol{x}(t),t\big)$ are defined by equations (3.4 B) and

(3.4 c), and $\boldsymbol{R}$ is the rotation matrix of an angle equal to $\frac{\pi}{2}$, defined as

$$\boldsymbol{R} = \begin{bmatrix} 0 & -1 \\ 1 & 0 \end{bmatrix}.$$

Clearly, the reference heading angle θ^{r} is an approximation of the gradient's argument $\theta_{\mathrm{g}}(\boldsymbol{x}(t)) = \arg \nabla f(\boldsymbol{x}(t))$; moreover, the expression for $\dot{\theta}^{\mathrm{r}}$ is an approximation of its time-derivative, $\dot{\theta}_{\mathrm{g}}(\boldsymbol{x}(t)) = \frac{\mathrm{d}\theta_{\mathrm{g}}(t)}{\mathrm{d}t}$. Indeed, by the chain rule,

$$\dot{\theta}_{\mathrm{g}}(\boldsymbol{x}(t)) = \frac{\partial \theta_{\mathrm{g}}(\boldsymbol{x}(t))}{\partial \boldsymbol{x}} \cdot \dot{\boldsymbol{x}}(t).$$

Here,

$$\dot{\boldsymbol{x}}(t) = v \begin{bmatrix} \cos\theta(t) \\ \sin\theta(t) \end{bmatrix}$$

by (3.1), while the spacial derivatives of $\theta_{\mathrm{g}}(\boldsymbol{x})$ are computed from the expression $\theta_{\mathrm{g}}(\boldsymbol{x}) = \arctan \frac{\partial f(\boldsymbol{x})/\partial x_2}{\partial f(\boldsymbol{x})/\partial x_1}$, as follows:

$$\begin{bmatrix} \frac{\partial \theta_{\mathrm{g}}(\boldsymbol{x})}{\partial x_1} \\ \frac{\partial \theta_{\mathrm{g}}(\boldsymbol{x})}{\partial x_2} \end{bmatrix} = \frac{1}{\left[1 + \left(\frac{\partial f(\boldsymbol{x})/\partial x_2}{\partial f(\boldsymbol{x})/\partial x_1}\right)^2\right] \left(\frac{\partial f(\boldsymbol{x})}{\partial x_1}\right)^2} \begin{bmatrix} \frac{\partial^2 f(\boldsymbol{x})}{\partial x_1 \partial x_2} \frac{\partial f(\boldsymbol{x})}{\partial x_1} - \frac{\partial f(\boldsymbol{x})}{\partial x_2} \frac{\partial^2 f(\boldsymbol{x})}{\partial x_1^2} \\ \frac{\partial^2 f(\boldsymbol{x})}{\partial x_2^2} \frac{\partial f(\boldsymbol{x})}{\partial x_1} - \frac{\partial f(\boldsymbol{x})}{\partial x_2} \frac{\partial^2 f(\boldsymbol{x})}{\partial x_1 \partial x_2} \end{bmatrix} =$$

$$= \frac{\boldsymbol{H}(\boldsymbol{x}) \boldsymbol{R} \nabla f(\boldsymbol{x})}{\|\nabla f(\boldsymbol{x})\|^2}.$$

3.4 Simulation Results

As a simulation example, we consider a heated plane corresponding to the one in example 2.2. In particular, we propose to have a rectangular space 10×6 m wide, with a circular heater of 5 cm of radius in its middle and an opening on the back-side. The heater imposes the condition $f(\boldsymbol{x}) = f_{\mathrm{s}}$; the borders are perfectly isolating, so as to impose the Neumann boundary condition $\nabla f(\boldsymbol{x}) \cdot \hat{\boldsymbol{n}} = 0$, while the side opening, 6 m wide, imposes the boundary condition on the value of the temperature $f(\boldsymbol{x}) = f_{\mathrm{ex}}$.

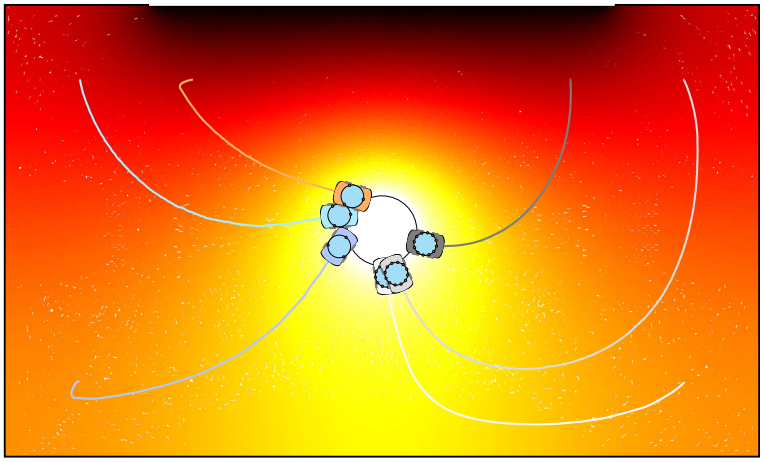

Figure 3.2. Trajectories of heat-seeking vehicles equipped with noiseless sensors; the vehicles on the left have 3 sensors each, the ones on the right 12 sensors.

Figure 3.2 shows the trajectories of a set of robots such as those depicted in figure 3.1A, described by the motion law (3.1), starting from different random initial positions and with different initial orientations. The temperature of the heater is $f_s = 45$ °C, while the external one is equal to $f_{ex} = 5$ °C, and each robot moves with a constant velocity of $v = 0.2\,\mathrm{m/s}$ and with the sensors arranged on a circumference of radius $r = 10\,\mathrm{cm}$; the control parameters in equation (3.5) are chosen as $k_1 = 49$ and $k_2 = 14$. In this first case we supposed perfectly noiseless measurements; the vehicles on the left are endowed with $N = 3$ sensors, while the ones on the right have $N = 12$ sensors. We can observe that a lower number of sensors results in a trajectory which is not exactly oriented with the gradient of f, but the robots are nonetheless able to quickly reach the source.

A simulation with the same initial conditions and parameters and the same number of sensors for each of the two subsets of vehicles, but with each measurement corrupted by white Gaussian noise of standard deviation $\sigma = 0.75$, is shown in figure 3.3. As we can see, all vehicles reach the source, with trajectories almost perpendicular to the contour lines of the temperature, which have a small dithering due to the noise in the measurements; we can also notice the better filtering achieved by the 12-sensor robots.

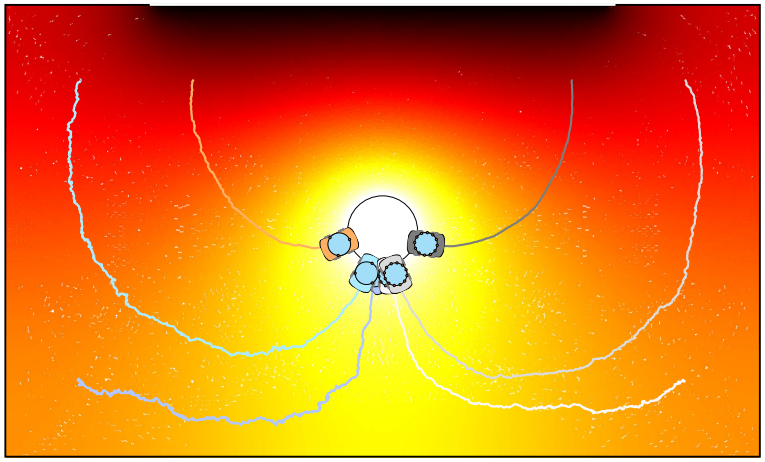

Figure 3.3. Trajectories of heat-seeking vehicles equipped with noisy sensors; the vehicles on the left have 3 sensors each, the ones on the right 12 sensors.

3.5 Experimental Practical Implementation

In the framework of a master internship project of a M.Sc. student (Yvan Gaudfrin) from the University of Bristol (England, UK), we developed a prototype planar robot to test the source-localisation control which we have previously described. The project was held at Gipsa-lab, under the supervision of eng. Jonathan Dumon and Ruggero Fabbiano.

3.5.1 Description of the Project

In this experiment, whose goal is to validate via a hardware implementation our 2D source-seeking control, the source-localisation task will be carried out by a planar robot equipped with a camera, moving on the top of a wide picture representing a real-life diffusion process, *i.e.*, a source of hot water discharge which is spreading into the sea (figure 3.4). The circular set of sensors which provide point-wise measurements will be obtained, in such case, by selecting appropriate pixels on a circular shape on the camera view. Using these sensors, the robot should move on that picture and roll toward the source. We note that, as in every real-life

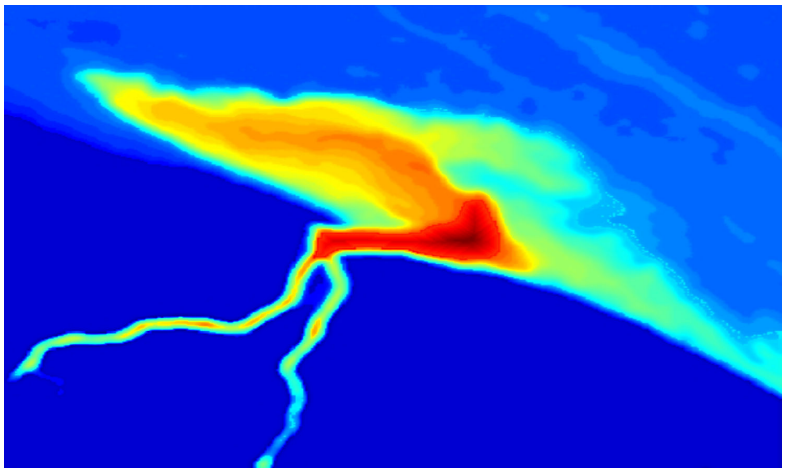

Figure 3.4. Image of the thermal plume used for the practical source-localisation case study; the temperature follows a colour scale from dark blue (cold/normal) to dark red (hot/polluted). Source: Science Education through Earth Observation for High Schools (SEOS).

application, the theoretical assumptions under which we developed our control law are not satisfied: indeed the function describing the diffusion process that we can see in figure 3.4 is nonharmonic and has also local maxima; therefore, another goal of the project is to see how such system can operate in practice, when the real diffusion process does not completely match with the assumptions of the ideal case.

After a pre-processing of the image to make it suitable to the case study, the project has been divided in several tasks listed below.

1. Simulation: the source-localisation algorithm described in the previous sections was adapted to our case study, and a fully-working Simulink® scheme, integrating both the robot model and the camera model, has been developed and used to test the algorithm itself.

2. Hardware selection and configuration: choice of the components and their configuration and construction of the wheeled robot.

3. Software implementation: this part required to do some suitable modification to the preliminary model, as well as some image pro-

cessing, so as to allow to program the robot taking into account its physical and device constraints.

In the following subsections we will give a brief overview of the three phases; an exhaustive description of the project can be found in the master thesis of Yvan Gaudfrin [33].

3.5.2 Simulation

The first step has been to create a simulation model in order to test the source-seeking algorithm, with a preliminary robot model integrated in it, before the hardware implementation; this phase allowed also to test the effectiveness of our algorithm when our assumptions are not satisfied. Figure 3.5 shows some simulations of the Simulink® model on the scenario given by the diffusion picture 3.4 for some random initial positions; the black dots represent the initial position, while the small black arrows represent the final one. The algorithm demonstrated to be highly successful even when the robot was located in the water plume (initial position at the bottom of the picture), where the assumptions are strongly violated, if only the radius of the given sensing device is correctly sized to sense a variation in the surrounding environment.

Clearly, in wide ocean (flat blue zone) it is then not possible to compute a significant gradient. A simple solution could be to implement a switched control which imposes a spiraled motion if the variance of the point-wise measurements is lower than a given threshold; such motion would persist until the vehicle starts to sense significant values, and thus compute a useful gradient. Nevertheless, it should be taken into account that such motions are low efficient in terms of time and energy consumption (the vehicle might have to cover long distances before sensing useful measurements).

3.5.3 Robot Design

Regarding the robot design, the two main constraints to take into account were:

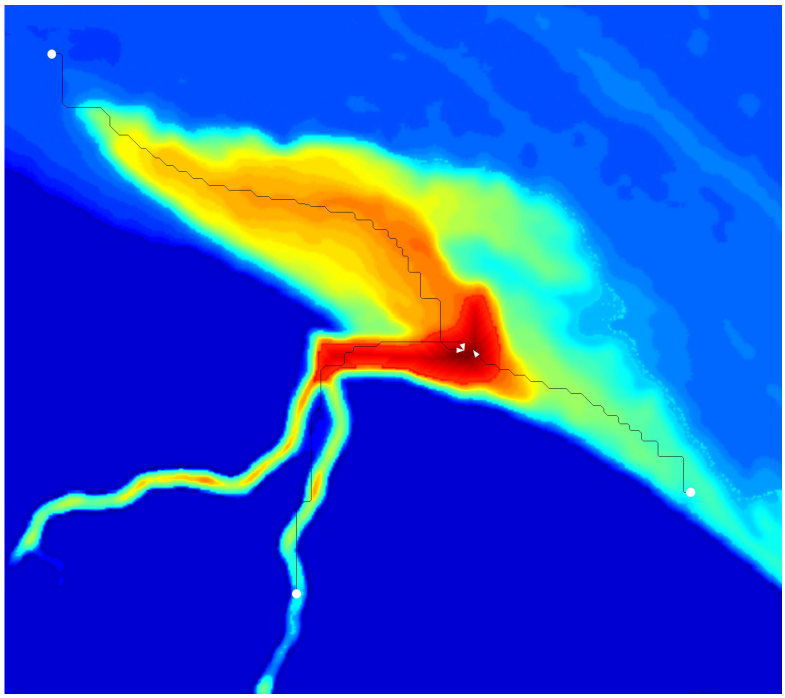

Figure 3.5. Some simulations on the scenario of the practical case study; the white circles represent the initial positions, the arrows the final positions.

A. In order to provide maximum liberty of motion, the components of the robot should not be connected to external wires for image transmission to the terminal; thus, the information and the data should be transmitted via a wireless signal.

B. The transmission of the image should be as fast as possible to be able to operate in real time with continuous correction of the robot's trajectory.

Clearly, these two constraints required to carefully choose the devices and properly process the captured image before sending it, in order to get the smallest amount of data and send it as fast as possible via a wireless communication.

Sensing Device

For these reasons, as a sensing device of the robot it has been decided to use a GigE Vision® camera. Such camera can use the Gigabit Ethernet vision communication protocol to communicate with the external world; usually used for high-performance industrial camera, this standard permits a rapid transfer of images using low cost standard cables, even over long distances. Nonetheless, to avoid the use of wires (*i.e.*, the Ethernet cables), the device has been combined with two Wi-Fi access points (APs) using the Wi-Fi communication protocols IEEE 802.11 group to make the link between the camera and the computer. Still the quality and the format of the transmitted image had to be adapted to the data rate in order to be able to operate on-line.

In the last part of the project, this device has been substituted with a small wireless camera combined with a USB 2 video converter from The Imaging Source®. This camera transmits the image via an antenna to a video receptor, which is then connected via a video wire to the USB 2 converter that processes the image format and send it to the terminal via a USB cable. Such choice had the advantages that no big size problems, and hence strict data formatting, were necessary; furthermore, this camera is very light (about 22 grams).

Since the camera is supposed to operate at a few centimetres above the diffusion image, a "fish-eye" lens has been chosen; such kind of lens is able to transmit a larger image sample compared to a common lens. Moreover, for the same reason, the captured area resulted too dark to clearly distinguish the different colours, giving sometimes false colour translations, and thus false measurements. To counter such problem two LEDs have been fixed around the lens to provide a constant intensity of light and thus better colour definition (which meant better gradient estimation). To avoid falsified measures, a colour temperature of 6500 K (white light, similar to Sun light) was chosen.

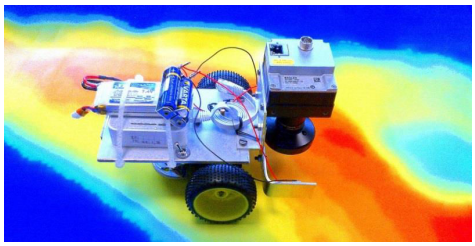

(A) First design: GigE Vision® camera.

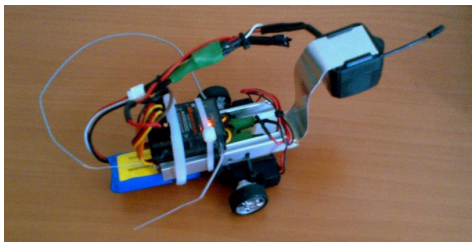

(B) Second design: wireless camera with USB converter.

Figure 3.6. The robots built for the practical study case.

Drive

To drive the robot, a differential drive with two motorised wheels and a castor wheel was chosen; to receive the driving instructions from the computer, in order to control the rotation of the wheels, we selected a basic model-making receptor (Spektrum® AR600), as it is quite simple to use and to configure.

The motors that have been used to command the wheels were basic model-making servos controlled in angle; those kinds of servos are mechanical combinations of a DC motor, a servomotor, a potentiometer and an electronic control system. The motor can rotate at an angle which depends on the servomotor (there is a mechanical stop that prevents it from going any further), and the potentiometer enables to know the position of the servomotor's axis, *i.e.*, the angle formed by the axis of the motor with the mechanical stop. Thus, in order to make our control law operate without any rotational limitation, some mechanical modifications were necessary inside each servo: first, we had to remove the mechanical stop by using some pliers, then it was necessary to fix the potentiometer when on the zero degree position or about.

The two final prototypes, with the two different cameras used, are shown in figure 3.6.

3.5.4 Software Implementation and Final Tests

We provide here a summary of the integration of the software and the hardware components, omitting the details about the configuation of all the different devices mounted on the robot and about the image processing (mainly due to the problem that the colours were not identically interpreted by MATLAB® and by the camera, which brought us to define a manually calibrated colour-map), which can be found in [33] along with the full Simulink® scheme of the final implementation.

Once the algorithm and the devices had been set up, the next step was to create a hardware-in-the-loop (HIP) Simulink® model with the real robot. As the motion strategy involved a tuned angular velocity, the rotational velocity of each wheel has to differ depending on the direction of the gradient estimation (*i.e.*, the orientation that the robot has to take); thus, the control input will be sent to each wheel as an increment of the rotational speed for the outer wheel with respect to the curvature to take, and a decrement for the inner one. Moreover, since now we are controlling directly the rotational speed, we used the simpler control

$$u(t) = \dot{\theta}(t) = k\Big(\theta^{\mathrm{r}}\big(\boldsymbol{x}(t), t\big) - \theta(t)\Big);$$

therefore, the speed of each wheel will linearly depend on the gradient computation. Finally, to take into account the physical behaviour of the actuator, it has been necessary to introduce a hysteresis cycle to avoid oscillations around the control value of 180°.

The planar source-seeking prototype demonstrated to be fully effective in the scenario we have used, even considering its nonharmonicity. If the initial conditions were such that it could get meaningful measurements, it always managed to reach the zone of the picture representing the diffusion source, as shown by figure 3.7, which reports an approximation of the path traced by the robot during some validation experiments. For a better understanding of the robot's behaviour, we refer to

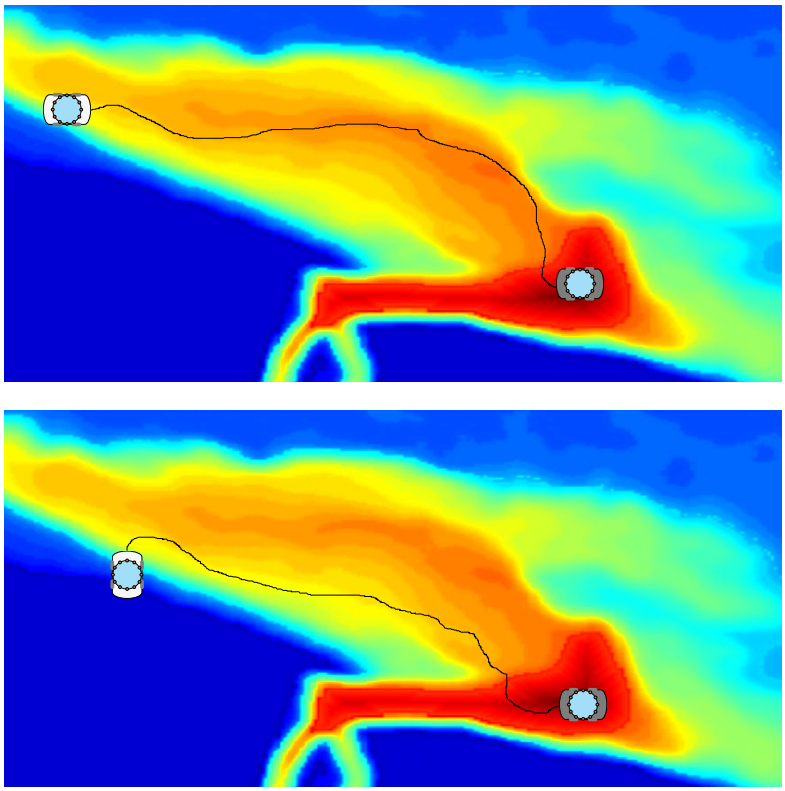

Figure 3.7. Reproduction of the trajectories followed by the source-seeking robot; the white vehicle indicates the initial position, the gray one the final position.

the website of the NeCS team[1] for the videos of the robot at work.

[1]http://necs.inrialpes.fr/pages/platforms.php#sourceLoc

Chapter 4

Tridimensional Source-Seeking

In this chapter we extend the previous results to a tridimensional framework. Even though it is less immediate how to approximate the Poisson integral in three dimensions, as we will see, nonetheless the simplicity and ease of implementation of the proposed solution remains still valid. We also deepen our analysis, with respect to the introductory bidimensional case, giving theoretical results in addition to wider simulation examples.

4.1 Vehicle Dynamics and Feedback Design

We consider an underactuated vehicle, described by the kinematic motion law

$$\begin{aligned} \dot{\boldsymbol{x}}(t) &= v \begin{bmatrix} \cos\theta_1(t)\sin\theta_2(t) \\ \sin\theta_1(t)\sin\theta_2(t) \\ \cos\theta_2(t) \end{bmatrix} \\ \begin{bmatrix} \dot{\theta}_1(t) \\ \dot{\theta}_2(t) \end{bmatrix} &= \boldsymbol{u}(t), \end{aligned} \tag{4.1}$$

where $\boldsymbol{x}$ indicates the position of the centre of mass of the agent, and θ_1 and θ_2 are the yaw and pitch angles respectively. In this model the forward velocity v is supposed to be constant (even though other strategies can be devised), and the heading angle is controlled by the control $\boldsymbol{u}$ that

steers the angular velocity. Such a choice for the vehicle's dynamics may represent, in three dimensions, a simplified model for a submarine or an autonomous underwater vehicle.

We would like to perform a gradient-ascent method using the Poisson formulas obtained in the previous chapter. Our objective is to follow the gradient of the signal function $\nabla f(\boldsymbol{x}(t))$, but we consider the case where it is possible to control the angular velocity only, and not to change instantaneously the orientation of the vehicle. Thus, we define the control references as the headings given by the direction of the gradient estimated at the current centre of mass of the vehicle $\boldsymbol{x}(t)$:

$$\theta_1^{\mathrm{r}}(\boldsymbol{x}(t)) = \arctan \frac{g_2(\boldsymbol{x}(t))}{g_1(\boldsymbol{x}(t))}$$

$$\theta_2^{\mathrm{r}}(\boldsymbol{x}(t)) = \arccos \frac{g_3(\boldsymbol{x}(t))}{\|\boldsymbol{g}(\boldsymbol{x}(t))\|},$$

where $\boldsymbol{g}(\boldsymbol{x}(t)) = \widehat{\nabla f}(\boldsymbol{x}(t))$ is the approximate gradient, so that the references are approximations of the gradient angles. Then, we define a control law with a term involving the time derivative of the reference headings:

$$\boldsymbol{u}(t) = k \begin{bmatrix} \theta_1^{\mathrm{r}}(\boldsymbol{x}(t)) - \theta_1(t) \\ \theta_2^{\mathrm{r}}(\boldsymbol{x}(t)) - \theta_2(t) \end{bmatrix} + \begin{bmatrix} \dot{\theta}_1^{\mathrm{r}}(\boldsymbol{x}(t)) \\ \dot{\theta}_2^{\mathrm{r}}(\boldsymbol{x}(t)) \end{bmatrix}. \tag{4.2}$$

Analogously to the 2D case, the expressions for the time-derivative of the heading references, which are approximations of the time derivatives of the respective gradient's angles, can be computed as

$$\dot{\theta}_1^{\mathrm{r}}(\boldsymbol{x}(t)) = \begin{bmatrix} \frac{\partial \theta_1^{\mathrm{r}}(\boldsymbol{x}(t))}{\partial x_1} \\ \frac{\partial \theta_1^{\mathrm{r}}(\boldsymbol{x}(t))}{\partial x_2} \\ \frac{\partial \theta_1^{\mathrm{r}}(\boldsymbol{x}(t))}{\partial x_3} \end{bmatrix} \cdot \dot{\boldsymbol{x}}(t) =$$

$$= \frac{1}{\|\boldsymbol{A}\boldsymbol{g}(\boldsymbol{x}(t))\|^2} \begin{bmatrix} \frac{\partial g_2(\boldsymbol{x}(t))}{\partial x_1} g_1(\boldsymbol{x}(t)) - g_2(\boldsymbol{x}(t)) \frac{\partial g_1(\boldsymbol{x}(t))}{\partial x_1} \\ \frac{\partial g_2(\boldsymbol{x}(t))}{\partial x_2} g_1(\boldsymbol{x}(t)) - g_2(\boldsymbol{x}(t)) \frac{\partial g_1(\boldsymbol{x}(t))}{\partial x_2} \\ 0 \end{bmatrix} \cdot \dot{\boldsymbol{x}}(t) =$$

$$= \frac{\boldsymbol{B}\hat{\boldsymbol{H}}(\boldsymbol{x}(t))\boldsymbol{A}\boldsymbol{g}(\boldsymbol{x}(t)) \cdot \dot{\boldsymbol{x}}(t)}{\|\boldsymbol{A}\boldsymbol{g}(\boldsymbol{x}(t))\|^2} \quad (4.3\,\text{A})$$

and, similarly,

$$\dot{\theta}_2^{\mathrm{r}}(\boldsymbol{x}(t)) = \begin{bmatrix} \frac{\partial \theta_2^{\mathrm{r}}(\boldsymbol{x}(t))}{\partial x_1} \\ \frac{\partial \theta_2^{\mathrm{r}}(\boldsymbol{x}(t))}{\partial x_2} \\ \frac{\partial \theta_2^{\mathrm{r}}(\boldsymbol{x}(t))}{\partial x_3} \end{bmatrix} \cdot \dot{\boldsymbol{x}}(t) =$$

$$= \frac{g_3(\boldsymbol{x}(t))\hat{\boldsymbol{H}}(\boldsymbol{x}(t))\boldsymbol{g}(\boldsymbol{x}(t)) - \|\boldsymbol{g}(\boldsymbol{x}(t))\|^2 \hat{\boldsymbol{H}}(\boldsymbol{x}(t))\boldsymbol{a}}{\|\boldsymbol{A}\boldsymbol{g}(\boldsymbol{x}(t))\|}, \quad (4.3\,\text{B})$$

where $\boldsymbol{A}$, $\boldsymbol{B}$ and $\boldsymbol{a}$ are the following matrices:

$$\boldsymbol{A} = \begin{bmatrix} 0 & -1 & 0 \\ 1 & 0 & 0 \\ 0 & 0 & 0 \end{bmatrix}, \qquad \boldsymbol{B} = \begin{bmatrix} 1 & 0 & 0 \\ 0 & 1 & 0 \\ 0 & 0 & 0 \end{bmatrix}, \qquad \boldsymbol{a} = \begin{bmatrix} 0 \\ 0 \\ 1 \end{bmatrix}.$$

In the next section we show how to compute the approximations of the gradient and the Hessian of $f(\boldsymbol{x})$.

4.2 Implementation Details

Steering the vehicle towards the source can be obtained by performing a gradient-ascent method based on the formulæ derived previously, with the gradient and the Hessian being estimated by collecting point-wise measurements of the quantity of interest. Hence, we need the vehicle to be equipped with a sensing device that can take suitable measurements on a sphere.

4.2.1 Derivative Computation

The expressions for the approximate gradient $\boldsymbol{g}$ and Hessian $\hat{\boldsymbol{H}}$ of the function f used in equations (4.3) can be obtained from equations (2.5)-(2.9), considering that, using the spherical coordinates

$$\boldsymbol{r} = r \begin{bmatrix} \cos\gamma \sin\varphi \\ \sin\gamma \sin\varphi \\ \cos\varphi \end{bmatrix},$$

where $\gamma \in [0, 2\pi)$ and $\varphi \in [0, \pi]$ are respectively the azimuth and altitude angle, we have that $n = 3$, $\Omega_3 = 4\pi$ and $\mathrm{d}S = r^2 \sin\varphi \,\mathrm{d}\gamma \,\mathrm{d}\varphi$, so that equations (2.5), (2.7) and (2.9) take the form

$$f\big(\boldsymbol{x}(t)\big) = \frac{1}{4\pi} \int_0^{\pi} \sin\varphi \int_0^{2\pi} f(\bar{\boldsymbol{x}}(\gamma,\varphi)) \,\mathrm{d}\gamma \,\mathrm{d}\varphi \tag{4.4 A}$$

$$\nabla f\big(\boldsymbol{x}(t)\big) = \frac{3}{4\pi r} \int_0^{\pi} \sin\varphi \int_0^{2\pi} \hat{\boldsymbol{r}}(\gamma,\varphi) f(\bar{\boldsymbol{x}}(\gamma,\varphi)) \,\mathrm{d}\gamma \,\mathrm{d}\varphi \tag{4.4 B}$$

$$\boldsymbol{H}\big(\boldsymbol{x}(t)\big) = \frac{5}{4\pi r^2} \int_0^{\pi} \sin\varphi \int_0^{2\pi} \boldsymbol{H}_P(\gamma,\varphi) f(\bar{\boldsymbol{x}}(\gamma,\varphi)) \,\mathrm{d}\gamma \,\mathrm{d}\varphi, \tag{4.4 C}$$

where

$$\boldsymbol{H}_P(\gamma,\varphi) = 3\hat{\boldsymbol{r}}(\gamma,\varphi)\hat{\boldsymbol{r}}^{\mathsf{T}}(\gamma,\varphi) - \mathbf{I} =$$

$$= \begin{bmatrix} 3\cos^2\gamma \sin^2\varphi - 1 & 3\cos\gamma \sin\gamma \sin^2\varphi & 3\cos\gamma \cos\varphi \sin\varphi \\ 3\cos\gamma \sin\gamma \sin^2\varphi & 3\sin^2\gamma \sin^2\varphi - 1 & 3\sin\gamma \cos\varphi \sin\varphi \\ 3\cos\gamma \cos\varphi \sin\varphi & 3\sin\gamma \cos\varphi \sin\varphi & 3\cos^2\varphi - 1 \end{bmatrix}.$$

4.2.2 Sensing Device

As a device to sense the environment and get a reliable gradient estimation, we have to consider now a sphere on which we have to dispose a set of sensors in a suitable way. We can suppose that the device is solidly connected to the vehicle, and that the centre of mass of the vehicle $\boldsymbol{x}$ is at

a small distance from the centre of the sphere $\boldsymbol{x}^{\mathrm{c}}$; however, for the sake of simplicity, we will assume that the two centres coincide, and that the gradient is estimated in the correct point.

For the computation of the integrals, we consider a suitable approximation with a discrete sum of a finite number of measurements. Differently from the two-dimensional case, where there is a very natural way to dispose the sensors (at uniformly spaced angles, see figure 3.1A), in three dimensions it is not trivial to choose the disposition of the sensors. Many algorithms have been devised in the literature with the aim of finding the best partition for a spheric surface from different points of view; for a deeper study of this topic we refer to [43, 64]. We choose here a simple division, that aims at maintaining a simple computation while trying to keep the sensors as equispaced as possible.

Given a total number of sensors N, we want to position them along circular stripes ("parallels") with equal angular width ζ, in a way that gives us a mesh of the sphere surface with almost regular quadrilateral elements, each having a side length approximatively equal to $b = \zeta r$. This results in an approximate width of $\tilde{\zeta} = 2\sqrt{\frac{\pi}{N}}$, and in $N_{\mathrm{p}} = \left[\frac{\pi}{\tilde{\zeta}}\right]$ parallels centered at latitudes

$$\varphi_i = (i - 0.5)\zeta, \quad i = 1, 2, \ldots, N_{\mathrm{p}},$$

where the square brackets indicate rounding to nearest integer and where $\zeta = \frac{\pi}{N_{\mathrm{p}}}$ is the correction of $\tilde{\zeta}$ such that the distance between two consecutive parallels is correctly estimated. Along each parallel we place a number N_i of sensors which decreases with the distance from the equator, so as to avoid an accumulation of sensors close to the poles, since the same angular distance would result in smaller distances; thus, each sensor has an azimuthal position of

$$\gamma_{i,j} = j\Delta\gamma_i = j\frac{2\pi}{N_i},$$

where N_i is chosen such that $N_i = \left[\frac{2\pi \sin\varphi_i}{\zeta}\right]$. As shown in figure 4.1 for two different values of ζ (specifically, for $N = 6$ and $N = 64$), each sensor

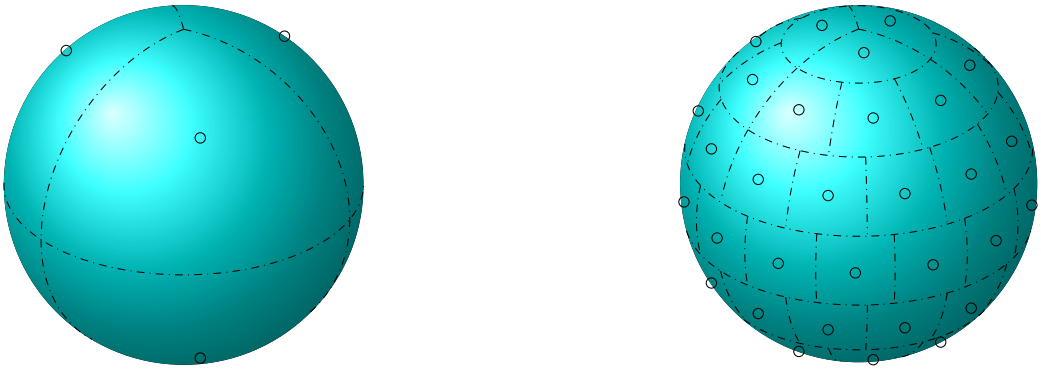

(a) $N = 6$ sensors (that corresponds to $\zeta = 90°$).

(b) $N = 64$ sensors (that corresponds to $\zeta \approx 25.7°$).

Figure 4.1. Sensor placement on the spheric device.

occupies the center of an element at a position

$$\boldsymbol{x}_{i,j} = \boldsymbol{x}^{\mathbf{c}} + \boldsymbol{r}_{i,j} = \boldsymbol{x}^{\mathbf{c}} + r \begin{bmatrix} \cos\gamma_{i,j} \sin\varphi_i \\ \sin\gamma_{i,j} \sin\varphi_i \\ \cos\varphi_i \end{bmatrix}.$$

We note that, using such an algorithm, N cannot take all possible values, due to the approximation made to have an integer number of parallels, together with trying to have equispaced sensors; this happens because our algorithm is conceived to dispose in an automatic and simple way a generic high number of sensors, but different strategies can be devised for a specific number of sensors at hand. Clearly, the sensors should be enough to guarantee a good gradient estimation; considering a bi-dimensional scenario, a correct estimation for a field with elliptical level sets can be proven by following a similar reasoning to the Lyapunov analysis used in [55, theorems 1 and 2], showing that the condition $\nabla f(\boldsymbol{x}) \cdot \widehat{\nabla f}(\boldsymbol{x}) = \frac{2}{Nr} \nabla f(\boldsymbol{x}) \cdot \sum_{i=1}^{N} \hat{\boldsymbol{r}}_i \hat{f}_i(\boldsymbol{x}) \geq 0$ (corresponding to the opposite of the derivative of the Lyapunov function in the cited reference) holds for $N \geq 3$.

4.2.3 Derivative Approximation

For such a choice for the position of the sensors it is now possible to compute the approximate values for (4.4): denoting the measurement of sensor (i, j) with

$$\hat{f}_{i,j}\big(\boldsymbol{x}(t), t\big) = f\big(\boldsymbol{x}_{i,j}(t)\big) + e_{i,j}^{(f)}(t),$$

where $e_{i,j}^{(f)}$ is the measurement error affecting sensor (i, j) at time t, we have that

$$\hat{f}(\boldsymbol{x}(t), t) \approx \frac{1}{4\pi} \sum_{i=1}^{N_\mathrm{p}} \zeta \sin\varphi_i \sum_{j=1}^{N_i} \Delta\gamma_i \hat{f}_{i,j}(\boldsymbol{x}(t), t).$$

Then, we note that, according to the initial choice of having equilateral elements, $\Delta\gamma_i \sin\varphi_i = \zeta$ (up to a small rounding error); by applying the same reasoning to (4.4 B) and (4.4 C), we can finally propose the following approximate formulæ:

$$\hat{f}\big(\boldsymbol{x}(t), t\big) = \frac{\zeta}{4N_\mathrm{p}} \sum_{i=1}^{N_\mathrm{p}} \sum_{j=1}^{N_i} \hat{f}_{i,j}\big(\boldsymbol{x}(t), t\big)$$

$$\widehat{\nabla f}\big(\boldsymbol{x}(t), t\big) = \frac{3\zeta}{4N_\mathrm{p} r} \sum_{i=1}^{N_\mathrm{p}} \sum_{j=1}^{N_i} \hat{\boldsymbol{r}}_{i,j} \hat{f}_{i,j}\big(\boldsymbol{x}(t), t\big)$$

$$\hat{\boldsymbol{H}}\big(\boldsymbol{x}(t), t\big) = \frac{5\zeta}{4N_\mathrm{p} r^2} \sum_{i=1}^{N_\mathrm{p}} \sum_{j=1}^{N_i} (3\hat{\boldsymbol{r}}_{i,j} \hat{\boldsymbol{r}}_{i,j}^{\mathsf{T}} - \mathbf{I}) \hat{f}_{i,j}\big(\boldsymbol{x}(t), t\big).$$

4.3 Convergence Analysis

In the next statements we study the convergence of our algorithm. We consider the problem solved, and speak about *convergence*, if either the vehicle touches the border of the source, or approaches it for $t \to \infty$, as stated in the following definition; in the first case, we consider our problem of interest for $t \leq t_\mathrm{s}$ and concluded at t_s, since handling the vehicle's behaviour in the neighbourhood of the source, once it has been

reached, is application-specific (*e.g.*, the search vehicle might need to avoid crashing on the source).

Definition 4.1 (Convergence to the source). Let the source's location be a point $\boldsymbol{x}_\mathrm{s} \in D_\mathrm{s}$, with

$$D_\mathrm{s}\colon f(\boldsymbol{x}) = f_\mathrm{s} = \max_{\boldsymbol{x}\in\bar{D}} f(\boldsymbol{x}), \quad \forall \boldsymbol{x} \in \partial D_\mathrm{s}.$$

A trajectory $\boldsymbol{x}(t)$ is said to be convergent to the source if either one of the following is true:

$$\exists t_\mathrm{s} < \infty \text{ such that } \boldsymbol{x}(t_\mathrm{s}) \in \partial D_\mathrm{s} \tag{4.5 A}$$

$$\lim_{t\to\infty} \operatorname{dist}(\boldsymbol{x}(t), \partial D_\mathrm{s}) = 0. \qquad \bullet \tag{4.5 B}$$

We will show now a trigonometric property that we will need later, and then we prove the convergence of our source-localisation control law.

Lemma 4.1. Given two vectors $\boldsymbol{b}_1, \boldsymbol{b}_2 \in \mathbb{R}^3$, expressed in spherical coordinates by the pair of angles (γ_1, φ_1) and (γ_2, φ_2), such that

$$|\gamma_2 - \gamma_1| \leq \bar{\gamma} < \frac{\pi}{2} \qquad\qquad |\varphi_2 - \varphi_1| \leq \bar{\varphi} < \frac{\pi}{2}, \tag{4.6}$$

then

$$\boldsymbol{b}_1 \cdot \boldsymbol{b}_2 \geq \|\boldsymbol{b}_1\|\|\boldsymbol{b}_2\| \cos(\bar{\gamma} + \bar{\varphi}).$$

Proof. Taking the unit vectors for simplicity, computing the dot product we get

$$\hat{\boldsymbol{b}}_1 \cdot \hat{\boldsymbol{b}}_2 = \cos(\gamma_2 - \gamma_1) \sin\varphi_1 \sin\varphi_2 + \cos\varphi_1 \cos\varphi_2.$$

Let us start by considering the case $\cos\varphi_1 \cos\varphi_2 \geq 0$. Thus, $\cos\varphi_1 \cos\varphi_2 \geq \cos\varphi_1 \cos\varphi_2 \cos(\gamma_2 - \gamma_1)$, that implies

$$\hat{\boldsymbol{b}}_1 \cdot \hat{\boldsymbol{b}}_2 \geq \cos(\gamma_2 - \gamma_1) \cos(\varphi_2 - \varphi_1) \geq \cos\bar{\gamma} \cos\bar{\varphi} \geq \cos(\bar{\gamma} + \bar{\varphi}).$$

Consider now the case $\cos\varphi_1 \cos\varphi_2 < 0$. Thanks to (4.6), this implies $\sin\varphi_1 \sin\varphi_2 > 0$, and hence

$$\sin\varphi_1 \sin\varphi_2 \cos(\gamma_2 - \gamma_1) \geq \sin\varphi_1 \sin\varphi_2 \cos\bar{\gamma};$$

also, since $\cos\bar{\gamma} + \sin\bar{\gamma} \geq 1$, we have

$$\cos\varphi_1 \cos\varphi_2 \geq \cos\varphi_1 \cos\varphi_2(\cos\bar{\gamma} + \sin\bar{\gamma}).$$

Thus,

$$\begin{aligned}\hat{\boldsymbol{b}}_1 \cdot \hat{\boldsymbol{b}}_2 &\geq \cos(\gamma_2 - \gamma_1) \sin\varphi_1 \sin\varphi_2 + (\cos\bar{\gamma} + \sin\bar{\gamma}) \cos\varphi_1 \cos\varphi_2 \geq \\ &\geq \cos\bar{\gamma} \sin\varphi_1 \sin\varphi_2 + (\cos\bar{\gamma} + \sin\bar{\gamma}) \cos\varphi_1 \cos\varphi_2 \geq \\ &\geq \cos\bar{\gamma} \cos(\varphi_1 - \varphi_2) + \sin\bar{\gamma} \cos\varphi_1 \cos\varphi_2.\end{aligned}$$

Finally, noting that

$$\begin{aligned}\cos\varphi_1 \cos\varphi_2 &= \cos\varphi_1 \cos\big(\varphi_1 + (\varphi_2 - \varphi_1)\big) = \\ &= \cos^2\varphi_1 \cos(\varphi_2 - \varphi_1) - \cos\varphi_1 \sin\varphi_1 \sin(\varphi_2 - \varphi_1) \geq \\ &\geq -\cos\varphi_1 \sin\varphi_1 \sin(\varphi_2 - \varphi_1) \geq -\sin(\varphi_2 - \varphi_1) \geq -\sin\bar{\varphi},\end{aligned}$$

we can write $\hat{\boldsymbol{b}}_1 \cdot \hat{\boldsymbol{b}}_2 \geq \cos\bar{\gamma}\cos\bar{\varphi} - \sin\bar{\gamma}\sin\bar{\varphi} = \cos(\bar{\gamma} + \bar{\varphi})$. ✓

Proposition 4.1 (Global convergence of the source-localisation algorithm). Let $D = \mathbb{R}^3 \setminus \bar{D}_\mathrm{s}$, and let f be a function harmonic in D, continuous on $\bar{D}$, and with compact sub-level sets $D_g = \{\, \boldsymbol{x} \in \bar{D} \colon f(\boldsymbol{x}) \leq g \,\}$. Consider the system (4.1) under the control law (4.2), where the references are given by the headings of $\nabla f(\boldsymbol{x}(t))$. Then, the system converges to the source in the sense of definition 4.1.

Proof. We prove that if condition (4.5 A) of definition 4.1 is false, then condition (4.5 B) holds.

Let us first define the heading error as

$$\boldsymbol{e}\big(\boldsymbol{x}(t),t\big) = \begin{bmatrix} \theta_1^{\mathrm{r}}(\boldsymbol{x}(t)) - \theta_1(t) \\ \theta_2^{\mathrm{r}}(\boldsymbol{x}(t)) - \theta_2(t) \end{bmatrix},$$

and notice that $\dot{\boldsymbol{e}}\big(\boldsymbol{x}(t),t\big) = -k\boldsymbol{e}\big(\boldsymbol{x}(t),t\big)$, which implies that

$$\lim_{t\to\infty} \boldsymbol{e}(\boldsymbol{x}(t),t) = \mathbf{0}.$$

In particular, there exists a time $\bar{t}$ such that $|e_1\big(\boldsymbol{x}(t),t\big)| \leq \bar{e}_1$ and $|e_2\big(\boldsymbol{x}(t),t\big)| \leq \bar{e}_2$, with $\bar{e}_1 + \bar{e}_2 < \frac{\pi}{2}$, for all $t \geq \bar{t}$.

Consider now the Lyapunov-like function

$$V(\boldsymbol{x}(t)) = f_{\mathrm{s}} - f(\boldsymbol{x}(t)) \geq 0,$$

which is continuous on $\bar{D}$, and where $V = 0 \iff \boldsymbol{x} \in \partial D_{\mathrm{s}}$. Its time derivative along trajectories is given by

$$\dot{V}(\boldsymbol{x}(t)) = -\nabla f(\boldsymbol{x}(t)) \cdot \dot{\boldsymbol{x}}(t),$$

with $\dot{\boldsymbol{x}}(t)$ given by equation (4.1); using lemma 4.1 we can write

$$\dot{V}(\boldsymbol{x}(t)) \leq -\|\nabla f(\boldsymbol{x}(t))\| v \cos(\bar{e}_1 + \bar{e}_2) < 0 \ \forall t \geq \bar{t}. \tag{4.7}$$

If condition (4.5 A) is false, then $\dot{V}(\boldsymbol{x}(t)) < 0 \ \forall t \in [\bar{t}, \infty]$, which means that V is strictly decreasing and there exists $\lim_{t\to\infty} V(\boldsymbol{x}(t)) = h \geq 0$. We prove that $h = 0$.

Let us suppose, by contradiction, that $h > 0$. Then, $V(\boldsymbol{x}(t)) \geq h$ for all $t \geq \bar{t}$. Since $\dot{V}$ is continuous and negative on the compact set $\big\{\, \boldsymbol{x} \in \bar{D} \colon V(\boldsymbol{x}(t)) \leq V(\boldsymbol{x}(\bar{t})) \,\big\} \cap \big\{\, \boldsymbol{x} \in \bar{D} \colon V(\boldsymbol{x}(t)) \geq h \,\big\}$, it attains a negative maximum $-m_1$. Thus,

$$V(\boldsymbol{x}(t)) = V(\boldsymbol{x}(\bar{t})) + \int_{\bar{t}}^{t} \dot{V}(\boldsymbol{x}(\tau))\,\mathrm{d}\tau \leq V(\boldsymbol{x}(t)) - m_1(t - \bar{t}),$$

which implies that $\lim_{t\to\infty} V(\boldsymbol{x}(t)) = -\infty$, that is a contradiction since

$V(\boldsymbol{x}(t)) \geq 0$ for all t.

Having proved that

$$\lim_{t\to\infty} V(\boldsymbol{x}(t)) = 0, \tag{4.8}$$

we want to conclude that $\operatorname{dist}(\boldsymbol{x}(t), \partial D) \to 0$ as well. Let us suppose, by contradiction, that there exists $l > 0$ such that, for all t, there exists $\tilde{t} > t$ such that $\operatorname{dist}\big(\boldsymbol{x}(\tilde{t}), \partial D\big) \geq l$. Hence,

$$\boldsymbol{x}(\tilde{t}) \in \{\, \boldsymbol{x}(t) \colon V(\boldsymbol{x}(t)) \leq V(\boldsymbol{x}(\bar{t})) \,\} \cap \{\, \boldsymbol{x}(t) \colon \operatorname{dist}\big(\boldsymbol{x}(t), \partial D\big) \geq l \,\},$$

which is a compact set, so that V has a minimum $m_2 > 0$ on this set. This implies that $V(\boldsymbol{x}(\tilde{t})) \geq m_2$, thus $\exists\, m_2 > 0 \colon \forall t\ \exists\, \tilde{t} > t \colon V(\boldsymbol{x}(\tilde{t})) \geq m_2$, which contradicts (4.8). ✓

The result of proposition 4.1 holds also if θ_1^{r} and θ_2^{r} are perturbed estimations of the gradient angles, *i.e.*,

$$\begin{aligned}
\theta_1^{\mathrm{r}}\big(\boldsymbol{x}(t), t\big) &= \theta_1^{(\nabla f)}\big(\boldsymbol{x}(t)\big) + e_{\theta_1}(t) \\
\theta_2^{\mathrm{r}}\big(\boldsymbol{x}(t), t\big) &= \theta_2^{(\nabla f)}\big(\boldsymbol{x}(t)\big) + e_{\theta_2}(t),
\end{aligned}$$

with e_{θ_1} and e_{θ_1} being the uncertainties, continuous on $\bar{D}$ and differentiable in D, and such that $|e_{\theta_1}(t)| + |e_{\theta_1}(t)| \leq \tilde{e} < \frac{\pi}{2}$. In this case, equation (4.7) in proposition 4.1 becomes

$$\dot{V}(\boldsymbol{x}(t)) = -\nabla f(\boldsymbol{x}(t)) \cdot \dot{\boldsymbol{x}}(t) \leq -\|\nabla f(\boldsymbol{x}(t))\| v \cos(\bar{e}_1 + \bar{e}_2 + \tilde{e}) \leq 0$$

for all $t > \hat{t}$ such that $\bar{e}_1 + \bar{e}_2 < \frac{\pi}{2} - \tilde{e}$. This guarantees that $V(\boldsymbol{x}(t))$ will be decreasing, and thus that $\boldsymbol{x}(t) \to D_{\mathrm{s}}$.

4.4 Simulation Results

The proposed algorithm has been simulated on a scenario given by the diffusion of an isotropic source emitting at a constant rate in an unbounded domain (unperturbed by borders), a simplified model of a pollutant

leakage underwater in a wide sea or ocean, in which a sensing device is seeking a source whose signal decays away from the source according to the expression given in example 2.3

$$f(\boldsymbol{x}) = \frac{a}{\|\boldsymbol{x} - \boldsymbol{x}_{\mathrm{s}}\|_2},$$

where $\boldsymbol{x}_{\mathrm{s}}$ is the position of the source, and a is a coefficient whose choice influences the amplitude of the signal.

The vehicle, which has no knowledge about $f(\boldsymbol{x})$, has a constant velocity $v = 0.1\,\mathrm{m/s}$, and the control parameter is set as $k = 0.95$; its initial orientation is chosen as $\theta_1(0) = \arctan\frac{x_2(0)}{x_1(0)}$ and $\theta_2(0) = \arccos\frac{x_3(0)}{\|\boldsymbol{x}(0)\|}$, and the initial angular velocities are set as $\dot{\theta}_1(0) = \dot{\theta}_2(0) = 0$. The amplitude of the signal function is chosen to be $a = 25$.

4.4.1 Sensitivity to the Sensing Parameters

To study the impact of the number of sensors on the convergence of the vehicle to the source, we simulated the same scenario for up to 100 sensors, *i.e.*, for $N \in \{\, 6, 12, 20, 32, 46, 64, 82 \,\}$. Each vehicle has a unit radius, and the source is set at the origin. We run a Monte Carlo simulation with 100 different initial positions for each value of N, and compute the mean of the average velocity and of the maximum errors on the yaw and pitch angles, defined as

$$\begin{aligned}
\bar{v}_i(N) &= \frac{\|\boldsymbol{x}_i(0)\| - r}{t_i^{\mathrm{s}}(N)} \\
J_i^{\mathrm{y}}(N) &= \max_t \left| \theta_1^{(\nabla f)}\big(\boldsymbol{x}_i(N,t)\big) - \theta_1^{\mathrm{r}}\big(\boldsymbol{x}_i(N,t)\big) \right| \\
J_i^{\mathrm{p}}(N) &= \max_t \left| \theta_2^{(\nabla f)}\big(\boldsymbol{x}_i(N,t)\big) - \theta_2^{\mathrm{r}}\big(\boldsymbol{x}_i(N,t)\big) \right|
\end{aligned} \tag{4.9}$$

where $t_i^{\mathrm{s}}(N)$ is the time to reach the source, starting from initial position i and with N sensors.

The results are summarised in table 4.1. For $N = 6$ there is no convergence, while for the other configurations, the largest error on the estimated

N	E[$\bar{v}$] [m/s]	E[J_1] [°]	E[J_2] [°]
6	–	–	–
12	0.0290	0.1479	3.0034
20	0.0845	0.0700	2.6763
32	0.0977	0.0279	2.6372
46	0.0990	0.0202	2.6018
64	0.0992	0.0077	2.6096
82	0.0993	0.0049	2.5895

Table 4.1. Mean values of the parameters (4.9) for a varying number of sensors N.

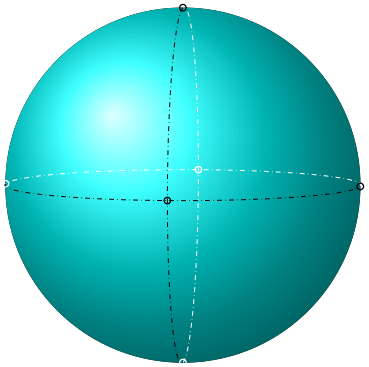

Figure 4.2. 6-sensor configuration that provides convergence.

direction is of about 3°, even for $N = 12$. Figure 4.3 A shows an example of the trajectories, for the same starting point and three different values of N. We note that with 6 sensors the algorithm fails because of the specific way in which they are automatically placed. An *ad hoc* configuration for $N = 6$, that provides convergence, can be obtained by placing two sensors in correspondence of the elevation angles $\varphi = 0$ and $\varphi = \pi$, and four of them equispaced on the great circle of elevation $\varphi = \frac{\pi}{2}$ (figure 4.2).

Figure 4.3 B depicts the trajectories for a varying length of the radius r of the ball on which the sensors are placed, and a fixed value of $N = 46$; we kept the same values as before for the other parameters. As we can see, the trajectory approaches the ideal oneas the radius is not too small. Indeed, while formulæ (4.4) are exact regardless of the radius value, when we approximate it with a finite sum a bigger radius is useful to attenuate

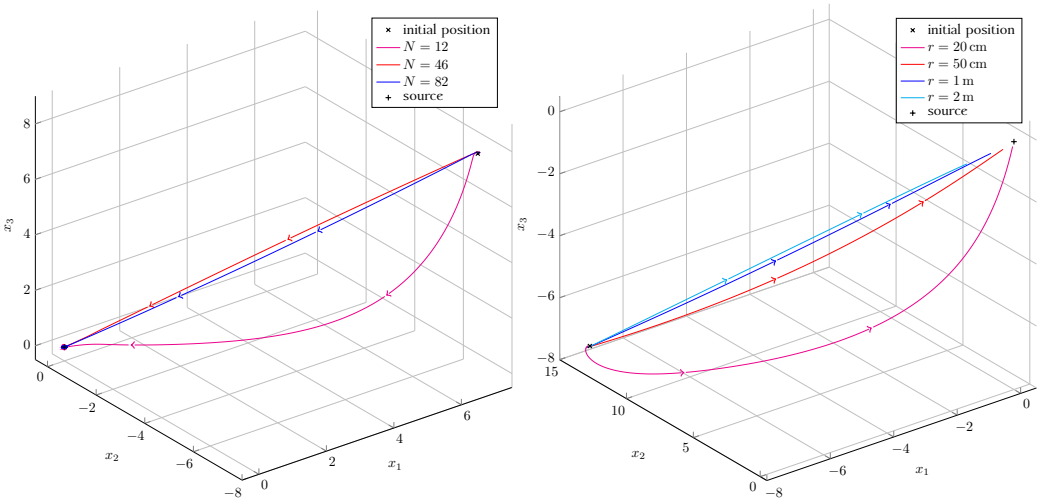

(A) Varying N **(B)** Varying r

Figure 4.3. Trajectories of the 3D source-seeking vehicle for different numbers of sensors and radius length.

the effect of quantisation (and possibly of measurement noise).

4.4.2 Noise Influence

We consider now the case where each sensor gives a measurement of the emitted signal corrupted by noise. We fix the values of N and r to $N = 46$ and $r = 1\,\mathrm{m}$, and run a Monte Carlo simulation with sensors affected by a white Gaussian noise of increasing standard deviation σ. For each value of σ, we run 100 simulations; the simulation was considered to be failed if time got over 10 times the minimum time to reach the source $t^* = \|\boldsymbol{x}(0)\|/v$, and the process stopped when all the trials, for a given σ, failed. The result is summarised in table 4.2, while in figure 4.4 A we can see the trajectories resulting from a simulation with $N = 12$, and some different values of σ. We can see that, except for the oscillation due to the noise, the vehicles settle on a small ball around the source.

The results of a simulation for $N = 46$, $\sigma = 0.75$ and different values of r are shown in figure 4.4 B.

Table 4.2. Percentage of successful simulations, and mean of the normalised time to reach the source, for increasing noise.

σ	%	$\mathrm{E}\left[\frac{t}{t^*}\right]$
0.5	100	2.0469
1	100	3.6287
1.5	100	5.3099
2	91	6.3628
2.5	73	7.2335
3	47	7.7745
3.5	35	8.1791
4	21	8.5948
4.5	9	8.2819
5	10	8.5013
5.5	7	8.7760
6	4	9.1355

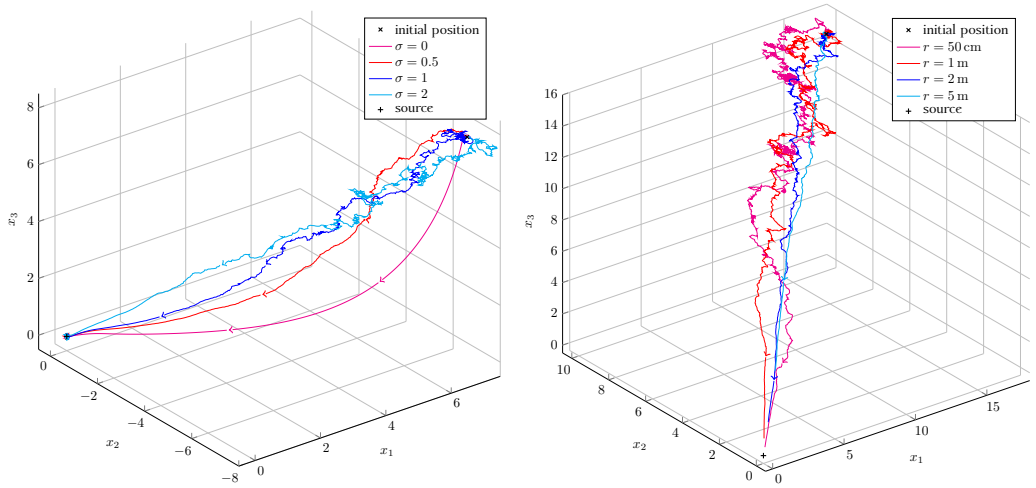

(A) $N = 12$, varying σ **(B)** $N = 46$, $\sigma = 0.75$, varying r

Figure 4.4. Trajectories of the source-seeking vehicle with measurements corrupted by noise.

4.4.3 Non-harmonic Diffusion Process

The proposed method relies on the assumptions of an isotropic source, and of the harmonicity of the solution of the PDE associated to the diffusion process. Experimental results (see section 3.5) suggest that the method may have a good behavior also when the properties are not fulfilled, if the gradient error introduced by the non-harmonicity is bounded, as shown in proposition 4.1. Moreover, a class of functions for which the gradient estimated with the Poisson formula is exact, although such functions are in general non-harmonic, is represented by quadratic functions, as shown in section 2.3.

We propose here a simulation example when these assumptions are not satisfied. The vehicle is equipped with 20 sensors disposed on a sphere with unit radius, and is seeking a source whose signal decays according to the non-harmonic function

$$\tilde{f}(\boldsymbol{x}) = 25\mathrm{e}^{-\frac{2.2x_1^2+0.7x_2^2+1.3x_3^2}{10}}.$$

Figure 4.5 depicts the result of such simulation, for the same control parameters as before.

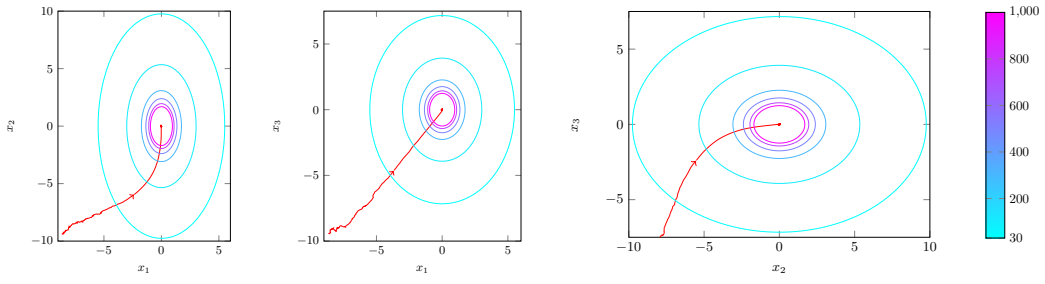

Figure 4.5. Trajectory for a vehicle seeking a source whose diffusion is described by the non-harmonic function $\tilde{f}(\boldsymbol{x})$.

Chapter 5

Distributed Source-Seeking

We present here a distributed control law to steer a group of autonomous communicating sensors towards the source of a diffusion process, based on the same hypotheses defined in chapter 2. We assume to have a set of autonomous sensors (each sensor is autonomously moving, and they are not organised in a fixed fashion as in the previous chapters), and suppose that each sensor is able to measure, in addition to the diffusing quantity of interest, only the relative bearing angle with respect to its neighbour, but has no absolute position information, and does not know any relative distance; the sensors can communicate to each other, and the graph describing the communication links has a time-invariant ring-topology.

Using multiple sensors makes it possible to have a fast gradient estimation also in wide environments (*e.g.*, under the sea), and in cases in which the function describing the diffusion process is low changing in space, where a single sensor may have to travel long distances before having a good gradient estimation. Our approach is based on a twofold control law, which is able to bring and keep the set of sensors on a circular equispaced formation, and to steer the circular formation towards the source via a gradient-ascent technique; the effectiveness of the proposed algorithm is both theoretically proven and supported by simulation results.

The framework is close to the one of previous works as [12, 55], but

our contribution differs as we suppose to have no full position information (which may be unavailable in various operating environments such as underwater or indoor vehicles, or in applications where inertial navigation systems are too expensive or not sufficiently accurate). We tackled the same problem, proposing a different solution, in our preliminary work [28]; in that paper, though, our twofold objective was expressed in an antagonistic control law, which, together with a formation control algorithm without any theoretical stability guarantee (taken from [57]), resulted in a weaker convergence, with no theoretical proof.

5.1 Problem Formulation

We consider a group of N autonomous communicating sensors moving in a region $D \subset \mathbb{R}^2$ where a diffusion process is taking place. The dynamics of each sensor is described by the nonlinear unicycle model

$$\begin{aligned} \dot{\boldsymbol{x}}_i(t) &= v_i(t) \begin{bmatrix} \cos\theta_i(t) \\ \sin\theta_i(t) \end{bmatrix} \\ \begin{bmatrix} v_i(t) \\ \dot{\theta}_i(t) \end{bmatrix} &= \boldsymbol{u}_i(t); \end{aligned} \tag{5.1}$$

where $\boldsymbol{x}_i$ represents the position of the sensor in the plane, and $\theta_i(t)$ is its heading angle. This is a particular non-holonomic model extensively considered in the robotics and automatic control, used to represent dynamics of ground vehicles, AUVs and unmanned aerial vehicles (UAVs). In such model the state of each agent is denoted by the vector $\big(x_1(t),\ \ x_2(t),\ \ \theta(t)\big)$, and $\big(v(t),\ \ \dot{\theta}(t)\big)$ are the control inputs.

The sensors, which can take point-wise measurements of the emitted quantity, have no position information, but know the value of N and are able to measure the bearing angle with respect to their following neighbour, *i.e.*, the angle between the orientation of an agent and the vector

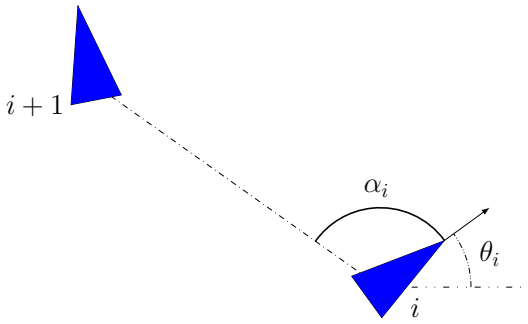

Figure 5.1. Graphical representation of the relative bearing angle α_i.

from itself to its neighbour, as explained in figure 5.1, defined by

$$\alpha_i(t) = \arg\left(\boldsymbol{x}_{i+1}(t) - \boldsymbol{x}_i(t)\right) - \theta_i(t). \tag{5.2}$$

Finally, we consider a communication network having a time-invariant directed ring topology, *i.e.*, where sensor i communicates with sensor $i+1$ (always intended $\bmod N$) irrespective of the sensor positions and of time.

Our control objective is twofold: on the one hand, we want to steer all the sensors in the approximated gradient direction, so that the gradient ascent search brings them to the source; on the other hand, the approximated gradient will be computed with a formula which requires measurements along a circle, and for this reason we aim at bringing the sensors to a circular formation, translating the gradient-ascent objective with respect to the formation's centroid.

5.2 Feedback Design

Steering the autonomous sensors towards the source can be obtained by performing a gradient-ascent method based on the formulæ derived in chapter 2, with the gradient being estimated by exchanging the point-wise measurements of the quantity of interest. Hence, we need to develop an algorithm which is able to both steer the sensors towards the gradient's direction, and bring them on a circular formation, such that the gradient itself is correctly estimated.

We introduce a control law assuming that each sensor i is able to compute the difference

$$\tilde{\theta}_i(t) = \theta^{\mathrm{r}}(t) - \theta_i(t),$$

where θ^{r} is a common reference (we will discuss in section 5.3 how to obtain it). Let $v_{\mathrm{c}} > 0$ and $v_{\mathrm{r}} > v_{\mathrm{c}}$, with $\tilde{v} = \frac{v_{\mathrm{c}}}{v_{\mathrm{r}}}$, be fixed parameters; we propose the following control law:

$$\boldsymbol{u}_i(t) = \begin{bmatrix} v_i(t) \\ \dot{\theta}_i(t) \end{bmatrix} = \begin{bmatrix} v_{\mathrm{c}} \cos\tilde{\theta}_i(t) + \sqrt{v_{\mathrm{r}}^2 - v_{\mathrm{c}}^2 \sin^2\tilde{\theta}_i(t)} \\ b_i(t)\dot{\theta}^{\mathrm{r}}(t) + \big(1 - b_i(t)\big)\omega_i(t) \end{bmatrix}, \tag{5.3 A}$$

where

$$b_i(t) = \frac{v_{\mathrm{c}}}{v_i(t)} \cos\tilde{\theta}_i(t) \tag{5.3 B}$$

$$\omega_i(t) = k\Big(\alpha_i(t) + \arcsin\big(\tilde{v}\sin\tilde{\theta}_i(t)\big)\Big), \tag{5.3 C}$$

$k > 0$ is a positive constant gain, and α_i is defined as in (5.2). We note that such control law only involves local variables, as it is function of only the measured relative bearing angle and the angle $\tilde{\theta}_i$, which is an angle difference and therefore independent of the coordinate system.

We will show that this control law brings the autonomous sensors to settle on an equispaced circular formation around a centre moving along the reference direction. As a first step, the following proposition shows an equivalent description of the closed-loop system described by the dynamics (5.1) and the control (5.3).

Proposition 5.1. The closed-loop system given by dynamics (5.1), under the control law (5.3 A–5.3 B), is equivalent to the system

$$\dot{\boldsymbol{x}}_i(t) = v_{\mathrm{c}} \begin{bmatrix} \cos\theta^{\mathrm{r}}(t) \\ \sin\theta^{\mathrm{r}}(t) \end{bmatrix} + v_{\mathrm{r}} \begin{bmatrix} \cos\eta_i(t) \\ \sin\eta_i(t) \end{bmatrix} \tag{5.4 A}$$

$$\dot{\eta}_i(t) = \omega_i(t). \tag{5.4 B}$$

Proof. To show such equality, let us start from system (5.4 A). We have that

$$\|\dot{\boldsymbol{x}}_i(t)\| = \left\| v_{\mathrm{c}} \begin{bmatrix} \cos\theta^{\mathrm{r}}(t) \\ \sin\theta^{\mathrm{r}}(t) \end{bmatrix} + v_{\mathrm{r}} \begin{bmatrix} \cos\eta_i(t) \\ \sin\eta_i(t) \end{bmatrix} \right\| \tag{5.5 A}$$

$$\arg\dot{\boldsymbol{x}}_i(t) = \arctan \frac{v_{\mathrm{c}}\sin\theta^{\mathrm{r}}(t) + v_{\mathrm{r}}\sin\eta_i(t)}{v_{\mathrm{c}}\cos\theta^{\mathrm{r}}(t) + v_{\mathrm{r}}\cos\eta_i(t)}; \tag{5.5 B}$$

moreover,

$$\begin{aligned} \cos\eta_i(t) &= \frac{\|\dot{\boldsymbol{x}}_i(t)\|\cos\big(\arg\dot{\boldsymbol{x}}_i(t)\big) - v_{\mathrm{c}}\cos\theta^{\mathrm{r}}(t)}{v_{\mathrm{r}}} \\ \sin\eta_i(t) &= \frac{\|\dot{\boldsymbol{x}}_i(t)\|\sin\big(\arg\dot{\boldsymbol{x}}_i(t)\big) - v_{\mathrm{c}}\sin\theta^{\mathrm{r}}(t)}{v_{\mathrm{r}}}. \end{aligned} \tag{5.5 C}$$

Developing (5.5 A) we get

$$\begin{aligned} \|\dot{\boldsymbol{x}}_i(t)\|^2 &= \big(v_{\mathrm{c}}\cos\theta^{\mathrm{r}}(t) + v_{\mathrm{r}}\cos\eta_i(t)\big)^2 + \big(v_{\mathrm{c}}\sin\theta^{\mathrm{r}}(t) + v_{\mathrm{r}}\sin\eta_i(t)\big)^2 = \\ &= v_{\mathrm{c}}^2 + 2v_{\mathrm{c}}v_{\mathrm{r}}\big(\cos\theta^{\mathrm{r}}(t)\cos\eta_i(t) + \sin\theta^{\mathrm{r}}(t)\sin\eta_i(t)\big) + v_{\mathrm{r}}^2; \end{aligned} \tag{5.6}$$

using (5.5 C) we get

$$\cos\theta^{\mathrm{r}}(t)\cos\eta_i(t) + \sin\theta^{\mathrm{r}}(t)\sin\eta_i(t) =$$

$$= \frac{\cos\theta^{\mathrm{r}}(t)\Big(\|\dot{\boldsymbol{x}}_i(t)\|\cos\big(\arg\dot{\boldsymbol{x}}_i(t)\big) - v_{\mathrm{c}}\cos\theta^{\mathrm{r}}(t)\Big)}{v_{\mathrm{r}}} +$$

$$+ \frac{\sin\theta^{\mathrm{r}}(t)\Big(\|\dot{\boldsymbol{x}}_i(t)\|\sin\big(\arg\dot{\boldsymbol{x}}_i(t)\big) - v_{\mathrm{c}}\sin\theta^{\mathrm{r}}(t)\Big)}{v_{\mathrm{r}}} =$$

$$= \frac{\|\dot{\boldsymbol{x}}_i(t)\|\Big(\cos\theta^{\mathrm{r}}(t)\cos\big(\arg\dot{\boldsymbol{x}}_i(t)\big) + \sin\theta^{\mathrm{r}}(t)\sin\big(\arg\dot{\boldsymbol{x}}_i(t)\big)\Big) - v_{\mathrm{c}}}{v_{\mathrm{r}}} =$$

$$= \frac{\|\dot{\boldsymbol{x}}_i(t)\| \cos\left(\theta^{\mathrm{r}}(t) - \arg \dot{\boldsymbol{x}}_i(t)\right) - v_{\mathrm{c}}}{v_{\mathrm{r}}} \tag{5.7}$$

and, by substituting it back into (5.6), it yields the quadratic equation

$$\|\dot{\boldsymbol{x}}_i(t)\|^2 = 2v_{\mathrm{c}} \cos\left(\theta^{\mathrm{r}}(t) - \arg \dot{\boldsymbol{x}}_i(t)\right) \|\dot{\boldsymbol{x}}_i(t)\| - v_{\mathrm{c}}^2 + v_{\mathrm{r}}^2. \tag{5.8}$$

Solving and taking the positive root, we obtain the expression for the velocity:

$$\begin{aligned}
&\|\dot{\boldsymbol{x}}_i(t)\| = \\
&= v_{\mathrm{c}} \cos\left(\theta^{\mathrm{r}}(t) - \arg \dot{\boldsymbol{x}}_i(t)\right) + \sqrt{\left(\cos^2\left(\theta^{\mathrm{r}}(t) - \arg \dot{\boldsymbol{x}}_i(t)\right) - 1\right) v_{\mathrm{c}}^2 + v_{\mathrm{r}}^2} = \\
&= v_{\mathrm{c}} \cos\left(\theta^{\mathrm{r}}(t) - \arg \dot{\boldsymbol{x}}_i(t)\right) + \sqrt{v_{\mathrm{r}}^2 - v_{\mathrm{c}}^2 \sin^2\left(\theta^{\mathrm{r}}(t) - \arg \dot{\boldsymbol{x}}_i(t)\right)}.
\end{aligned} \tag{5.9}$$

Computing the time derivative of (5.5 b) we get

$$\begin{aligned}
&\frac{\mathrm{d} \arg \dot{\boldsymbol{x}}_i(t)}{\mathrm{d}t} = \\
&= \frac{\left(v_{\mathrm{c}} \dot{\theta}^{\mathrm{r}}(t) \cos\theta^{\mathrm{r}}(t) + v_{\mathrm{r}} \dot{\eta}_i(t) \cos\eta_i(t)\right)\left(v_{\mathrm{c}} \cos\theta^{\mathrm{r}}(t) + v_{\mathrm{r}} \cos\eta_i(t)\right)}{\left(v_{\mathrm{c}} \sin\theta^{\mathrm{r}}(t) + v_{\mathrm{r}} \sin\eta_i(t)\right)^2 + \left(v_{\mathrm{c}} \cos\theta^{\mathrm{r}}(t) + v_{\mathrm{r}} \cos\eta_i(t)\right)^2} + \\
&\quad + \frac{\left(v_{\mathrm{c}} \sin\theta^{\mathrm{r}}(t) + v_{\mathrm{r}} \sin\eta_i(t)\right)\left(v_{\mathrm{c}} \dot{\theta}^{\mathrm{r}}(t) \sin\theta^{\mathrm{r}}(t) + v_{\mathrm{r}} \dot{\eta}_i(t) \sin\eta_i(t)\right)}{\left(v_{\mathrm{c}} \sin\theta^{\mathrm{r}}(t) + v_{\mathrm{r}} \sin\eta_i(t)\right)^2 + \left(v_{\mathrm{c}} \cos\theta^{\mathrm{r}}(t) + v_{\mathrm{r}} \cos\eta_i(t)\right)^2} = \\
&\qquad = \frac{v_{\mathrm{c}} \dot{\theta}^{\mathrm{r}}(t) \left[v_{\mathrm{c}} + v_{\mathrm{r}}\left(\cos\theta^{\mathrm{r}}(t) \cos\eta_i(t) + \sin\theta^{\mathrm{r}}(t) \sin\eta_i(t)\right)\right]}{v_{\mathrm{c}}^2 + 2v_{\mathrm{c}}v_{\mathrm{r}}\left(\cos\theta^{\mathrm{r}}(t) \cos\eta_i(t) + \sin\theta^{\mathrm{r}}(t) \sin\eta_i(t)\right) + v_{\mathrm{r}}^2} + \\
&\qquad\quad + \frac{v_{\mathrm{r}} \dot{\eta}_i \left[v_{\mathrm{r}} + v_{\mathrm{c}}\left(\cos\theta^{\mathrm{r}}(t) \cos\eta_i(t) + \sin\theta^{\mathrm{r}}(t) \sin\eta_i(t)\right)\right]}{v_{\mathrm{c}}^2 + 2v_{\mathrm{c}}v_{\mathrm{r}}\left(\cos\theta^{\mathrm{r}}(t) \cos\eta_i(t) + \sin\theta^{\mathrm{r}}(t) \sin\eta_i(t)\right) + v_{\mathrm{r}}^2};
\end{aligned}$$

substituting again (5.7):

$$\frac{\mathrm{d} \arg \dot{\boldsymbol{x}}_i(t)}{\mathrm{d}t} = \frac{v_{\mathrm{c}} \|\dot{\boldsymbol{x}}_i(t)\| \cos\left(\theta^{\mathrm{r}}(t) - \arg \dot{\boldsymbol{x}}_i(t)\right) \dot{\theta}^{\mathrm{r}}(t)}{2v_{\mathrm{c}} \|\dot{\boldsymbol{x}}_i(t)\| \cos\left(\theta^{\mathrm{r}}(t) - \arg \dot{\boldsymbol{x}}_i(t)\right) - v_{\mathrm{c}}^2 + v_{\mathrm{r}}^2} +$$

$$+\frac{\left(v_{\mathrm{r}}^2+v_{\mathrm{c}}\|\dot{\boldsymbol{x}}_i(t)\|\cos\left(\theta^{\mathrm{r}}(t)-\arg\dot{\boldsymbol{x}}_i(t)\right)-v_{\mathrm{c}}^2\right)\dot{\eta}_i(t)}{2v_{\mathrm{c}}\|\dot{\boldsymbol{x}}_i(t)\|\cos\left(\theta^{\mathrm{r}}(t)-\arg\dot{\boldsymbol{x}}_i(t)\right)-v_{\mathrm{c}}^2+v_{\mathrm{r}}^2}$$

and, finally, by (5.8),

$$\begin{aligned}\frac{\mathrm{d}\arg\dot{\boldsymbol{x}}_i(t)}{\mathrm{d}t}=&\frac{v_{\mathrm{c}}\|\dot{\boldsymbol{x}}_i(t)\|\cos\left(\theta^{\mathrm{r}}(t)-\arg\dot{\boldsymbol{x}}_i(t)\right)}{\|\dot{\boldsymbol{x}}_i(t)\|^2}\dot{\theta}^{\mathrm{r}}(t)+\\&+\frac{\left(\|\dot{\boldsymbol{x}}_i(t)\|^2-v_{\mathrm{c}}\|\dot{\boldsymbol{x}}_i(t)\|\cos\left(\theta^{\mathrm{r}}(t)-\arg\dot{\boldsymbol{x}}_i(t)\right)\right)}{\|\dot{\boldsymbol{x}}_i(t)\|^2}\dot{\eta}_i(t)=\\=&\frac{v_{\mathrm{c}}\cos\left(\theta^{\mathrm{r}}(t)-\arg\dot{\boldsymbol{x}}_i(t)\right)}{\|\dot{\boldsymbol{x}}_i(t)\|}\dot{\theta}^{\mathrm{r}}(t)+\left(1-\frac{v_{\mathrm{c}}\cos\left(\theta^{\mathrm{r}}(t)-\arg\dot{\boldsymbol{x}}_i(t)\right)}{\|\dot{\boldsymbol{x}}_i(t)\|}\right)\dot{\eta}_i(t).\end{aligned}\tag{5.10}$$

We can notice that (5.9) and (5.10) correspond to our choice of $\boldsymbol{u}_i$ in (5.3 A) for $v_i(t)=\|\dot{\boldsymbol{x}}_i(t)\|$ and $\theta_i(t)=\arg\dot{\boldsymbol{x}}_i(t)$, showing the equivalence between system (5.1, 5.3 A, 5.3 B) and system (5.4). ✓

We can see from this equivalence that the dynamics of each sensor is given by the superposition of a motion with speed v_{c} in the common direction $\theta^{\mathrm{r}}(t)$ and a motion with speed v_{r} and heading $\eta_i(t)$ such that $\dot{\eta}_i(t)=\omega_i(t)$. In particular, since the direction $\theta^{\mathrm{r}}(t)$ is common to each autonomous sensor, the motion with speed v_{c} results in a translation of the whole formation in such direction. We need to show that our law ensures that the sensors settle on a circular equispaced formation (thus allowing for a gradient estimation based on the Poisson integral formula), *i.e.*, that they asymptotically tend to a formation in which each sensor has position and velocity

$$\begin{aligned}\boldsymbol{x}_i(t)&=\boldsymbol{x}^{\mathrm{c}}(t)+r\begin{bmatrix}\cos\gamma_i(t)\\\sin\gamma_i(t)\end{bmatrix}\\\dot{\boldsymbol{x}}_i(t)&=v_{\mathrm{c}}\begin{bmatrix}\cos\theta^{\mathrm{r}}(t)\\\sin\theta^{\mathrm{r}}(t)\end{bmatrix}+v_{\mathrm{r}}\begin{bmatrix}\cos\eta_i(t)\\\sin\eta_i(t)\end{bmatrix},\end{aligned}$$

with $\gamma_i(t) = \gamma_0(t) + \frac{2\pi}{N} i$ and $\eta_i(t) = \gamma_i(t) + \frac{\pi}{2}$.

5.2.1 Convergence to the Formation

We show here how the control law (5.3) can bring the sensors on a desired formation. We start by recalling some results by Marshall *et al.* [45–47].

Let us consider a fleet of autonomous under-actuated vehicles described by the dynamics (5.1). By a suitable change of coordinates [45], each subsystem (5.1) can be described by the new state variables

$$d_i(t) = \|\boldsymbol{x}_{i+1}(t) - \boldsymbol{x}_i(t)\| \tag{5.11a}$$

$$\alpha_i(t) = \arg\left(\boldsymbol{x}_{i+1}(t) - \boldsymbol{x}_i(t)\right) - \theta_i(t) \tag{5.11b}$$

$$\beta_i(t) = \theta_i(t) - \theta_{i+1}(t) - \pi. \tag{5.11c}$$

With such state variables we lose any information about the absolute positioning of each vehicle; nonetheless, they are more suitable to describe the formation reached, as they define the position of each vehicle in terms of relative variables with respect to each other's neighbours, such as the relative distance d_i and the relative bearing angle α_i.

The authors propose the control law

$$\begin{aligned} v_i(t) &= \tilde{v}, \quad \forall i \\ \dot{\theta}_i(t) &= k\alpha_i(t), \end{aligned}$$

with $\tilde{v}, k > 0$ constant parameters, and show that the dynamics of each

subsystem in the state variables (5.11) becomes

$$\begin{aligned}\dot{d}_i(t) &= -\tilde{v}\Big(\cos\alpha_i(t) + \cos\big(\alpha_i(t)+\beta_i(t)\big)\Big)\\ \dot{\alpha}_i(t) &= \frac{\tilde{v}\Big(\sin\alpha_i(t) + \sin\big(\alpha_i(t)+\beta_i(t)\big)\Big)}{d_i(t)} - k\alpha_i(t)\\ \dot{\beta}_i(t) &= k\big(\alpha_i(t)-\alpha_{i+1}(t)\big).\end{aligned} \tag{5.12}$$

Their main result is to show that the equilibrium points of such dynamics correspond to the vehicles disposed as the vertices of an ordinary regular polygon, and thus being equispatially disposed on a circle (whose radius is given by $r = \frac{N\tilde{v}}{k\pi}$). We will briefly recall their result, and will show later on how it can be applied to our control law.

Proposition 5.2 ([46, theorem 5 and corollary 4]). Each system (5.12) has $2N-1$ equilibrium points, among which the two locally asymptotically stable described by

$$\bar{d}_i = \bar{d} = \frac{2\tilde{v}}{k\bar{\alpha}}\sin\bar{\alpha} \tag{5.13 A}$$

$$\bar{\alpha}_i = \bar{\alpha} = \pm\frac{\pi}{N} \tag{5.13 B}$$

$$\bar{\beta}_i = \bar{\beta} = \pi - 2\bar{\alpha}. \qquad \bullet \tag{5.13 C}$$

Since our control law is different than the one proposed in the aforementioned result, also our closed-loop dynamics will differ from (5.12), and the result of proposition 5.2 does not apply directly. Nevertheless, defining the variables

$$\tilde{\alpha}_i(t) = \arg\big(\boldsymbol{x}_{i+1}(t) - \boldsymbol{x}_i(t)\big) - \eta_i(t) \tag{5.14 A}$$

$$\tilde{\beta}_i(t) = \eta_i(t) - \eta_{i+1}(t) - \pi, \tag{5.14 B}$$

with $\eta_i(t)$ as in (5.5 C), we show that in the new state $\big(d_i(t),\ \tilde{\alpha}_i(t),\ \tilde{\beta}_i(t)\big)$ also our closed-loop systems converge to the same equilibrium points (5.13).

Proposition 5.3. For the system (5.4), with $\omega_i(t)$ as in (5.3 c), the dynamics in the state variables (5.11 a, 5.14) is

$$\begin{aligned}
\dot{d}_i(t) &= -v_{\mathrm{r}}\Big(\cos\tilde{\alpha}_i(t) + \cos\big(\tilde{\alpha}_i(t)+\tilde{\beta}_i(t)\big)\Big) \\
\dot{\tilde{\alpha}}_i(t) &= \frac{v_{\mathrm{r}}\Big(\sin\tilde{\alpha}_i(t) + \sin\big(\tilde{\alpha}_i(t)+\tilde{\beta}_i(t)\big)\Big)}{d_i(t)} - k\tilde{\alpha}_i(t) \\
\dot{\tilde{\beta}}_i(t) &= k\big(\tilde{\alpha}_i(t) - \tilde{\alpha}_{i+1}(t)\big).
\end{aligned} \tag{5.15}$$

Proof. We start by showing that, if ω_i is defined as in (5.3 c), the control law (5.4 b) is equivalent to the control law $\dot{\eta}_i(t) = k\tilde{\alpha}_i(t)$. Let

$$\delta_i(t) = \theta_i(t) - \eta_i(t)$$

be the difference between the heading $\theta_i(t)$ and the direction $\eta_i(t)$; from (5.5 c) we have that

$$\sin\delta_i(t) = \sin\theta_i(t)\cos\eta_i(t) - \cos\theta_i(t)\sin\eta_i(t);$$

using (5.5 c),

$$\begin{aligned}
\sin\delta_i(t) =& \sin\theta_i(t)\frac{v_i(t)\cos\theta_i(t) - v_{\mathrm{c}}\cos\theta^{\mathrm{r}}(t)}{v_{\mathrm{r}}} + \\
&- \cos\theta_i(t)\frac{v_i(t)\sin\theta_i(t) - v_{\mathrm{c}}\sin\theta^{\mathrm{r}}(t)}{v_{\mathrm{r}}} = \\
&= \frac{v_{\mathrm{c}}}{v_{\mathrm{r}}}\big(\cos\theta_i(t)\sin\theta^{\mathrm{r}}(t) - \sin\theta_i(t)\cos\theta^{\mathrm{r}}(t)\big) = \tilde{v}\sin\tilde{\theta}_i(t),
\end{aligned} \tag{5.16}$$

from which it follows that $\delta_i(t) = \arcsin\big(\tilde{v}\sin\tilde{\theta}_i(t)\big)$. Therefore, we have that

$$\dot{\eta}_i(t) = k\big(\alpha_i(t)+\delta_i(t)\big) = k\big(\arg(\boldsymbol{x}_{i+1}(t)-\boldsymbol{x}_i(t)\big) - \theta_i(t) + \theta_i(t) - \eta_i(t)\big) = k\tilde{\alpha}_i(t).$$

Now we have

$$\dot{\boldsymbol{x}}_i(t) = v_{\mathrm{c}} \begin{bmatrix} \cos\theta^{\mathrm{r}}(t) \\ \sin\theta^{\mathrm{r}}(t) \end{bmatrix} + v_{\mathrm{r}} \begin{bmatrix} \cos\eta_i(t) \\ \sin\eta_i(t) \end{bmatrix}$$

$$\dot{\eta}_i(t) = k\tilde{\alpha}_i(t).$$

Similarly to [47], we can now find the dynamics in the new state variables. Starting with d_i, we have

$$\dot{d}_i(t) = \frac{\mathrm{d}\|\boldsymbol{x}_{i+1}(t) - \boldsymbol{x}_i(t)\|}{\mathrm{d}t} = \frac{\left(x_{i+1}^{(1)}(t) - x_i^{(1)}(t)\right)\left(\dot{x}_{i+1}^{(1)}(t) - \dot{x}_i^{(1)}(t)\right)}{\|\boldsymbol{x}_{i+1}(t) - \boldsymbol{x}_i(t)\|} + \\ + \frac{\left(x_{i+1}^{(2)}(t) - x_i^{(2)}(t)\right)\left(\dot{x}_{i+1}^{(2)}(t) - \dot{x}_i^{(2)}(t)\right)}{\|\boldsymbol{x}_{i+1}(t) - \boldsymbol{x}_i(t)\|};$$

noting that

$$\boldsymbol{x}_{i+1}(t) = \boldsymbol{x}_i(t) + d_i(t) \begin{bmatrix} \cos\left(\tilde{\alpha}_i(t) + \eta_i(t)\right) \\ \sin\left(\tilde{\alpha}_i(t) + \eta_i(t)\right) \end{bmatrix}$$

we get the following equalities:

$$\boldsymbol{x}_{i+1}(t) - \boldsymbol{x}_i(t) = d_i(t) \begin{bmatrix} \cos\left(\tilde{\alpha}_i(t) + \eta_i(t)\right) \\ \sin\left(\tilde{\alpha}_i(t) + \eta_i(t)\right) \end{bmatrix}$$

$$\dot{\boldsymbol{x}}_{i+1}(t) - \dot{\boldsymbol{x}}_i(t) = v_{\mathrm{r}} \left(\begin{bmatrix} \cos\eta_{i+1}(t) \\ \sin\eta_{i+1}(t) \end{bmatrix} - \begin{bmatrix} \cos\eta_i(t) \\ \sin\eta_i(t) \end{bmatrix} \right)$$

and hence we can compute

$$\begin{aligned} \dot{d}_i(t) =& v_{\mathrm{r}} \left[\cos\left(\tilde{\alpha}_i(t) + \eta_i(t)\right)\left(\cos\eta_{i+1}(t) - \cos\eta_i(t)\right) + \right. \\ &\left. + \sin\left(\tilde{\alpha}_i(t) + \eta_i(t)\right)\left(\sin\eta_{i+1}(t) - \sin\eta_i(t)\right)\right] = \\ =& v_{\mathrm{r}} \left[\cos\left(\tilde{\alpha}_i(t) + \eta_i(t)\right)\cos\eta_{i+1}(t) + \right. \\ &- \left(\cos\tilde{\alpha}_i(t)\cos\eta_i(t) - \sin\tilde{\alpha}_i(t)\sin\eta_i(t)\right)\cos\eta_i(t) + \\ &\left. - \left(\cos\tilde{\alpha}_i(t)\cos\eta_i(t) - \sin\tilde{\alpha}_i(t)\sin\eta_i(t)\right)\cos\eta_i(t) + \right. \end{aligned}$$

$$
\begin{aligned}
&+ \sin\big(\tilde{\alpha}_i(t) + \eta_i(t)\big) \sin\eta_{i+1}(t) + \\
&- \big(\cos\tilde{\alpha}_i(t) \sin\eta_i(t) + \sin\tilde{\alpha}_i(t) \cos\eta_i(t)\big) \sin\eta_i(t)\big] = \\
&= v_{\mathrm{r}}\Big(\cos\big(\tilde{\alpha}_i(t) + \eta_i(t) - \eta_{i+1}(t)\big) - \cos\tilde{\alpha}_i(t)\Big) = \\
&= v_{\mathrm{r}}\Big(\cos\big(\tilde{\alpha}_i(t) + \tilde{\beta}_i(t) + \pi\big) - \cos\tilde{\alpha}_i(t)\Big) = \\
&= -v_{\mathrm{r}}\Big(\cos\big(\tilde{\alpha}_i(t) + \tilde{\beta}_i(t)\big) + \cos\tilde{\alpha}_i(t)\Big). \qquad (5.17\,\text{A})
\end{aligned}
$$

Similarly, computing $\dot{\tilde{\alpha}}_i(t)$ yields

$$
\begin{aligned}
\dot{\tilde{\alpha}}_i(t) &= \frac{\mathrm{d}}{\mathrm{d}t}\left(\arctan\frac{x_{i+1}^{(2)}(t) - x_i^{(2)}(t)}{x_{i+1}^{(1)}(t) - x_i^{(1)}(t)} - \eta_i(t)\right) = \\
&= \frac{\big(x_{i+1}^{(1)}(t) - x_i^{(1)}(t)\big)\big(\dot{x}_{i+1}^{(2)}(t) - \dot{x}_i^{(2)}(t)\big)}{\big(x_{i+1}^{(1)}(t) - x_i^{(1)}(t)\big)^2 + \big(x_{i+1}^{(2)}(t) - x_i^{(2)}(t)\big)^2} + \\
&\quad - \frac{\big(x_{i+1}^{(2)}(t) - x_i^{(2)}(t)\big)\big(\dot{x}_{i+1}^{(1)}(t) - \dot{x}_i^{(1)}(t)\big)}{\big(x_{i+1}^{(1)}(t) - x_i^{(1)}(t)\big)^2 + \big(x_{i+1}^{(2)}(t) - x_i^{(2)}(t)\big)^2} - k\tilde{\alpha}_i(t) = \\
&= \frac{v_{\mathrm{r}}}{d_i(t)}\big[\cos\big(\tilde{\alpha}_i(t) + \eta_i(t)\big)\big(\sin\eta_{i+1}(t) - \sin\eta_i(t)\big) + \\
&\quad - \sin\big(\tilde{\alpha}_i(t) + \eta_i(t)\big)\big(\cos\eta_{i+1}(t) - \cos\eta_i(t)\big)\big] - k\tilde{\alpha}_i(t) = \\
&= \frac{v_{\mathrm{r}}}{d_i(t)}\Big(\sin\big(\tilde{\alpha}_i(t) + \tilde{\beta}_i(t)\big) + \sin\tilde{\alpha}_i(t)\Big) - k\tilde{\alpha}_i(t), \qquad (5.17\,\text{B})
\end{aligned}
$$

and the expression of $\dot{\tilde{\beta}}_i$ follows directly from its definition:

$$
\dot{\tilde{\beta}}_i(t) = \frac{\mathrm{d}\big(\eta_i(t) - \eta_{i+1}(t) - \pi\big)}{\mathrm{d}t} = k\big(\tilde{\alpha}_i(t) - \tilde{\alpha}_{i+1}(t)\big), \qquad (5.17\,\text{C})
$$

showing the equivalence between dynamics (5.15) and (5.17). ✓

Corollary 5.1. Each system (5.11 A, 5.14) has $2N - 1$ equilibrium points,

among which the two locally asymptotically stable described by

$$\begin{aligned} \bar{d}_i =& \bar{d} = \frac{2v_{\mathrm{r}}}{k\bar{\alpha}} \sin\bar{\alpha} \\ \bar{\tilde{\alpha}}_i =& \bar{\alpha} = \pm\frac{\pi}{N} \\ \bar{\tilde{\beta}}_i =& \bar{\beta} = \pi - 2\bar{\alpha}. \end{aligned} \tag{5.18}$$

Proof. By proposition 5.3 the system $\big(d_i(t),\ \tilde{\alpha}_i(t),\ \tilde{\beta}_i(t)\big)$ has dynamics equivalent to (5.12). Hence, applying proposition 5.2 yields to the equilibria (5.18). ✓

Proposition 5.4. At the equilibria (5.18), the relative positions $\boldsymbol{x}_{i+1}(t) - \boldsymbol{x}_i(t)$ draw an ordinary regular polygon.

Proof. The internal angle between sensors $\big(\boldsymbol{x}_{i-1}(t), \boldsymbol{x}_i(t), \boldsymbol{x}_{i+1}(t)\big)$ (see figure 5.2) can be expressed as

$$\begin{aligned} \kappa_i(t) &= \arg\big(\boldsymbol{x}_i(t) - \boldsymbol{x}_{i-1}(t)\big) + \pi - \arg\big(\boldsymbol{x}_{i+1}(t) - \boldsymbol{x}_i(t)\big) = \\ &= \tilde{\alpha}_{i-1}(t) + \eta_{i-1}(t) + \pi - \tilde{\alpha}_i(t) - \eta_i(t) = \tilde{\alpha}_{i-1}(t) - \tilde{\beta}_{i-1}(t) - \tilde{\alpha}_i(t); \end{aligned}$$

at the equilibrium, $\tilde{\alpha}_i = \bar{\alpha}$ and $\tilde{\beta}_i = \bar{\beta}$, $\forall i$, which yields

$$\kappa_i(t) = -\bar{\beta}, \quad \forall i.$$

Therefore, the relative positions at the equilibrium are both equilateral (because $\bar{d}_i = \bar{d}\ \forall i$) and equiangular, and thus represent an ordinary regular polygon. ✓

5.2.2 Gradient-Ascent Motion of the Formation Centroid

Our goal is to use the sensors' measurements to compute a discrete approximation of the gradient formula (2.7), and then to perform a gradient ascent using the (approximated) gradient's argument as reference θ^{r} for the

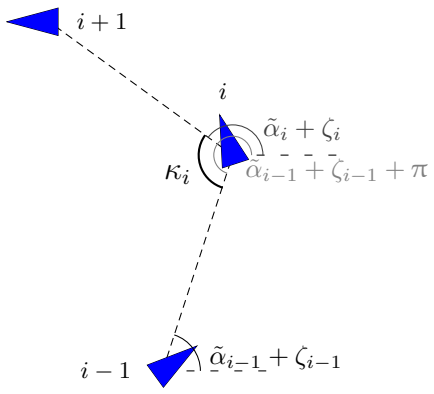

Figure 5.2. Representation of the internal angle κ_i between consecutive sensors.

control law (5.3). The computation of the gradient approximation will be discussed in section 5.3, while here we discuss how the control law (5.3) indeed drives the centroid of the formation to follow the reference direction and perform gradient ascent towards the source.

Proposition 5.5. If the initial conditions of the agents are such that the corresponding system (5.15) is in the attractive basin of one of the two locally asymptotically stable equilibria (5.18), then

$$\arg \dot{\boldsymbol{x}}^{\mathbf{c}}(t) - \theta^{\mathrm{r}}(t) \to 0.$$

Proof. The dynamics of the formation centroid (*i.e.*, the barycentre of positions $\boldsymbol{x}_i$) is given by

$$\dot{\boldsymbol{x}}^{\mathbf{c}}(t) = \frac{1}{N}\sum_{i=1}^{N} \dot{\boldsymbol{x}}_i(t) = v_{\mathrm{c}} \begin{bmatrix} \cos\theta^{\mathrm{r}}(t) \\ \sin\theta^{\mathrm{r}}(t) \end{bmatrix} + \frac{v_{\mathrm{r}}}{N}\sum_{i=1}^{N} \begin{bmatrix} \cos\eta_i(t) \\ \sin\eta_i(t) \end{bmatrix}.$$

We can easily show that, at any of the equilibria (5.18),

$$\dot{\boldsymbol{x}}^{\mathbf{c}}(t) = v_{\mathrm{c}} \begin{bmatrix} \cos\theta^{\mathrm{r}}(t) \\ \sin\theta^{\mathrm{r}}(t) \end{bmatrix}.$$

Indeed, the result of proposition 5.4 implies that, at equilibria (5.18), they occupy positions $\boldsymbol{x}_i(t)$ which are equispaced along a circle; in particular,

equation (5.14 B) implies that $\eta_{i+1}(t) - \eta_i(t) = -\tilde{\beta}_i(t) - \pi \ \forall i$ which, at the equilibria (5.18), gives $\eta_i(t) = \eta_0(t) + \frac{2\pi}{N} i$ for all i, and hence

$$\sum_{i=1}^{N} \begin{bmatrix} \cos \eta_i(t) \\ \sin \eta_i(t) \end{bmatrix} = 0.$$

Then, the asymptotic stability of such equilibria ensures the asymptotic convergence of

$$\dot{\boldsymbol{x}}^{\mathbf{c}}(t) - v_{\mathrm{c}} \begin{bmatrix} \cos \theta^{\mathrm{r}}(t) \\ \sin \theta^{\mathrm{r}}(t) \end{bmatrix} = \frac{v_{\mathrm{r}}}{N} \sum_{i=1}^{N} \begin{bmatrix} \cos \eta_i(t) \\ \sin \eta_i(t) \end{bmatrix}$$

to zero, and hence also ensures that $\arg \dot{\boldsymbol{x}}^{\mathbf{c}}(t) - \theta^{\mathrm{r}}(t) \to 0$. ✓

This proposition means that, if the agents have initial positions such that they will converge to circular formation, then, while this convergence happens, their barycentre will follow with increasing precision the reference direction. In particular, given any $\varepsilon > 0$, there exists a time $\bar{t}$ such that, for all $t \geq \bar{t}$, $|\arg \dot{\boldsymbol{x}}^{\mathbf{c}}(t) - \theta^{\mathrm{r}}(t)| \leq \varepsilon$; moreover, velocities of individual agents and of the formation centroid are all bounded by $v_{\mathrm{c}} + v_{\mathrm{r}}$, so that there is no risk of divergence in finite time.

In next section we will discuss how to compute a reference $\theta^{\mathrm{r}}(t)$ which is an approximation of the argument of the gradient $\nabla f(\boldsymbol{x}^{\mathbf{c}}(t))$ (at least for sufficiently large times, when the circular formation is nearly attained). Now, let us assume that such a reference is given, and that for all $t \geq \tilde{t}$, $|\theta^{\mathrm{r}}(t) - \arg \nabla f(\boldsymbol{x}^{\mathbf{c}}(t))| \leq \tilde{\varepsilon}$ for some time $\tilde{t}$ and for some error bound $\tilde{\varepsilon} < \frac{\pi}{2}$. Then, we can clearly find ε such that $\varepsilon + \tilde{\varepsilon} < \frac{\pi}{2}$, and a time $\bar{t} \geq \tilde{t}$ such that, for all $t \geq \bar{t}$,

$$|\arg \dot{\boldsymbol{x}}^{\mathbf{c}}(t) - \arg \nabla f(\boldsymbol{x}^{\mathbf{c}}(t))| \leq \varepsilon + \tilde{\varepsilon} < \frac{\pi}{2}.$$

This inequality ensures that the formation centroid performs gradient ascent, namely that $f(\boldsymbol{x}^{\mathbf{c}}(t))$ increases along trajectories; indeed, the derivative of f along trajectories of $\boldsymbol{x}^{\mathbf{c}}(t)$ is given by $\nabla f(\boldsymbol{x}^{\mathbf{c}}(t)) \cdot \dot{\boldsymbol{x}}^{\mathbf{c}}(t)$, which is positive since $|\arg \dot{\boldsymbol{x}}^{\mathbf{c}}(t) - \arg \nabla f(\boldsymbol{x}^{\mathbf{c}}(t))| < \frac{\pi}{2}$.

Gradient ascent is usually applied to convex functions, while here we

are considering harmonic functions, which might not be convex. However, the local maximum principle (proposition 2.2) ensures that f does not have any local maximum inside D: hence, the gradient ascent search is ensured not to get trapped in any local maximum, except possibly on the outer boundary $\partial\tilde{D}$; some simple rule can be introduced that allows to distinguish the external boundary from the source, *e.g.*, some rough bound on the source intensity.

5.3 Distributed Implementation

We discuss here how to implement the control law proposed previously. We make the restrictive assumption to not have any absolute position information available (and very little relative): this means that the sensors neither know their absolute position, nor their relative one with respect to the formation centroid or to each other, and they do not know their absolute orientation θ_i either. They are only able to measure the pointwise value of the diffusing quantity at their position, *i.e.*, $f(\boldsymbol{x}_i(t))$, and the relative bearing angle with respect to their neighbour α_i; in addition, they know the common parameters v_c, v_r, k and their total number N.

To drive the sensors to the source location we make use of a control input which involves the difference $\tilde{\theta}_i(t)$ between the reference input $\theta^r(t)$ and the current heading of the sensor $\theta_i(t)$, and where we want the reference $\theta^r(t)$ to be the angle of the approximation, computed by each sensor i, of the gradient at the formation centroid. To obtain such an approximation we propose a discrete-time algorithm, involving an exchange of messages among the agents, which is run within every sampling time; the value of the gradient approximation $\boldsymbol{g}_i(t)$, and consequently of its argument, is then held constant until the next value is available. The algorithm is designed to use the information collected by each sensor and produce, in a distributed way, a discrete approximation of the integral formula (3.3 B), *i.e.*, to

compute the Riemann sum

$$\widehat{\nabla f}\big(\boldsymbol{x}^{\mathbf{c}}(t)\big) = \frac{2}{Nr^2}\sum_{i=1}^{N} f\big(\boldsymbol{x}_i(t)\big)\big(\boldsymbol{x}_i(t) - \boldsymbol{x}^{\mathbf{c}}(t)\big) \tag{5.19}$$

(which is equivalent to the (3.4 B)), and then obtain the difference $\tilde{\theta}_i(t) = \theta^{\mathrm{r}}(t) - \theta_i(t)$, where ideally $\theta^{\mathrm{r}}(t) = \arg\widehat{\nabla f}(\boldsymbol{x}^{\mathbf{c}}(t))$ (the difficulty lies in the fact that the vector $\boldsymbol{x}_i(t) - \boldsymbol{x}^{\mathbf{c}}(t)$ is not directly available, as we assumed not to have any position information); we propose the following technique.

During every time interval $(t,\ t + \Delta t)$, with Δt sufficiently long, each sensor i performs $h = 1, 2, \ldots, N-1$ iterations which involve an exchange of messages with its preceding and following neighbours: each sensor i receives the current value computed by its predecessors, rotates it of an angle $\frac{2\pi}{N}$, adds its own measurement $f(\boldsymbol{x}_i)$ and sends it to its successor.

In the sequel we will suppose for simplicity to be in the attractive region of the equilibrium with $\bar{\alpha} > 0$, *i.e.*, a counter-clockwise rotation (this assumption is justified by the local stability property of the equilibria, which justify also the choice of a time-invariant ring topology for the communication graph), hence, we will use a rotation angle of $\lambda = -\frac{2\pi}{N}$. Anyway, a general implementation would be to have a rotation angle depending on the current relative bearing angle measured, *i.e.*, $\lambda_i(t) = -\operatorname{sign}\big(\alpha_i(t)\big)\frac{2\pi}{N}$.

The argument of the vector obtained in this way is the ith reference, which is then used to compute the difference $\tilde{\theta}_i$ and then, together with the relative bearing angle α_i which each sensor i measure with respect to its follower, the new control $\boldsymbol{u}_i$. The details are shown in algorithm 5.1.

We are going to show, in the following proposition, the effectiveness of the proposed algorithm if the sensors are already at the equilibrium.

Proposition 5.6. If the N sensors described by the dynamics (5.15) are at the equilibrium (5.18) with $\bar{\alpha} > 0$, then $\tilde{\theta}_i$ computed with algorithm 5.1 corresponds to the difference

$$\tilde{\theta}_i(t) = \arg\widehat{\nabla f}(\boldsymbol{x}^{\mathbf{c}}(t)) - \theta_i(t).$$

Algorithm 5.1 Distributed source-seeking

$\boldsymbol{g}_i(0) = \begin{bmatrix} f(\boldsymbol{x}_i) \\ 0 \end{bmatrix}$ {initialisation}
for $h = 1, 2, \ldots, N-1$ **do**
  $\boldsymbol{g}_i(h) \leftarrow \boldsymbol{g}_{i-1}(h-1)$ {node i receives from $i-1$}
  $\boldsymbol{g}_i(h) \leftarrow \begin{bmatrix} \cos\lambda & \sin\lambda \\ -\sin\lambda & \cos\lambda \end{bmatrix} \boldsymbol{g}_i(h) + \begin{bmatrix} f(\boldsymbol{x}_i) \\ 0 \end{bmatrix}$ {update}
end for
$\theta_i^{\mathrm{r}} = \arg \boldsymbol{g}_i(N-1)$
$\delta_i = -\arctan \frac{v_{\mathrm{c}} \cos\theta_i^{\mathrm{r}}}{v_{\mathrm{r}} + v_{\mathrm{c}} \sin\theta_i^{\mathrm{r}}}$
$\tilde{\theta}_i = \theta_i^{\mathrm{r}} - \delta_i - \frac{\pi}{2}$

Proof. When the sensors are at the equilibrium (5.18) with $\bar{\alpha} > 0$, they are turning equispaced in circle around their centroid $\boldsymbol{x}^{\mathbf{c}}$, hence we have that

$$\eta_i(t) = \begin{cases} \arg\left(\boldsymbol{x}_i(t) - \boldsymbol{x}^{\mathbf{c}}(t)\right) + \frac{\pi}{2} \\ \eta_0(t) + \frac{2\pi}{N} i \end{cases}, \quad \forall i; \tag{5.20}$$

in particular, the second one implies that $\eta_j(t) = \eta_i(t) + \frac{2\pi}{N}(j-i)$ for all i, j. Using these properties, we can rewrite the argument of the Riemann sum in (5.19) as

$$\arg \widehat{\nabla f}(\boldsymbol{x}^{\mathbf{c}}(t)) = \arg \sum_{j=1}^{N} f\left(\boldsymbol{x}_j(t)\right) \begin{bmatrix} \cos\left(\eta_j(t) - \frac{\pi}{2}\right) \\ \sin\left(\eta_j(t) - \frac{\pi}{2}\right) \end{bmatrix} =$$

$$= \arg \sum_{j=1}^{N} f\left(\boldsymbol{x}_j(t)\right) \begin{bmatrix} \cos\left(\eta_i(t) + \frac{2\pi}{N}(j-i) - \frac{\pi}{2}\right) \\ \sin\left(\eta_i(t) + \frac{2\pi}{N}(j-i) - \frac{\pi}{2}\right) \end{bmatrix}, \quad \forall i.$$

Node i, at the end of the $N-1$ iterations in algorithm 5.1, has computed

$$\boldsymbol{g}_i(N-1) = \sum_{j=1}^{N} f\left(\boldsymbol{x}_j(t)\right) \begin{bmatrix} \cos\frac{2\pi}{N}(j-i) \\ \sin\frac{2\pi}{N}(j-i) \end{bmatrix},$$

so that

$$\theta_i^{\mathrm{r}}(t) = \arg \boldsymbol{g}_i(N-1) = \arg \widehat{\nabla f}(\boldsymbol{x}^{\mathbf{c}}(t)) - \eta_i(t) + \frac{\pi}{2}. \tag{5.21}$$

We want to show that the solution of system

$$\delta_i(t) = -\arctan \frac{v_{\mathrm{c}} \cos \theta_i^{\mathrm{r}}(t)}{v_{\mathrm{r}} + v_{\mathrm{c}} \sin \theta_i^{\mathrm{r}}(t)} \tag{5.22 A}$$

$$\tilde{\theta}_i(t) = \theta_i^{\mathrm{r}}(t) - \delta_i(t) - \frac{\pi}{2} \tag{5.22 B}$$

and the one of

$$\delta_i(t) = \theta_i(t) - \eta_i(t) \tag{5.23 A}$$

$$\tilde{\theta}_i(t) = \arg \widehat{\nabla f}(\boldsymbol{x}^{\mathbf{c}}(t)) - \theta_i(t) \tag{5.23 B}$$

coincide, thus showing that system (5.22) used in the algorithm correctly compute the quantities of interest defined by (5.23). We already know from equation (5.16) that $\delta_i(t) = \theta_i(t) - \eta_i(t)$ implies $\sin \delta_i(t) = \tilde{v} \sin \tilde{\theta}_i(t)$; thus, combining it with equation (5.21), system (5.23) becomes

$$\begin{aligned} \sin \delta_i(t) &= \tilde{v} \sin \tilde{\theta}_i(t) \\ \tilde{\theta}_i(t) &= \theta_i^{\mathrm{r}}(t) + \eta_i(t) - \frac{\pi}{2} - \theta_i(t) = \theta_i^{\mathrm{r}}(t) - \delta_i(t) - \frac{\pi}{2}. \end{aligned}$$

Solving for $\sin \tilde{\theta}_i(t)$ we get

$$\sin \tilde{\theta}_i(t) = \begin{cases} \frac{\sin \delta_i(t)}{\tilde{v}} \\ -\cos \theta_i^{\mathrm{r}}(t) \cos \delta_i(t) - \sin \theta_i^{\mathrm{r}}(t) \sin \delta_i(t); \end{cases}$$

equating the solutions and multiplying by $\frac{\tilde{v}}{\cos \delta_i(t)}$ yields

$$\tan \delta_i(t) = -\frac{\tilde{v} \cos \theta_i^{\mathrm{r}}(t)}{1 + \tilde{v} \sin \theta_i^{\mathrm{r}}(t)},$$

and assuming that $\delta_i(t) \in \left[-\frac{\pi}{2}, \frac{\pi}{2}\right]$ and $\tilde{\theta}_i(t) \in [-\pi, \pi]$ we obtain

$$\delta_i(t) = -\arctan \frac{v_c \cos \theta_i^r(t)}{v_r + v_c \sin \theta_i^r(t)}. \qquad \checkmark$$

As one may notice, this algorithm gives the argument of the correct gradient approximation only when the sensors are in formation. Otherwise, not only θ_i^r is not ensured to be a good approximation of the gradient's argument, but it is not a common reference either, *i.e.*, $\tilde{\theta}_i(t) + \theta_i(t)$ is not the same for all i (while it should be equal to a common reference in order to apply proposition 5.1). Indeed, equation (5.20) holds only at the formation. This contradicts the assumption we made about the reference θ^r being the same for every sensors, which guarantees the convergence to the equilibria (5.18) and thus to a circular equispaced formation; nevertheless, we proposed this implementation for its simplicity, since it shows a good behaviour in simulations, as we will show in section 5.4. In the next subsection we will provide an alternative algorithm to ensure a common reference θ^r for each sensor i regardless their relative positions and orientations.

Alternative Implementation

We propose here an alternative algorithm which ensures that all the sensors have always a common reference. To do so, we need to design a sensor as the leader, say sensor $i = 1$. Moreover, we need the measure of the relative bearing angle with respect to the predecessor.; *i.e.*, in addition to the already defined angle α_i, we assume that each sensor i can also measure the angle

$$\alpha_i^-(t) = \arg\left(\boldsymbol{x}_{i-1}(t) - \boldsymbol{x}_i(t)\right) - \theta_i(t).$$

The idea is to perform, after a first phase as in algorithm 5.1, a second communication round enforcing $\tilde{\theta}_i(t) = \theta^r(t) - \theta_i(t)$ for every i, with $\theta^r(t) = \tilde{\theta}_1(t) + \theta_1(t)$.

Proposition 5.7. If each sensor i computes $\tilde{\theta}_i$ as in algorithm 5.2, then

Algorithm 5.2 Distributed source-seeking - enforced common reference

$\boldsymbol{g}_i(0) = \begin{bmatrix} f(\boldsymbol{x}_i) \\ 0 \end{bmatrix}$ {initialisation}
for $h = 1, 2, \ldots, N-1$ **do**
  $\boldsymbol{g}_i(h) \leftarrow \boldsymbol{g}_{i-1}(h-1)$ {node i receives from $i-1$}
  $\boldsymbol{g}_i(h) \leftarrow \begin{bmatrix} \cos\lambda & \sin\lambda \\ -\sin\lambda & \cos\lambda \end{bmatrix} \boldsymbol{g}_i(h) + \begin{bmatrix} f(\boldsymbol{x}_i) \\ 0 \end{bmatrix}$ {update}
end for
$\theta_1^{\mathrm{r}} = \arg \boldsymbol{g}_1(N-1)$ {only node 1}
$\delta = -\arctan \frac{v_{\mathrm{c}} \cos\theta_1^{\mathrm{r}}}{v_{\mathrm{r}} + v_{\mathrm{c}} \sin\theta_1^{\mathrm{r}}}$ {only node 1}
$\tilde{\theta}_1 = \theta_1^{\mathrm{r}} - \delta - \frac{\pi}{2}$ {only node 1}
for $i = 1, 2, \ldots, N-1$ **do**
  $\iota = \tilde{\theta}_i - \alpha_i - \frac{\pi}{2}$ {node i}
  node $i+1$ receives ι from i
  $\tilde{\theta}_{i+1} = \iota + \alpha_{i+1}^{-} - \frac{\pi}{2}$ {node $i+1$}
end for

$\tilde{\theta}_i(t) = \theta^{\mathrm{r}}(t) - \theta_i(t)\ \forall i$, where $\theta^{\mathrm{r}}(t) = \tilde{\theta}_1(t) + \theta_1(t)$, and $\tilde{\theta}_1$ is the same as in algorithm 5.1.

Proof. It is easy to see that, in algorithm 5.2, for all $i \neq 1$ $\tilde{\theta}_i$ is computed as $\tilde{\theta}_i = \tilde{\theta}_{i-1} + \mu_i$, where $\mu_i = \theta_{i-1} - \theta_i$:

$$\mu_i = \alpha_i^{-} - \alpha_{i-1} - \pi = \arg(\boldsymbol{x}_{i-1} - \boldsymbol{x}_i) - \theta_i - \arg(\boldsymbol{x}_i - \boldsymbol{x}_{i-1}) + \theta_{i-1} - \pi = \\ = \theta_{i-1} - \theta_i.$$

Therefore, $\tilde{\theta}_i = \tilde{\theta}_{i-1} + \theta_i - \theta_{i-1}$ and, recursively, $\tilde{\theta}_i = \tilde{\theta}_1 + \theta_1 - \theta_i$. ✓

5.4 Simulations

To validate our algorithm we consider the search of a heat source in a 2-dimensional space 20×12 m large; the borders are considered perfectly isolating, and we suppose to have an opening imposing an external temperature of $f_{\mathrm{ex}} = 5$ °C, and a circular heater of $f_{\mathrm{s}} = 50$ °C in the middle. Our scenario is thus described by the problem with mixed Dirichlet-Neumann

boundary conditions given in example 2.2.

We consider a set of $N = 5$ sensors with dynamics (5.1) and with the control law described in (5.3), starting from random initial positions and with random initial orientations, with velocities of $v_\mathrm{r} = 0.5$ and $v_\mathrm{c} = 0.1$ m/s; the values for the control constant is chosen such to have a formation radius of $r = 50\,\mathrm{cm}$, *i.e.*, $k = \frac{N v_\mathrm{r}}{\pi r} \approx 1.5915$.

Figure 5.3 shows the result of some simulations obtained with algorithm 5.1. We can see the trajectories of the sensors as well as the one of their centroids (in black); the white-bordered triangles represent the initial conditions of each sensor, while the black-bordered ones show their position and orientation when the formation reached the heater (the red circle in the middle). The sensors reach soon a circular configuration, and then keep moving towards the source following the gradient of the field. The trajectories of the formation's centroids are not exactly aligned with the gradient's argument because of the discrete (backward) approximation of the reference's time-derivative $\dot{\theta}^\mathrm{r}$. Figure 5.4 shows simulations for the same initial conditions, with both the temperature and the bearing angle measurements corrupted by white Gaussian noise of standard deviation $\sigma = 0.5$.

From the analysis of the simulation results we can remark also that, even if the theoretical convergence is local, the algorithm demonstrated to be effective also for random generated initial conditions; moreover, despite the theoretical request to have the same common reference for each sensor, there is no practical difference between the two algorithm: as we can see, the formation centroids follow the gradient (even with the deviation introduced by the discrete approximation and noise) even using the algorithm 5.1, which does not fulfill such assumption.

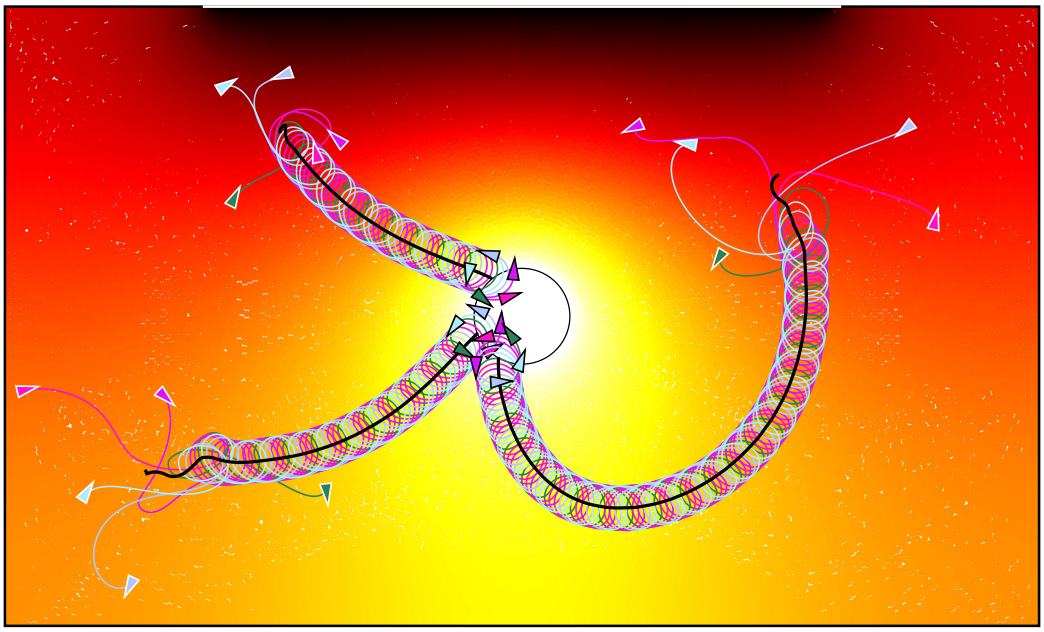

Figure 5.3. Simulation results for random initial conditions; the white-bordered triangles represent the initial conditions, the black-bordered ones the final conditions.

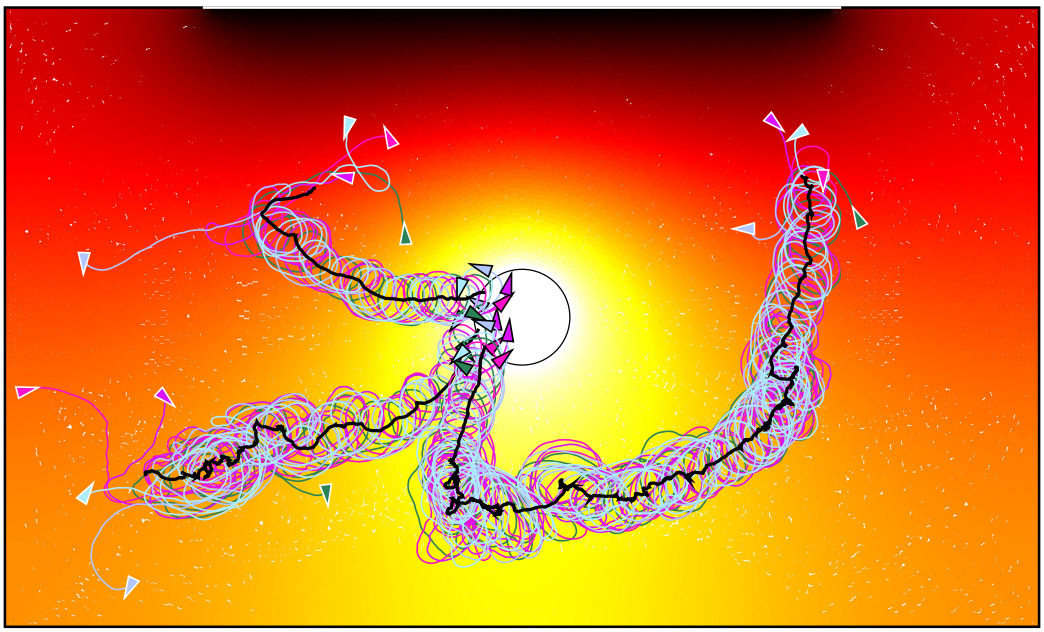

Figure 5.4. Simulation results for random initial conditions and noisy measurements; the white-bordered triangles represent the initial conditions, the black-bordered ones the final conditions.

Chapter 6

Conclusions

In this dissertation we have faced the problem of localising an emitting source by multiple moving sensors, able to take point-wise measurements of the emitted quantity, without position information.

By making some assumptions on the diffusion process, we develop a model which allows the source-seeking agents to compute a simple approximation of the gradient of the function describing the diffusion process, making it possible to perform a gradient ascent and find the source's location, which is considered to be the point where such function has its maximum.

6.1 Review of the Contributions

6.1.1 Formalisation of Previous Methods

We have provided a mathematical formalisation (chapter 2) of methods already used in the literature, *i.e.*, the approximation of the function's gradient by a weighted sum of some values of the function itself (see for example [12, 55]. While such method results to be effective in many practical case, as we have shown its validity has theoretical bases when certain assumption on the diffusion process are made. Moreover, this allowed for an easy extension of such method in n dimensions (*e.g.*, for tridimensional

source localisation), and not only for the computation of the gradient, but potentially of derivatives of any order.

6.1.2 Positionless Multi-Dimensional Source-Seeking

The theory developed has been applied to solve the problem of localising a source by single vehicles equpped with several sensors and without position information. After a demonstration of the applicability of the proposed solution in two dimensions (accompanied by practical tests with a prototype robot), we have used such solution to give a contribution on the source-seeking problem in 3 dimensions, formally proving the convergence to the source.

6.1.3 Positionless Distributed Source-Seeking

We have considered the problem where each source-seeking vehicle is a single sensor, and thus the agents has to exchange information to find the source's location in a cooperative way. We have proposed a distributed control law which combines two objectives, *i.e.*, the disposition of the agents in a circular fashion, necessary for a correct gradient estimation, and the motion of the whole formation towards the source, by still assuming to not have any full position measurement, but only the relative bearing angle, that brings the agents to move around a common centre without knowing the position of the centre itself. The effectiveness of such control law has been theoretically proven.

6.2 Extensions and Future Works

The main contributions previously presented have been developed considering several assumptions, on the model of the diffusion process; nevertheless, some preliminary experiments suggest that the proposed solution remains still valid even when when such assumptions are not fully satisfied. A first line of research that can open is to fully understand and

formalise why and in which cases this can happen, and under what limits the proposed gradient estimation is still a good reference to reach the source. A limit case in this direction is to adapt the method to turbulent environments, where a simple gradient search can not be applied: on this purpose we cite the works of prof. Fumin Zhang and Wencen Wu [15, 76], that introduced a suitable transformation to map the highly irregular field given by the concentration of the emitted quantity subject to plume spikes, to a smooth one representing the frequency of spike detections, thus allowing for simple maximum search.

Also, we have supposed here to have a time invariant communication graph between the agents; thus, it would be interesting (and more realistic) to develop a solution based on an information exchange with the closest neighbours.

French Summary

Introduction

Le problème de la localisation de sources consiste à trouver, par un ou plusieurs agents, qui peuvent être fixes ou mobiles de manière autonome, la source d'une substance — chimique, lumineuse, sonore, polluante, de chaleur, et ainsi de suite — qui est produite à un endroit particulier, mais se répand sur une région à travers un processus de diffusion. Résoudre cette tâche est non seulement pertinent pour de nombreuses applications humaines, mais est crucial aussi bien dans la nature : les animaux ont développé une grande variété de stratégies complexes de localisation de source afin d'atteindre une grande variété d'objectifs. La localisation de sources sonores est cruciale pour survivre, autant pour les chasseurs que les proies ; des formes plus simples de vie (par exemple, les bactéries ou les insectes) suivent les signaux chimiques pour trouver de la nourriture ou des partenaires pour la reproduction, tandis que les espèces plus complexes effectuent de la localisation de sources d'odeurs pour atteindre les mêmes objectifs.

Les scientifiques ont investi un énorme effort dans l'étude et la compréhension de ces mécanismes complexes, dans le but de reproduire ces comportements dans ce qui est connu sous le nom de "localisation de sources bio-inspirée". Par exemple, les crabes bleus (*callinectes sapidus*, figure 1), utilisent les signals captés par des capteurs chimiques pour chercher de la nourriture dans les panaches d'eau : les capteurs chimiques sur les antennules, qui sont élevés sur le corps du crabe, contrôlent le

Figure 1. Les crabs bleus utilisent capteurs chimiques sur les antennules et sur les pattes pour contrôler leur localisation de nourriture.

mouvement en avant vers la source odorante, tandis que les capteurs sur les pattes, qui sont séparés spatialement et à proximité du substrat, sont soupçonnés de servir de médiateur du mouvement inter-flux par rapport à la structure du panache d'eau [75]. Encore, les papillons de nuit mâles (figure 2) sont capables de détecter et de localiser les papillons de nuit femelles jusqu'à plusieurs centaines de mètres tandis qu'elles sécrètent des quantités infimes de phéromones dispersées dans les panaches turbulents ; ils résolvent cette tâche en combinant capteurs olfactifs hautement spécialisés, capteurs anémotactiques, et capteurs visuels avec stratégies spécifiques de traitement de l'information et de contrôle comportemental [61]. Enfin, les bactéries flagellées, comme l'*escherichia coli* (figure 3), ont un mouvement caractéristique qui se compose de deux phases qui leur permettent des marches aléatoires : ils peuvent utiliser leurs flagelles pour nager droit, ou se retourner, de sorte que quand ils recommencent à nager ils se déplacent dans une direction aléatoire ; à son tour, la probabilité d'un changement de direction augmente tant que la concentration de la cible chimique détectée diminue.

Dans la recherche et l'ingénierie, le problème de la localisation de la source d'un signal a reçu un intérêt croissant au cours des dernières décennies, en particulier dans les applications où les agents doivent atteindre physiquement la position de la source et ont peu ou pas d'information de position. Cette question est pertinente dans de nombreuses applica-

tions concernant des sources émettant de la chaleur ou de la vapeur [60], telles que l'échantillonnage océanique, la surveillance, la cartographie et l'exploration de l'espace (voir [25, 42, 72, 82] et les références qui y sont), la détection d'explosifs, la détection de drogue, de fuites ou de produits chimiques dangereux, la détection de pollution et les études environnementales. Nous rappelons ici qu'il existe également de nombreux domaines dans lesquels il est pertinent de localiser la direction, et peut-être la distance, d'une source qui émet, et cela se fait par exemple en utilisant les différences de temps d'arrivée du signal par des capteurs statiques qui ne se déplacent pas vers la source ; en sont des exemples la localisation de sources sonores, ce qui est pertinente dans de nombreuses applications (par exemple dans les systèmes de conférences téléphoniques intelligents, qui permettent d'identifier les intervenants pour améliorer la qualité sonore et vidéo [80]), ou des études de médecine, par exemple en utilisant des capteurs de surface pour explorer l'activité interne du cerveau.

Nous allons dans les sections suivantes, donner un (non exhaustif) aperçu de la littérature à propos de la localisation de source.

Revue de la littérature sur la localisation de sources

La quête de la source peut être effectuée de manière statique, avec un réseau de capteurs qui collectent et échangent de l'information sur l'environnement et cherchent à identifier d'où un signal d'intérêt provient, ou par des véhicules autonomes, équipés de capteurs, qui atteignent physiquement la source. Le premier scénario est particulièrement adapté pour la localisation de sources sonores ou la localisation des signaux électromagnétiques, qui peuvent faire usage de méthodes qui nécessitent de mesures telles que l'intensité du signal, la triangularisation et la différence des temps d'arrivée de l'onde à différents capteurs. Comme nous l'avons déjà mentionné, nous sommes intéressés par ce deuxième scénario (la localisation par des capteurs qui atteignent la source) ; nous allons donc concentrer la revue sur ces sujets.

D'un point de vue mathématique, la distribution d'un signal est un champ scalaire décrit par une fonction spatiale $f(\boldsymbol{x})$, dont le maximum est en correspondance de la position de la source $\boldsymbol{x}^{\mathrm{s}}$. Il existe dans la littérature une grande variété de méthodes pour traiter le problème de la localisation de la source et des questions connexes, ce qui en fait une exposition exhaustive impossible ; mais la ligne commune est que, dans toutes ces missions, nous disposons de véhicules sans équipage, qui ont besoin de se déplacer et de prendre des mesures d'un tel champ scalaire inconnu, avec l'objectif d'utiliser ces mesures pour calculer la position de la source du signal. Par exemple, nous pouvons être intéressés par la localisation d'une source de chauffage, et dans ce cas le signal d'intérêt est donné par la température à des endroits donnés ; ou nous pouvons vouloir trouver la source d'une substance chimique qui pollue l'environnement, et donc nous allons nous intéresser à la concentration de ce produit chimique.

Problèmes inverses

De nombreuses techniques traitent de formulations associées aux processus de diffusion isotropes décrits par des équations de diffusion pour lesquelles une solution de forme fermée est connue ; puisque la solution explicite dépend (parmi d'autres paramètres) de l'emplacement de la source, plusieurs méthodes d'identification ont été conçus pour estimer la position de la source : dans [49] il est proposé une procédure d'identification en deux étapes, avec un réseau de capteurs fixes ; dans [60] il est formulé un problème similaire, mais avec des capteurs en mouvement, en utilisant une approche du maximum probabilistique pour estimer la position de la source, et des capteurs qui bougent de manière à minimiser leur erreur d'estimation. Des problèmes plus fondamentaux, tels que l'identifiabilité de la source et le placement optimal des capteurs, sont discutés en profondeur par [39] utilisant des concepts et des idées de la théorie du contrôle de systèmes. Les approches mentionnées ci-dessus peuvent être considérés comme des problèmes inverses pour les équations aux dérivées partielles, avec l'objectif de trouver les conditions initiales ou un terme de forçage.

En raison de leur nature, toutes ces méthodes partagent les inconvénients communs de calculs lourds et d'une grande sensibilité à la connaissance explicite de la solution en forme fermée de l'équation aux derivées partielles décrivant le processus de diffusion.

Localisation de sources basée sur le gradient

Une autre voie de recherche consiste à calculer le champ du gradient de la grandeur mesurée, et à se diriger vers la source en suivant la direction du gradient ; cela peut être fait soit directement, via une méthode développée *ad hoc* pour le problème particulier, soit implicitement, en estimant le gradient via différentes techniques. Une des premières contributions faisant usage d'un calcul explicite du gradient peut être trouvée dans [14], où l'agent obtient différentes mesures d'un panache hydrothermal et effectue un estimation du gradient pour se déplacer vers la source. Dans [6] des véhicules nonholonomes sont entraînés vers une source par une loi de contrôle liés à la géométrie du processus de diffusion. Une estimation du gradient est également utilisé dans [4] pour diriger un seul véhicule au maximum/minimum d'un champ scalaire. Dans [23] une méthode du gradient qui converge en un temps fini est développée ; dans cet ouvrage l'auteur présente les bases des méthodes de recherche basée sur le gradient.

En plus de cela, des résultats récents traitant de la localisation de source d'odeur [24, 37, 78] ont tenté de faire face à des panaches de sources, et doivent être capables de mesurer également le vent ou le débit qui crée ce panache, puisque dans ce cas une estimation de gradient directe est impossible. Dans ce cadre sont à noter des œuvres récentes de Zhang *et al.* [15, 76], où les auteurs ont développé une stratégie pour cartographier le champ discontinu donné par le panache dans un processus continu dans lequel le signal d'intérêt est la durée du panache, et étaient donc en mesure d'appliquer leur méthode précédente [77] pour effectuer une recherche normale basée sur le gradient sur cette dernière quantité.

Ces méthodes partagent l'avantage d'être en général plus simples que

Figure 2. Un papillon de nuit est capable de localiser une femme par ses phéromones dispersées dans les panaches d'air turbulents [61].

les suivantes, mais elles sont généralement basées sur des hypothèses fortes, comme une certaine régularité du profil du signal (ou la possibilité d'en mesurer directement le gradient), et peuvent nécessiter un temps de convergence long si elles sont effectuées par un seul agent.

Extremum seeking

Une autre approche pour la localisation de source est basée sur la technique dite *extremum seeking*, une contribution fondamentale dans le domaine de la commande adaptative [2]. Cette méthode peut encore être considérée comme une technique d'optimisation basée sur le gradient, car elle repose sur l'idée de réunir des informations assez riches pour approcher le gradient grâce à l'utilisation d'un signal de sondage périodique ; cependant, contrairement aux méthodes mentionnées précédemment, cette approche ne repose pas sur une structure ou une connaissance particulière de la solution du processus de diffusion, et pour cette raison elle s'applique uniquement aux capteurs mobiles. Dans l'*extremum seeking*, la caractéristique d'entrée-sortie à l'état stable est optimisée sans nécessiter aucune connaissance explicite sur la caractéristique elle-même, autre qu'elle existe et qu'elle a un extremum ; une telle situation se présente dans une large gamme d'applications d'ingénierie : réacteurs biochimiques, commande ABS des freins de l'automobile, vannes électromécaniques, com-

presseurs axiaux, robots mobiles, réseaux de capteurs mobiles, tuning PID, amplificateurs à fibre optique etc. [27, 74, 81, 83]. Bien que cette méthode remonte à la moitié du siècle dernier, la première analyse de stabilité locale de cette classe de contrôleurs a été donnée en 2000 par Krstić et Wang [41], étendue plus tard à l'analyse de stabilité semi-globale dans [69, 70]; pour d'autres études théoriques sur l'*extremum seeking*, voir [58, 71]. Une formalisation rigoureuse de sa théorie est donnée dans [1], tandis qu'une bonne enquête sur la littérature sur l'*extremum seeking* peut être trouvée dans [68].

Des contributions sur la localisation de source basée sur l'*extremum seeking* sont représentées par [18, 36, 79], où un monocycle non holonome est contrôlé respectivement par la vitesse d'avancement, puis par celle angulaire, et enfin par les deux ensemble; dans tous ces documents le scénario est donné par des sources avec des distributions spatiales inconnues et des véhicules non holonomes monocycles sans mesure de position. Dans le premier cas, le véhicule utilise une vitesse d'avancement constante positive, et la direction du véhicule dans le plan est effectuée en utilisant seulement la variation de la vitesse angulaire, tandis que dans la seconde la configuration opposée est étudiée; comme Ghods le souligne dans la troisième contribution, où soit la vitesse d'avancement ainsi soit celle angulaire sont contrôlées, aucune des deux premières stratégies n'est idéale, puisque la première sacrifie les transitoires, tandis que la seconde, même si c'est une stratégie raisonnable motivée par la mise en œuvre avec de véhicules aériens, conduit à une complexité du comportement asymptotique du véhicule, car il ne peut au mieux que converger vers un petit attracteur autour de la source.

Dans [51, 52], un contrôleur hybride est mis en œuvre pour améliorer les performances de la méthode *extremum seeking* appliquée à la localisation de source; dans ces œuvres, les auteurs développent une méthode d'optimisation avec des changements de cap successifs basés sur des vecteurs conjugués, et le système résultant est montré être pratiquement stable pour une certaine classe de distributions de l'intensité du signal. Une analyse de stabilité pour le problème de la localisation de source avec un

monocycle non holonome se trouve dans [19], et dans [22] ceci est appliqué à plusieurs scénarios. Des contributions sur la localisation de sources en 3D sont données par [17, 20, 21]. Une approche légèrement différente est proposée dans [50], où ils utilisent une stratégie avec des lois de commande *sliding mode* pour laquelle le véhicule n'a pas besoin de calculer le gradient de la distribution du signal pour atteindre la source.

Localisation de sources stochastique

Une autre technique digne de mention est donnée par les méthodes stochastiques, qui tentent de reproduire certains comportements biologiques comme des bancs de poissons ou les mouvements des bactéries, et de modéliser la quête de l'agent via une fonction de probabilité qui décrit le taux de changement de direction. Ainsi l'*Optimotaxis* [54] : dans le travail cité, les agents se déplacent d'une manière qui imite le mouvement de l'*escherichia coli*, c'est-à-dire un mouvement aléatoire où la probabilité d'un changement de direction augmente à mesure que la concentration détectée des aliments diminue ; ce procédé peut également être utilisé avec des profils de signaux non quadratiques, y compris ceux avec de multiples maxima. Une autre contribution est donnée par [53], où les auteurs localisent une source de substance polluante et suivent la limite de la région contaminée. Enfin, dans [44, 66] une nouvelle méthode est introduite, qui combine une approche stochastique avec l'algorithme *extremum seeking* mentionné précédemment.

Localisation de source de façon distribuée

Afin d'éviter les grandes distances parcourues par le véhicule, et les oscillations nécessaires par les techniques d'*extremum seeking*, certaines stratégies de collaboration peuvent être conçues. Un tel objectif est obtenu par un groupe de véhicules qui collectent — et éventuellement partagent — suffisamment d'informations sur le champ du signal pour résoudre le problème de recherche de la source ; cela ouvre de nouveaux défis, tels que trouver des algorithmes d'optimisation efficaces pour estimer le gradient

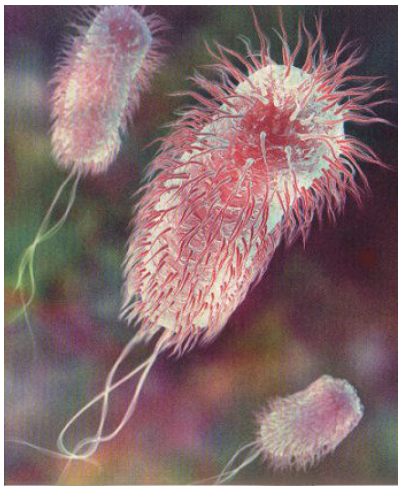

Figure 3. *Escherichia coli* tourne ses flagelles dans le sens antihoraire pour nager et dans le sens horaire pour changer de direction, effectuant de cette manière une localisation de source stochastique.

de manière distribuée (en général avec seulement des informations locales connues par chaque agent) ou encore gérer les contraintes de communication.

Une des premières contributions dans ce sens qui utilise une approche fondée sur le gradient est [56], où il est supposé que chaque véhicule, modélisé avec la dynamique de simple intégrateur, peut mesurer le gradient complet ; les auteurs développent un double algorithme avec un terme d'algorithme du gradient et des termes de forçage inter-véhicule. Une autre contribution basée sur le gradient est [59], où un groupe de planeurs équipés de capteurs estiment les paramètres du modèle du champ scalaire *via* la collecte de mesures de concentration à différents endroits, reconstruisent une valeur approximative du gradient du signal et utilisent cette information pour atteindre la source. Une application réelle d'une telle approche est présentée dans [30]. Des lois de contrôle collaboratives pour diriger une flotte de véhiculs sous-marins autonomes à la source d'une distribution en utilisant seulement des mesures de signaux directs par une formation circulaire d'agents sont présentés dans [12, 55]. Le gradient est estimé de manière implicite dans [77], où les auteurs prennent l'inspiration à partir des bancs de poissons pour concevoir un algorithme aussi adapté

pour la recherche de sources d'un écoulement turbulent [76].

L'*extremum seeking* est appliqué de façon collaborative dans [35], dans un cadre 1D, où les auteurs considèrent le problème du déploiement d'un groupe de véhicules autonomes dans une formation qui a une densité supérieure près de la source d'un signal mesurable, et inférieure loin de celle-ci. Dans [8], les auteurs conduisent une formation d'agents au maximum (ou minimum) d'un champ scalaire, en utilisant une approche multi-agents non collaborative : l'algorithme d'*extremum seeking* est effectivement mis en œuvre par un seul véhicule, le chef de file de la formation, et les agents restants suivent le leader en gardant une formation particulière. Enfin, une application très récente d'*extremum seeking* d'une manière répartie est [40], où une source est localisée à l'aide d'un algorithme en temps discret.

Deux localisations de source distribuées et stochastiques sont en [65], où un groupe de capteurs chimiques prend des mesures de valeurs de concentration du panache pour estimer la position de la source par l'intermédiaire d'une technique d'approximation stochastique, et [62], dans lequel les auteurs utilisent les mesures de capteurs pour estimer les paramètres du modèle du panache de concentration. Un approche mixte stochastique/*extremum-seeking* peut être trouvée aussi dans une approche distribuée, dans [34], où un groupe de véhicules autonomes entièrement actionnés sont déployés dans un champ de signal de plane ; ces contributions sont distribuées, mais non *coopératives*, car il n'y a pas d'échange d'information : chaque véhicule emploie une loi de commande stochastique *extremum seeking*, dont le but est de maximiser la valeur du signal mesuré ainsi que de minimiser simultanément une fonction des distances entre les agents voisins, ce qui produit un équilibre de Nash qui dépend des paramètres de contrôle des agents et de la distribution du signal inconnu.

Contributions de la thèse

L'originalité de la solution de localisation de source proposée réside dans le calcul du gradient à partir de l'intégrale de Poisson : en opposition à d'autres solutions publiées dans la littérature, d'une part il ne nécessite

pas de connaissances spécifiques de la solution du processus de diffusion, et il peut calculer la direction du gradient à partir des échantillons de concentration avec une petite charge de calcul ; d'autre part il ne nécessite pas l'utilisation d'un signal de test, et évite ainsi les oscillations nécessaires par les techniques *extremum seeking*. En outre, un tel procédé est facilement adaptable à toute dimension, et du fait que les dérivées sont calculées en utilisant les intégrales, la méthode est peu sensible au bruit de mesure, étant donné que ce calcul filtre intrinsèquement les hautes fréquences. Cette méthode représente une formalisation théorique de solutions antérieures proposées dans la littérature [11, 12, 55] ; en outre, il permet également le calcul des dérivées d'ordre supérieur (comme la matrice hessienne), ce qui permet de concevoir des lois de commande plus complexes.

Un tel procédé est appliqué de manière centralisée dans des scénarios en 2D ou en 3D, avec une preuve théorique de sa convergence ; nous proposons un algorithme distribué, dont l'efficacité est également prouvée théoriquement, qui diffère des précédentes contributions dès lors que nous supposons ne pas avoir des informations de position complètes (qui peuvent ne pas être disponibles dans différents environnements d'exploitation tels que les véhicules sous-marins ou à l'intérieur, ou dans des applications où les systèmes de navigation inertielle sont trop coûteux ou pas suffisamment précis), mais nous ne supposons que les capteurs autonomes sont capables de mesurer l'angle rélatif par rapport à leurs voisins.

Intégrale de Poisson et calcul du gradient

Modèle du processus de diffusion

Nous allons examiner, tout au long de notre mémoire, un processus de diffusion où la source est isotrope et la diffusion homogène ; cela signifie que les propriétés de la source, ainsi que le processus de diffusion lui-même, sont indépendants de la direction spatiale considérée. Cette diffusion est décrite par la célèbre équation aux dérivées partielles parabolique linéaire

avec des coefficients constants

$$\frac{\partial f(\boldsymbol{x},t)}{\partial t} - c\nabla^2 f(\boldsymbol{x},t) = 0, \quad \forall \boldsymbol{x} \in D,\ t \geq 0, \tag{1}$$

où f est la fonction de concentration, c est le coefficient de diffusion isotrope et D est un ouvert de $\mathbb{R}^n$ (voir [31]). Une telle équation est appropriée pour décrire divers phénomènes de diffusion : par exemple, f peut représenter la distribution de la température dans un environnement ou la concentration d'un produit chimique (polluant, salinité…).

Dans ce travail, nous supposons que le processus de diffusion est assez rapide, de sorte que notre intérêt est à étudier le comportement à l'état stable résultant de l'équation (1) ; par conséquent, nous limitons notre attention aux solutions de l'équation suivante, connue sous le nom d'*équation de Laplace* :

$$\nabla^2 f(\boldsymbol{x}) = 0, \quad \forall \boldsymbol{x} \in D. \tag{2}$$

Notre intérêt se concentre sur le cas où l'état d'équilibre a été atteint, mais une source émet toujours quelque part à un taux constant (cela se produit dans de nombreux cas d'intérêt pratique, par exemple dans un processus de chauffage ou dans la dispersion d'une substance chimique), ou que les variations possibles de la source sont lents dans l'échelle de temps d'intérêt, et notre objectif est de trouver l'emplacement de la source. En tant que modèle pour une telle source, nous supposons que la source occupe une partie de l'espace n'appartenant pas à D, et elle affecte les valeurs de f dans D en imposant une condition limite. Plus précisément, nous considérons un domaine ouvert $D = \tilde{D} \setminus D_{\mathrm{s}}$, où $\tilde{D} \subseteq \mathbb{R}^n$ est un ensemble connexe représentant la région dont l'étude nous intéresse, et D_{s} est un petit sous-ensemble connexe de $\tilde{D}$ qui représente la zone occupée par la source. Ainsi, la limite de D est formée par une partie intérieure, égale à la limite de la région de source D_{s} et notée ∂D_{in}, et peut-être une partie externe, égale à la limite de $\tilde{D}$ et notée ∂D_{ex} (figure 4).

Nous allons examiner ci-dessous un exemple explicatif.

Exemple (conditions aux limites mixtes de Dirichlet-Neumann).

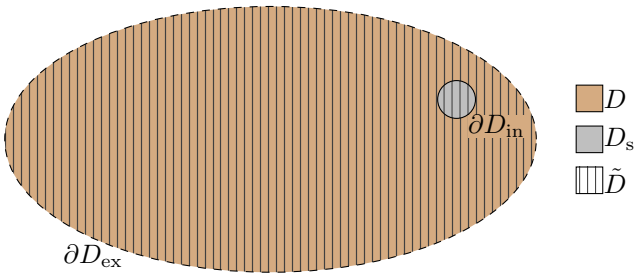

Figure 4. Représentation des domaines d'intérêt pour notre modèle de la source.

Dans certains cas, une fonction harmonique ne peut pas être écrite en forme fermée, mais elle peut être exprimée comme la solution d'un problème aux derivées partielles. À titre d'exemple, nous considérons un plan rectangulaire : un réchauffeur circulaire D_{s} est placé au milieu, et impose une condition à la limite constante $f(\boldsymbol{x}) = f_{\text{s}}$ pour toutes $\boldsymbol{x} \in \partial D_{\text{in}}$; sur les frontières, la condition limite est imposée non pas sur f, mais sur le dérivée de f dans le sens de l'unité extérieure normale $\hat{\boldsymbol{n}}$: nous supposons que $\nabla f(\boldsymbol{x}) \cdot \hat{\boldsymbol{n}} = 0$ au long des frontières, qui modélise des frontières parfaitement isolantes ; au milieu de l'une des plus longues frontières il y a une grande ouverture, qui impose une condition limite constante $f(\boldsymbol{x}) = f_{\text{ex}}$ en raison de la température extérieure plus froide. Le profil de température à l'état d'équilibre est obtenu par la solution du problème aux conditions mélangées de Dirichlet-Neumann

$$\begin{aligned} f(\boldsymbol{x}) &= f_{\text{s}} && \text{sur } \partial D_{\text{in}} = \partial D_{\text{s}} \\ f(\boldsymbol{x}) &= f_{\text{ex}} && \text{sur } [a_3, a_1 - a_3] \times a_2 \\ \nabla f(\boldsymbol{x}) \cdot \hat{\boldsymbol{n}} &= 0 && \text{sur } \partial D_{\text{ex}} \setminus [a_3, a_1 - a_3] \times a_2 \\ \nabla^2 f(\boldsymbol{x}) &= 0 && \text{dans } D = [0, a_1] \times [0, a_2] \setminus B_r(\boldsymbol{x}^{\mathbf{c}}), \end{aligned}$$

où a_1 est la longueur du côté le plus long, a_2 la longueur des plus courts, et l'ouverture extérieure a pour longueur $a_1 - 2a_3$; le réchauffeur est représenté par $B_r(\boldsymbol{x}^{\mathbf{c}})$, avec $r \ll \frac{a_2}{2}$. La figure 5 montre la température obtenue en résolvant le problème décrit ci-dessus par l'intermédiaire d'une méthode des éléments finis en utilisant le logiciel FreeFem++ (voir [38]), pour un domaine de 10 m de large et 6 m de long ; la fenêtre est de 6 m de large

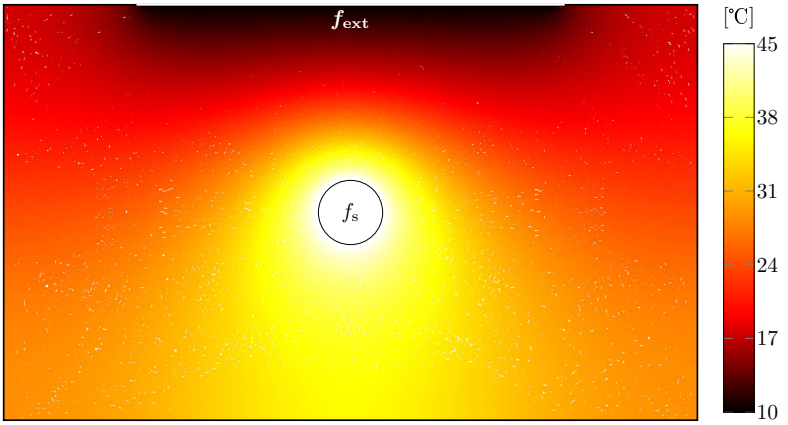

Figure 5. Solution du problème dans l'exemple ; les taches blanches sont dues à la solution obtenue par l'intermédiaire d'un approximation discret par éléments finis.

et le dispositif de chauffage occupe un cercle avec un rayon de 50 cm ; la température du réchauffeur est $f_{\text{s}} = 45$ °C et la température extérieure est $f_{\text{ex}} = 10$ °C.

Les solutions de l'équation de Laplace (2) sont appelées *harmoniques*, et ont de nombreuses propriétés intéressantes que nous rappelons ci-dessous[1].

Corollaire 1 (Principe du maximum). Soit $D \subset \mathbb{R}^n$ un ouvert borné, et soit $f\colon \bar{D} \to \mathbb{R}$ continue dans $\bar{D} = D \cup \partial D$ et harmonique dans D. Alors, la valeur maximale de f sur $\bar{D}$ est atteinte sur ∂D. •

Ce corollaire implique que sur un domaine borné une fonction harmonique est déterminée par ses valeurs limites, nous permettant ainsi de résoudre le problème de Dirichlet pour la boule, comme expliqué dans le paragraph prochain.

Proposition 1 (Principe du maximum local). Soit $D \subseteq \mathbb{R}^n$ un ouvert connexe, et soit $f\colon D \to \mathbb{R}$ une fonction harmonique sur D. Si f a un maximum local dans D, alors f est constante. •

[1]Pour une étude plus détaillée des propriétés des fonctions harmoniques nous renvoyons à [3, 31], d'où certaines des déclarations suivantes sont prises.

Parce que dans notre scénario le domaine intérieur ∂D_{s} représente la source, nous supposons que les valeurs de f sur ∂D_{in} sont plus élevées que les valeurs de f sur ∂D_{ex} (ou à l'infini) ; dans cette hypothèse, le principe du maximum garantit que la valeur maximale de f sur $\bar{D}$ est atteinte sur ∂D_{in}. Par conséquent, le problème de trouver la source peut être décrit comme le problème de trouver la valeur maximale de f sur $\bar{D}$; plus précisément, ayant assumé une valeur constante pour f long ∂D_{in}, nous allons considérer que le problème de recherche de la source est résolu si un point quelconque long ∂D_{in} a été atteint. En outre, le principe de maximum local assure que nous avons pas de maxima locaux à l'intérieur de D, ce qui rend possible l'utilisation d'une technique d'algorithme du gradient pour localiser la source sans se faire piéger dans des maxima locaux.

L'intégrale de Poisson

Considérons un domaine borné A et le problème de Dirichlet à condition limite homogène

$$\begin{aligned} f(\boldsymbol{x}) &= \bar{f}(\boldsymbol{x}) && \text{on } \partial A \\ \nabla^2 f(\boldsymbol{x}) &= 0 && \text{in } A. \end{aligned}$$

Grâce au corollaire précédent, la solution du problème de Dirichlet est unique ; pour toute fonction f qui est harmonique sur A et continue sur sa fermeture, $f(\boldsymbol{x})$ aux points à l'intérieur de A peut être calculée avec une formule impliquant uniquement les valeurs de la restriction de f à la limite ∂A et le noyau de Poisson, comme suit pour $A = B_r(\boldsymbol{x}^{\mathbf{c}}) = \{\, \boldsymbol{x} \colon \|\boldsymbol{x} - \boldsymbol{x}^{\mathbf{c}}\| < r \,\}$.

Théorème (Intégrale de Poisson pour la boule générique). Soit $f \colon \bar{B}_r(\boldsymbol{x}^{\mathbf{c}}) \to \mathbb{R}$ continue sur $\bar{B}_r(\boldsymbol{x}^{\mathbf{c}})$, harmonique sur $B_r(\boldsymbol{x}^{\mathbf{c}})$. Alors :

$$f(\boldsymbol{x}) = \frac{1}{\Omega_n r} \int_{\partial B_r(\boldsymbol{x}^{\mathbf{c}})} P_{B_r(\boldsymbol{x}^{\mathbf{c}})}(\boldsymbol{x}, \bar{\boldsymbol{x}}) f(\bar{\boldsymbol{x}}) \, \mathrm{d}S_{B_r(\boldsymbol{x}^{\mathbf{c}})}(\bar{\boldsymbol{x}}), \tag{3}$$

où $\boldsymbol{x} \in B_r(\boldsymbol{x}^{\mathbf{c}})$, et $P_{B_r(\boldsymbol{x}^{\mathbf{c}})}$ est le noyau de Poisson pour la boule générique, défini comme

$$P_{B_r(\boldsymbol{x}^{\mathbf{c}})}(\boldsymbol{x}, \bar{\boldsymbol{x}}) = \frac{r^2 - \|\boldsymbol{x} - \boldsymbol{x}^{\mathbf{c}}\|^2}{\|\boldsymbol{x} - \bar{\boldsymbol{x}}\|^n}. \qquad \bullet \tag{4}$$

En particulier, lorsqu'il est évalué dans le centre de la boule sur laquelle l'intégrale est calculée, le noyau de Poisson en (4) se réduit à

$$P_{B_r(\boldsymbol{x}^{\mathbf{c}})}(\boldsymbol{x}^{\mathbf{c}}, \bar{\boldsymbol{x}}) = \frac{r^2}{r^n} = \frac{1}{r^{n-2}},$$

et l'expression de $f(\boldsymbol{x})$ de (3) devient beaucoup plus simple :

$$f(\boldsymbol{x}^{\mathbf{c}}) = \frac{1}{\Omega_n r^{n-1}} \int_{\partial B_r(\boldsymbol{x}^{\mathbf{c}})} f(\bar{\boldsymbol{x}}) \, \mathrm{d}S_{B_r(\boldsymbol{x}^{\mathbf{c}})}(\bar{\boldsymbol{x}}). \tag{5 A}$$

Calcul des dérivées

La formule de l'intégrale de Poisson donnée dans (3) donne également une technique pour calculer les dérivées (gradient, matrice hessienne etc.) de f en tout point à l'intérieur de la boule $B_r(\boldsymbol{x}^{\mathbf{c}})$ avec une intégrale impliquant seulement les valeurs de f au long du cercle $\partial B_r(\boldsymbol{x}^{\mathbf{c}})$, comme indiqué dans la proposition suivante.

Proposition 2. Soit $D \subseteq \mathbb{R}^n$ un ouvert, et soit $f \colon D \to \mathbb{R}$ harmonique sur D. Pour tout $\boldsymbol{x}^{\mathbf{c}} \in D$, pour tout $r > 0$ tel que $\bar{B}_r(\boldsymbol{x}^{\mathbf{c}}) \subseteq D$, pour tout $\boldsymbol{x} \in B_r(\boldsymbol{x}^{\mathbf{c}})$, et pour tous entiers non-négatifs $g_1, g_2, \ldots, g_n$ tels que $\sum_{i=1}^n g_i = g$,

$$\frac{\partial^g f(\boldsymbol{x})}{\prod_{i=1}^n \partial x_i^{g_i}} = \frac{1}{\Omega_n r} \int_{\partial B_r(\boldsymbol{x}^{\mathbf{c}})} \frac{\partial^g P_{B_r(\boldsymbol{x}^{\mathbf{c}})}(\boldsymbol{x}, \bar{\boldsymbol{x}})}{\prod_{i=1}^n \partial x_i^{g_i}} f(\bar{\boldsymbol{x}}) \, \mathrm{d}S_{B_r(\boldsymbol{x}^{\mathbf{c}})}(\bar{\boldsymbol{x}}). \qquad \bullet$$

En applicant cette proposition il est facile d'obtenir l'expression du gradient $\nabla f(\boldsymbol{x}^{\mathbf{c}})$. Le gradient du noyau de Poisson peut être calculé à partir de (4), ce qui donne l'expression du gradient

$$\nabla f(\boldsymbol{x}^{\mathbf{c}}) = \frac{1}{\Omega_n r} \int_{\partial B_r(\boldsymbol{x}^{\mathbf{c}})} \nabla P_{B_r(\boldsymbol{x}^{\mathbf{c}})}(\boldsymbol{x}^{\mathbf{c}}, \bar{\boldsymbol{x}}) f(\bar{\boldsymbol{x}}) \, \mathrm{d}S_{B_r(\boldsymbol{x}^{\mathbf{c}})}(\bar{\boldsymbol{x}}) = \\ = \frac{n}{\Omega_n r^n} \int_{\partial B_r(\boldsymbol{x}^{\mathbf{c}})} \hat{\boldsymbol{r}} f(\bar{\boldsymbol{x}}) \, \mathrm{d}S_{B_r(\boldsymbol{x}^{\mathbf{c}})}(\bar{\boldsymbol{x}}). \quad (5\,\text{B})$$

De même, nous pouvons calculer la matrice hessienne de f au centre $\boldsymbol{H}(\boldsymbol{x}^{\mathbf{c}})$, en obtenant

$$\boldsymbol{H}(\boldsymbol{x}^{\mathbf{c}}) = \frac{1}{\Omega_n r} \int_{\partial B_r(\boldsymbol{x}^{\mathbf{c}})} \boldsymbol{H}_P(\boldsymbol{x}^{\mathbf{c}}, \bar{\boldsymbol{x}}) f(\bar{\boldsymbol{x}}) \, \mathrm{d}S_{B_r(\boldsymbol{x}^{\mathbf{c}})}(\bar{\boldsymbol{x}}) = \\ = \frac{n+2}{\Omega_n r^{n+1}} \int_{\partial B_r(\boldsymbol{x}^{\mathbf{c}})} (n \hat{\boldsymbol{r}} \hat{\boldsymbol{r}}^{\mathsf{T}} - \mathbf{I}) f(\bar{\boldsymbol{x}}) \, \mathrm{d}S_{B_r(\boldsymbol{x}^{\mathbf{c}})}(\bar{\boldsymbol{x}}). \quad (5\,\text{C})$$

Localisation de sources sur le plan

Véhicules mobiles planaires

Nous considérons des robots mobiles, chacun doté d'un ou plusieurs capteurs fournissant des mesures ponctuelles de concentration. La dynamique des robots peut être modélisée de différentes manières, en fonction de l'application à portée de main : à titre d'exemple, nous considérons des véhicules sous-actionnés modélisés comme des monocycles non holonomes avec la dynamique

$$\begin{aligned} \dot{\boldsymbol{x}}(t) &= v \begin{bmatrix} \cos\theta(t) \\ \sin\theta(t) \end{bmatrix} \\ \ddot{\theta}(t) &= u(t), \end{aligned} \quad (6)$$

commandé par le couple de torsion $u(t)$. La position du véhicule dans le plan est décrite par $\boldsymbol{x}(t)$, et $\theta(t)$ représente l'angle de position ; la vitesse d'avancement v est supposée ici constante par simplicité, même si différentes stratégies peuvent être élaborées.

Le point central est de concevoir le contrôle $u(t)$ en utilisant des informations provenant des capteurs pour atteindre l'emplacement de la source. Idéalement, nous aimerions que chaque robot soit capable de calculer le

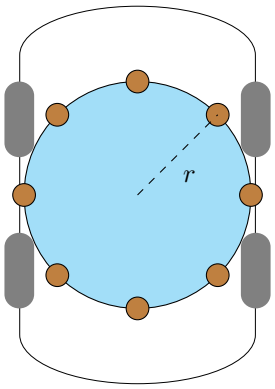

Figure 6. Possible déploiement des capteurs sur un véhicule autonome planaire : un réseau circulaire de capteurs avec des angles équidistants est fixé sur le robot.

gradient à sa position centrale $\boldsymbol{x}(t)$ en utilisant la formule de Poisson (5 B), avec $\boldsymbol{x}^{\mathbf{c}} = \boldsymbol{x}(t)$; pour atteindre cet objectif, il a besoin de recueillir des mesures sur un cercle $\partial B_r(\boldsymbol{x}^{\mathbf{c}})$ et de calculer l'intégrale de Poisson. Pour en obtenir une bonne approximation, un dispositif de détection efficace, décrit en figure 6, consiste en N capteurs disposés au long d'un réseau circulaire de rayon r, centré à la position centrale $\boldsymbol{x}(t)$ avec des angles équidistants ; c'est-à-dire, le $i^{\text{ème}}$ capteur est en position

$$\boldsymbol{x}_i(t) = \boldsymbol{x}(t) + r \begin{bmatrix} \cos\gamma_i \\ \sin\gamma_i \end{bmatrix}, \tag{7}$$

où $\gamma_i = \frac{2\pi}{N}(i-1)$. Le réseau de capteurs est solidement connecté au véhicule, et il tourne avec l'angle de position du robot ; par conséquent, le robot calcule le gradient dans le système de coordonnées local où sa position a une valeur fixe. Ensuite, l'intégrale est approchée par la somme de Riemann en utilisant les N valeurs mesurées.

Approximation des dérivées

Nous pouvons rapprocher les intégrales (5) par la somme de Riemann des N valeurs fournies par les capteurs disposés au long du cercle (voir figure 6).

En utilisant les coordonnées polaires $\boldsymbol{r} = r(\cos\gamma, \ \sin\gamma)$, avec $\gamma \in$

$[0, 2\pi)$, $\mathrm{d}S = r\,\mathrm{d}\gamma$ et la mesure du cercle unitaire égal à $\Omega_2 = 2\pi$, les formules de Poisson (5) en deux dimensions deviennent

$$f(\boldsymbol{x}(t)) = \frac{1}{2\pi}\int_0^{2\pi} f(\bar{\boldsymbol{x}}(\gamma))\,\mathrm{d}\gamma \tag{8 A}$$

$$\nabla f(\boldsymbol{x}(t)) = \frac{1}{\pi r}\int_0^{2\pi} \begin{bmatrix}\cos\gamma\\ \sin\gamma\end{bmatrix} f(\bar{\boldsymbol{x}}(\gamma))\,\mathrm{d}\gamma \tag{8 B}$$

$$\boldsymbol{H}(\boldsymbol{x}(t)) = \frac{2}{\pi r^2}\int_0^{2\pi} \begin{bmatrix}2\cos^2\gamma - 1 & 2\cos\gamma\sin\gamma\\ 2\cos\gamma\sin\gamma & 2\sin^2\gamma - 1\end{bmatrix} f(\bar{\boldsymbol{x}}(\gamma))\,\mathrm{d}\gamma. \tag{8 C}$$

En notant la mesure du capteur i au temps t par

$$\hat{f}_i\big(\boldsymbol{x}(t), t\big) = f\big(\boldsymbol{x}_i(t)\big) + e_i(t),$$

où $\boldsymbol{x}_i$, défini dans l'équation (7), est la discrétisation de $\bar{\boldsymbol{x}}$ et $e_i(t)$ est l'erreur due au bruit de mesure blanc gaussien affectant le capteur i, nous pouvons maintenant calculer l'approximation des équations (8) comme

$$\hat{f}\big(\boldsymbol{x}(t), t\big) = \frac{1}{N}\sum_{i=1}^{N} \hat{f}_i\big(\boldsymbol{x}(t), t\big) \tag{9 A}$$

$$\widehat{\nabla f}\big(\boldsymbol{x}(t), t\big) = \frac{2}{Nr}\sum_{i=1}^{N} \hat{\boldsymbol{r}}_i \hat{f}_i\big(\boldsymbol{x}(t), t\big) \tag{9 B}$$

$$\hat{\boldsymbol{H}}\big(\boldsymbol{x}(t), t\big) = \frac{4}{Nr^2}\sum_{i=1}^{N} \tilde{\boldsymbol{H}}_i \hat{f}_i\big(\boldsymbol{x}(t), t\big), \tag{9 C}$$

où $\hat{\boldsymbol{r}}_i = (\cos\gamma_i, \quad \sin\gamma_i)$ et, après quelques simples calculs trigonométriques sur la matrice dans (8 C), il vient

$$\tilde{\boldsymbol{H}}_i = \begin{bmatrix}\cos 2\gamma_i & \sin 2\gamma_i\\ \sin 2\gamma_i & -\cos 2\gamma_i\end{bmatrix}.$$

Nous notons que toutes les intégrales et les sommes de quantités vectorielles ou matricielles sont conçues comme des intégrales ou sommes des entrées simples.

Conception de la rétroaction

La stratégie de l'algorithme du gradient peut être mise en œuvre en définissant une référence d'orientation $\theta^{\mathrm{r}}(\boldsymbol{x})$ dans la direction du gradient de la fontion de diffusion au point $\boldsymbol{x}$, en utilisant la formule (9 B) et la matrice hessienne (9 C). Grâce à la facilité de calcul des formules précédentes, nous pouvons utiliser une loi de contrôle impliquant la matrice hessienne, par exemple en incluant un terme d'amortissement, utile puisque le système est du second ordre, impliquant les dérivées temporelles soit de l'angle de cap soit de sa référence θ^{r} ; ce terme peut être calculé à partir du gradient approximé (9 B) et de la matrice hessienne (9 C).
La rétroaction proposée est

$$u(t) = k_1\Big(\theta^{\mathrm{r}}\big(\boldsymbol{x}(t),t\big) - \theta(t)\Big) + k_2\Big(\dot{\theta}^{\mathrm{r}}\big(\boldsymbol{x}(t),t\big) - \dot{\theta}(t)\Big), \tag{10}$$

avec la référence et sa dérivée temporelle données par

$$\begin{aligned}
\theta^{\mathrm{r}}\big(\boldsymbol{x}(t),t\big) &= \arg\widehat{\nabla f}\big(\boldsymbol{x}(t),t\big)\\
\dot{\theta}^{\mathrm{r}}\big(\boldsymbol{x}(t),t\big) &= \frac{\dot{\boldsymbol{x}}^{\mathsf{T}}(t)\hat{\boldsymbol{H}}\big(\boldsymbol{x}(t),t\big)\boldsymbol{R}\widehat{\nabla f}\big(\boldsymbol{x}(t),t\big)}{\|\widehat{\nabla f}\big(\boldsymbol{x}(t),t\big)\|^2},
\end{aligned}$$

où $\widehat{\nabla f}\big(\boldsymbol{x}(t),t\big)$ et $\hat{\boldsymbol{H}}\big(\boldsymbol{x}(t),t\big)$ sont définies par les équations (9 B) et (9 C), et $\boldsymbol{R}$ est la matrice de rotation d'un angle égale à $\frac{\pi}{2}$, définie comme

$$\boldsymbol{R} = \begin{bmatrix} 0 & -1 \\ 1 & 0 \end{bmatrix}.$$

Résultats des simulations

À titre d'exemple de simulation, on considère un plan chauffé correspondant à l'exemple décrit précédemment. En particulier, nous proposons d'avoir un espace rectangulaire de 10×6 m de large, avec un radiateur circulaire de $5\,\mathrm{cm}$ de rayon dans son milieu et une ouverture sur le côté arrière. Le réchauffeur impose la condition $f(\boldsymbol{x}) = f_\mathrm{s}$; les frontières sont parfaitement isolantes, de manière à imposer la condition limite de Neumann $\nabla f(\boldsymbol{x}) \cdot \hat{\boldsymbol{n}} = 0$, tandis que l'ouverture latérale, de $6\,\mathrm{m}$ de large, impose la condition frontière sur la valeur de la température $f(\boldsymbol{x}) = f_\mathrm{ex}$.

La figure 7 montre les trajectoires d'un ensemble de robots tels que ceux décrits dans la figure 6, décrits par la loi de mouvement (6), à partir de différentes positions initiales aléatoires et avec différentes orientations initiales. La température de l'élément chauffant est $f_\mathrm{s} = 45$ °C, tandis que celle externe est égale à $f_\mathrm{ex} = 5$ °C, et chaque robot se déplace avec une vitesse constante de $v = 0,2$ m/s et avec des capteurs disposés sur une circonférence de rayon $r = 10\,\mathrm{cm}$; les paramètres de contrôle dans l'équation (10) sont choisis comme $k_1 = 49$ et $k_2 = 14$. Dans ce premier cas, nous supposons des mesures parfaites ; les véhicules sur la gauche sont dotés de $N = 3$ capteurs, tandis que ceux sur la droite en ont $N = 12$. Nous pouvons observer qu'un nombre inférieur de capteurs à pour résultat une trajectoire qui n'est pas exactement orientée avec le gradient de f, mais les robots sont néanmoins capables d'atteindre rapidement la source.

Une simulation avec les mêmes conditions et paramètres initiaux et le même nombre de capteurs pour chacun des deux sous-ensembles de véhicules, mais avec chaque mesure corrompue par un bruit blanc gaussien d'écart-type $\sigma = 0,75$, est représentée sur la figure 8. Comme nous pouvons le voir, tous les véhicules atteignent la source, avec des trajectoires presque perpendiculaires aux lignes de contour de la température, qui ont un petit tramage à cause du bruit dans les mesures ; nous pouvons également remarquer le meilleur filtrage réalisé par les robots à 12 capteurs.

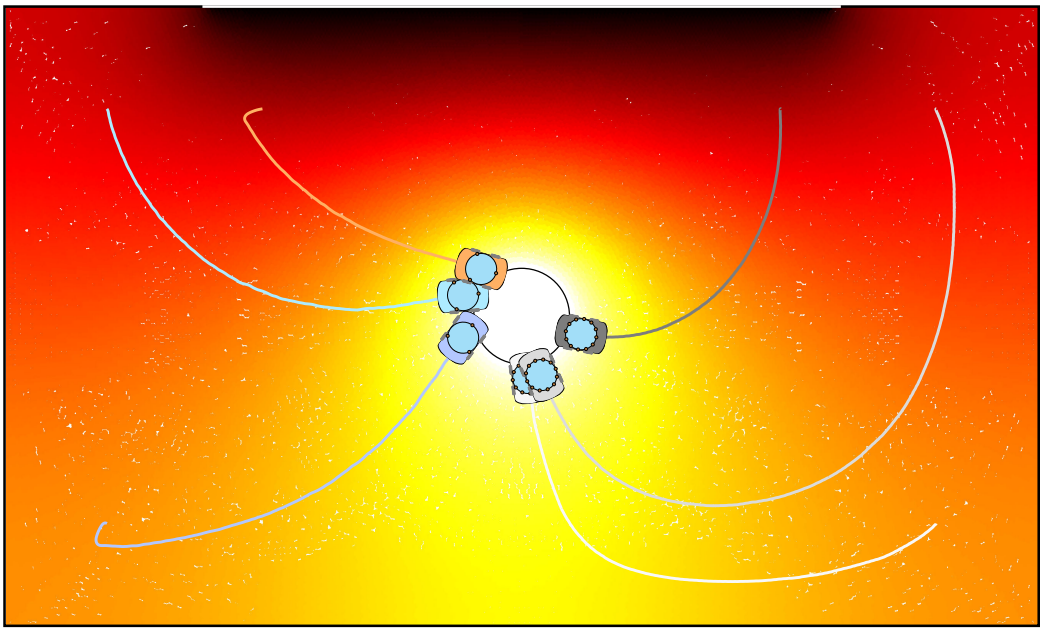

Figure 7. Trajectoires des véhicules cherchant une source thermique équipées de capteurs sans bruit ; les véhicules sur la gauche ont 3 capteurs chacun, les uns sur la droite 12 capteurs.

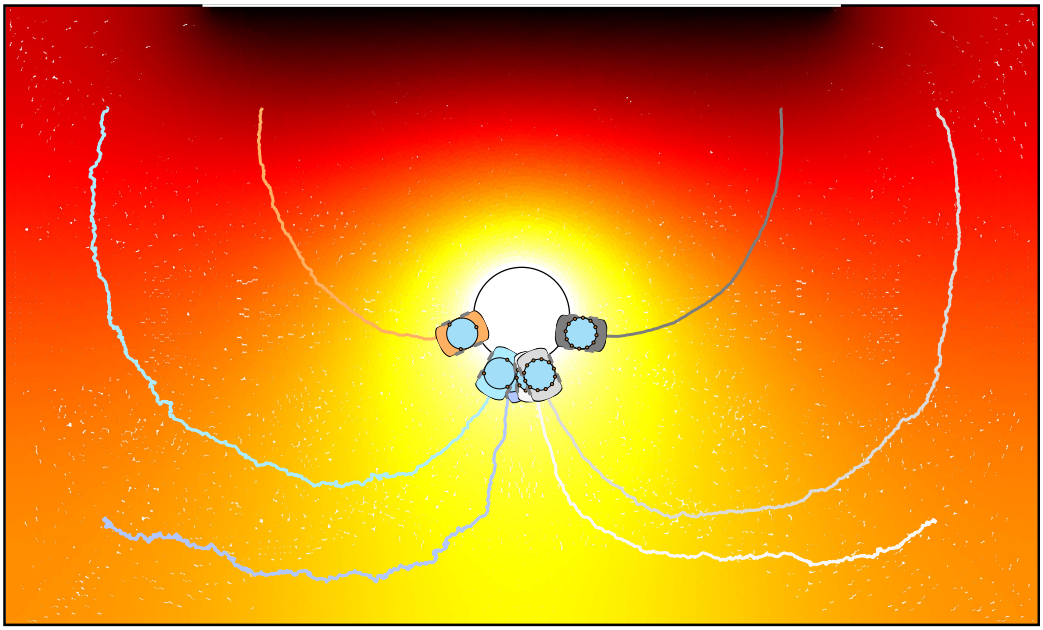

Figure 8. Trajectoires des véhicules cherchant une source thermique équipées de capteurs avec bruit ; les véhicules sur la gauche ont 3 capteurs chacun, les uns sur la droite 12 capteurs.

Mise en œuvre expérimentale

Dans le cadre d'un projet de stage de fin d'études d'un étudiant de master (Yvan Gaudfrin) de l'université de Bristol (Angleterre, Royaume-uni), nous avons développé un prototype de robot planaire pour tester la loi de contrôle de localisation de source que nous avons décrite précédemment. Le projet a eu lieu au GIPSA-lab, sous la supervision de l'ingénieur Jonathan Dumon et de Ruggero Fabbiano.

Description du projet et conception du robot

Dans cette expérience, dont l'objectif est de valider par une mise en œuvre pratique notre algorithme de recherche de source en 2D, la tâche sera effectuée par un robot planaire équipé d'une caméra, se déplaçant sur le dessus d'un large tableau représentant un réel processus de diffusion, c'est-à-dire une source de rejets d'eau chaude qui se répand dans la mer (figure 10). L'ensemble circulaire de capteurs qui fournissent des mesures ponctuelles sera obtenu, dans ce cas, en sélectionnant des pixels appropriés sur une forme circulaire de la vue de la caméra. En utilisant ces capteurs, le robot doit se déplacer sur cette photo et rouler vers la source. Nous notons que, comme dans toutes les applications de la vie réelle, les hypothèses théoriques en vertu desquelles nous avons développé notre loi de contrôle ne sont pas satisfaites : en effet la fonction décrivant le processus de diffusion que nous pouvons voir dans figure 10 est non harmonique et a également des maxima locaux ; par conséquent, un autre objectif du projet est de voir comment ce système peut fonctionner dans la pratique, lorsque le processus de diffusion réelle ne correspond pas complètement aux hypothèses du cas idéal.

Les deux prototypes finaux du robot réalisés, avec leur deux caméras utilisées, sont présentés dans figure 9.

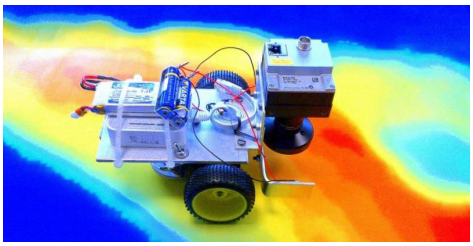

(A) Première conception : caméra GigE Vision®.

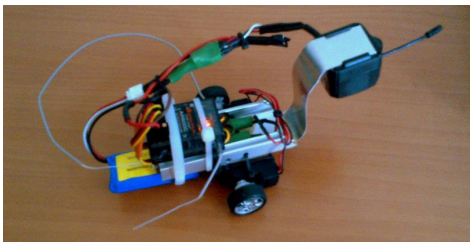

(B) Deuxième conception : caméra sans fil avec convertisseur USB.

Figure 9. Les robots construits pour le cas d'étude pratique.

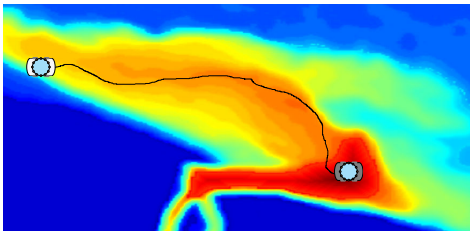

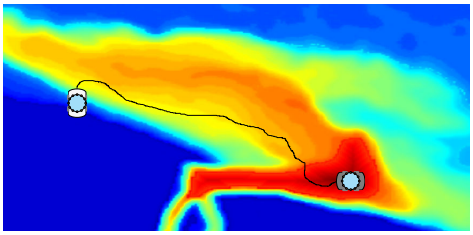

Figure 10. Reproduction des trajectoires suivies par le robot cherchant la source ; le véhicule blanc indique la position initiale, le gris la position finale.

Tests finaux

Le prototype planaire pour la recherche de sources a démontré être pleinement efficace dans le scénario utilisé, même compte tenu de son non harmonicité. Si les conditions initiales étaient telles qu'il pouvait obtenir des mesures significatives, il a toujours réussi à atteindre la zone de l'image qui représente la source de la diffusion, comme le montre la figure 10, qui montre une approximation de la voie tracée par le robot pendant quelques expériences de validation. Pour une meilleure compréhension du comportement du robot, nous nous référons au site web de l'équipe NeCS[2] pour les vidéos du robot au travail.

[2]http ://necs.inrialpes.fr/pages/platforms.php#sourceLoc

Recherche tridimensionnelle de sources

Dynamique du véhicule et conception de la rétroaction

Nous considérons un véhicule sous-actionné, décrit par la loi de mouvement cinématique

$$\begin{aligned} \dot{\boldsymbol{x}}(t) &= v \begin{bmatrix} \cos\theta_1(t)\sin\theta_2(t) \\ \sin\theta_1(t)\sin\theta_2(t) \\ \cos\theta_2(t) \end{bmatrix} \\ \begin{bmatrix} \dot{\theta}_1(t) \\ \dot{\theta}_2(t) \end{bmatrix} &= \boldsymbol{u}(t), \end{aligned} \tag{11}$$

où $\boldsymbol{x}$ indique la position du centre de masse de l'agent, et θ_1 et θ_2 sont les angles de lacet et de tangage respectivement ; l'angle de cap est contrôlé par la commande $\boldsymbol{u}$ qui dirige la vitesse angulaire. Un tel choix pour la dynamique du véhicule peut représenter, en trois dimensions, un modèle simplifié d'un véhicule sous-marin autonome.

Nous aimerions réaliser un algorithme du gradient en utilisant les formules de Poisson obtenus dans la section précédente. Notre objectif est de suivre le gradient de la fonction du signal $\nabla f(\boldsymbol{x}(t))$, mais nous considérons le cas où il est possible de contrôler la vitesse angulaire seulement, et non pas changer instantanément l'orientation du véhicule. Ainsi, nous définissons les références de la commande comme les orientations donnés par la direction du gradient estimé à l'actuel centre de masse du véhicule $\boldsymbol{x}(t)$:

$$\begin{aligned} \theta_1^{\mathrm{r}}(\boldsymbol{x}(t)) &= \arctan \frac{g_2(\boldsymbol{x}(t))}{g_1(\boldsymbol{x}(t))} \\ \theta_2^{\mathrm{r}}(\boldsymbol{x}(t)) &= \arccos \frac{g_3(\boldsymbol{x}(t))}{\|\boldsymbol{g}(\boldsymbol{x}(t))\|}, \end{aligned}$$

où $\boldsymbol{g}(\boldsymbol{x}(t)) = \widehat{\nabla f}(\boldsymbol{x}(t))$ est l'approximation du gradient, de sorte que les références sont des approximations des angles du gradient. Ensuite, nous

définissons une loi de commande avec une terme impliquant la dérivée temporelle des références :

$$\boldsymbol{u}(t) = k \begin{bmatrix} \theta_1^{\mathrm{r}}(\boldsymbol{x}(t)) - \theta_1(t) \\ \theta_2^{\mathrm{r}}(\boldsymbol{x}(t)) - \theta_2(t) \end{bmatrix} + \begin{bmatrix} \dot{\theta}_1^{\mathrm{r}}(\boldsymbol{x}(t)) \\ \dot{\theta}_2^{\mathrm{r}}(\boldsymbol{x}(t)) \end{bmatrix}. \tag{12}$$

De manière analogue au cas 2D, les expressions de la dérivée des références de cap peuvent être calculés comme

$$\begin{aligned} \dot{\theta}_1^{\mathrm{r}}(\boldsymbol{x}(t)) &= \frac{\boldsymbol{B}\hat{\boldsymbol{H}}\big(\boldsymbol{x}(t)\big)\boldsymbol{A}\boldsymbol{g}\big(\boldsymbol{x}(t)\big) \cdot \dot{\boldsymbol{x}}(t)}{\|\boldsymbol{A}\boldsymbol{g}\big(\boldsymbol{x}(t)\big)\|^2} \\ \dot{\theta}_2^{\mathrm{r}}(\boldsymbol{x}(t)) &= \frac{g_3\big(\boldsymbol{x}(t)\big)\hat{\boldsymbol{H}}\big(\boldsymbol{x}(t)\big)\boldsymbol{g}\big(\boldsymbol{x}(t)\big) - \|\boldsymbol{g}\big(\boldsymbol{x}(t)\big)\|^2\hat{\boldsymbol{H}}\big(\boldsymbol{x}(t)\big)\boldsymbol{a}}{\|\boldsymbol{A}\boldsymbol{g}\big(\boldsymbol{x}(t)\big)\|}, \end{aligned} \tag{13}$$

où $\boldsymbol{A}$, $\boldsymbol{B}$ et $\boldsymbol{a}$ sont les matrices suivantes :

$$\boldsymbol{A} = \begin{bmatrix} 0 & -1 & 0 \\ 1 & 0 & 0 \\ 0 & 0 & 0 \end{bmatrix}, \qquad \boldsymbol{B} = \begin{bmatrix} 1 & 0 & 0 \\ 0 & 1 & 0 \\ 0 & 0 & 0 \end{bmatrix}, \qquad \boldsymbol{a} = \begin{bmatrix} 0 \\ 0 \\ 1 \end{bmatrix}.$$

Détails d'implémentation

Calcul des dérivées

Les expressions de l'approximation du gradient $\boldsymbol{g}$ et de l'hessienne $\hat{\boldsymbol{H}}$ de la fonction f utilisée dans les équations (13) peuvent être obtenues à partir des équations (5), considérant que, en utilisant les coordonnées sphériques

$$\boldsymbol{r} = r \begin{bmatrix} \cos\gamma \sin\varphi \\ \sin\gamma \sin\varphi \\ \cos\varphi \end{bmatrix},$$

où $\gamma \in [0, 2\pi)$ et $\varphi \in [0, \pi]$ sont respectivement l'azimut et l'angle d'altitude, nous avons $n = 3$, $\Omega_3 = 4\pi$ et $\mathrm{d}S = r^2 \sin\varphi \,\mathrm{d}\gamma \,\mathrm{d}\varphi$, de sorte que les

équations (5) prennent la forme

$$\begin{aligned} f\big(\boldsymbol{x}(t)\big) &= \frac{1}{4\pi}\int_0^{\pi}\sin\varphi\int_0^{2\pi} f(\bar{\boldsymbol{x}}(\gamma,\varphi))\,\mathrm{d}\gamma\,\mathrm{d}\varphi \\ \nabla f\big(\boldsymbol{x}(t)\big) &= \frac{3}{4\pi r}\int_0^{\pi}\sin\varphi\int_0^{2\pi} \hat{\boldsymbol{r}}(\gamma,\varphi) f(\bar{\boldsymbol{x}}(\gamma,\varphi))\,\mathrm{d}\gamma\,\mathrm{d}\varphi \\ \boldsymbol{H}\big(\boldsymbol{x}(t)\big) &= \frac{5}{4\pi r^2}\int_0^{\pi}\sin\varphi\int_0^{2\pi} \boldsymbol{H}_P(\gamma,\varphi) f(\bar{\boldsymbol{x}}(\gamma,\varphi))\,\mathrm{d}\gamma\,\mathrm{d}\varphi, \end{aligned} \tag{14}$$

où

$$\begin{aligned} \boldsymbol{H}_P(\gamma,\varphi) &= 3\hat{\boldsymbol{r}}(\gamma,\varphi)\hat{\boldsymbol{r}}^{\mathsf{T}}(\gamma,\varphi) - \mathbf{I} = \\ &= \begin{bmatrix} 3\cos^2\gamma\sin^2\varphi - 1 & 3\cos\gamma\sin\gamma\sin^2\varphi & 3\cos\gamma\cos\varphi\sin\varphi \\ 3\cos\gamma\sin\gamma\sin^2\varphi & 3\sin^2\gamma\sin^2\varphi - 1 & 3\sin\gamma\cos\varphi\sin\varphi \\ 3\cos\gamma\cos\varphi\sin\varphi & 3\sin\gamma\cos\varphi\sin\varphi & 3\cos^2\varphi - 1 \end{bmatrix}. \end{aligned}$$

Dispositif de détection

Pour le calcul des intégrales, nous considérons une approximation convenable avec une somme discrète d'un nombre fini de mesures. Compte tenu d'un nombre total de capteurs N, nous voulons les placer le long de bandes circulaires avec une égale largeur angulaire ζ, d'une manière qui nous donne un maillage de la surface de la sphère avec des éléments presque réguliers ; il en résulte $N_{\mathrm{p}} = \left[\frac{\sqrt{\pi N}}{2}\right]$ parallèles centrées à des latitudes

$$\varphi_i = (i - 0.5)\zeta, \quad i = 1, 2, \ldots, N_{\mathrm{p}},$$

où les crochets indiquent l'arrondi à l'entier le plus proche et où $\zeta = \frac{\pi}{N_{\mathrm{p}}}$. Tout au long de chaque parallèle on place un certain nombre N_i de capteurs qui diminue avec la distance à l'équateur, de manière à éviter une accumulation de capteurs proches des pôles ; ainsi, chaque capteur a une position azimutale de

$$\gamma_{i,j} = j\Delta\gamma_i = j\frac{2\pi}{N_i},$$

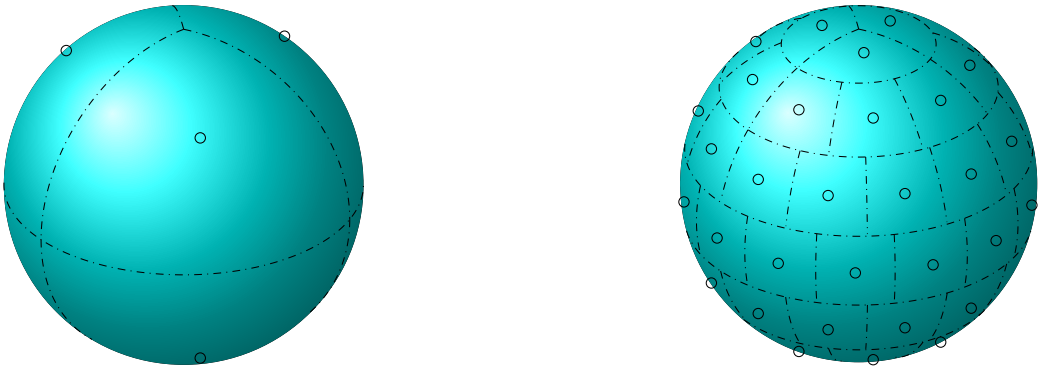

(A) $N = 6$ capteurs (qui correspond à $\zeta = 90°$).

(B) $N = 64$ capteurs (qui correspond à $\zeta = 25,7°$).

Figure 11. Placement des capteurs sur l'appareil sphérique.

où $N_i = \left[2N_\mathrm{p} \sin \varphi_i\right]$. Comme le montre la figure 11 pour deux valeurs différentes de ζ (plus précisément, pour $N = 6$ et $N = 64$), chaque capteur occupe le centre d'un élément dans une position

$$\boldsymbol{x}_{i,j} = \boldsymbol{x}^\mathbf{c} + \boldsymbol{r}_{i,j} = \boldsymbol{x}^\mathbf{c} + r \begin{bmatrix} \cos \gamma_{i,j} \sin \varphi_i \\ \sin \gamma_{i,j} \sin \varphi_i \\ \cos \varphi_i \end{bmatrix}.$$

Approximation des dérivées

Pour un tel choix de la position des capteurs, il est maintenant possible de calculer les valeurs approximatives pour (14) : désignant la mesure du capteur (i, j) avec

$$\hat{f}_{i,j}\big(\boldsymbol{x}(t), t\big) = f\big(\boldsymbol{x}_{i,j}(t)\big) + e_{i,j}^{(f)}(t),$$

où $e_{i,j}^{(f)}$ est l'erreur de mesure affectant le capteur (i, j) au temps t, nous pouvons proposer les formules approximatives suivantes :

$$\hat{f}\big(\boldsymbol{x}(t), t\big) = \frac{\zeta}{4N_\mathrm{p}} \sum_{i=1}^{N_\mathrm{p}} \sum_{j=1}^{N_i} \hat{f}_{i,j}\big(\boldsymbol{x}(t), t\big)$$

$$\widehat{\nabla f}\big(\boldsymbol{x}(t),t\big) = \frac{3\zeta}{4N_{\mathrm{p}}r}\sum_{i=1}^{N_{\mathrm{p}}}\sum_{j=1}^{N_i}\hat{\boldsymbol{r}}_{i,j}\hat{f}_{i,j}\big(\boldsymbol{x}(t),t\big)$$

$$\hat{\boldsymbol{H}}\big(\boldsymbol{x}(t),t\big) = \frac{5\zeta}{4N_{\mathrm{p}}r^2}\sum_{i=1}^{N_{\mathrm{p}}}\sum_{j=1}^{N_i}(3\hat{\boldsymbol{r}}_{i,j}\hat{\boldsymbol{r}}_{i,j}^{\mathsf{T}} - \mathbf{I})\hat{f}_{i,j}\big(\boldsymbol{x}(t),t\big).$$

Analyse de convergence

Dans ce qui suit nous étudions la convergence de notre algorithme. Nous considérons le problème résolu, et parlons de *convergence*, si le véhicule touche la frontière de la source, ou l'approche pour $t \to \infty$, comme indiqué dans la définition suivante.

Definition (Convergence à la source). Soit l'emplacement de la source un point $\boldsymbol{x}_{\mathrm{s}} \in D_{\mathrm{s}}$, avec

$$D_{\mathrm{s}}\colon f(\boldsymbol{x}) = f_{\mathrm{s}} = \max_{\boldsymbol{x}\in\bar{D}} f(\boldsymbol{x}), \quad \forall \boldsymbol{x} \in \partial D_{\mathrm{s}}.$$

Une trajectoire $\boldsymbol{x}(t)$ est dite convergente à la source si l'une des conditions suivantes est vraie :

$$\exists t_{\mathrm{s}} < \infty \text{ tel que } \boldsymbol{x}(t_{\mathrm{s}}) \in \partial D_{\mathrm{s}}$$
$$\lim_{t\to\infty} \operatorname{dist}(\boldsymbol{x}(t), \partial D_{\mathrm{s}}) = 0. \qquad \bullet$$

Nous pouvons prouver la convergence de notre loi de contrôle de localisation de source indiquée ci-dessous.

Proposition 3 (Convergence globale de l'algorithme de localisation de source). Soit $D = \mathbb{R}^3 \setminus \bar{D}_{\mathrm{s}}$, et soit f une fonction harmonique dans D, continue sur $\bar{D}$ et à sous-niveaux compacts $D_g = \{\, \boldsymbol{x} \in \bar{D}\colon f(\boldsymbol{x}) \le g \,\}$. Considérons le système (11) sous la loi de contrôle (12), où les références sont données par les orientations de $\nabla f(\boldsymbol{x}(t))$. Alors, le système converge vers la source dans le sens de la définition précédente. $\bullet$

Le résultat de la proposition tient également si θ_1^{r} et θ_2^{r} sont des esti-

mations perturbées des angles de gradient, c'est-à-dire,

$$\theta_1^{\mathrm{r}}\big(\boldsymbol{x}(t),t\big) = \theta_1^{(\nabla f)}\big(\boldsymbol{x}(t)\big) + e_{\theta_1}(t)$$
$$\theta_2^{\mathrm{r}}\big(\boldsymbol{x}(t),t\big) = \theta_2^{(\nabla f)}\big(\boldsymbol{x}(t)\big) + e_{\theta_2}(t),$$

avec e_{θ_1} et e_{θ_1} étant les incertitudes, continues sur $\bar{D}$ et différentiables dans D, et telles que $|e_{\theta_1}(t)| + |e_{\theta_1}(t)| \leq \tilde{e} < \frac{\pi}{2}$.

Résultats de simulation

L'algorithme proposé a été simulé sur un scénario donné par la diffusion d'une source isotrope émettant à une vitesse constante dans un domaine non borné, un modèle simplifié d'une fuite de polluant sous-marine, dans laquelle un dispositif de détection est à la recherche de la source dont le signal se dégrade selon l'expression

$$f(\boldsymbol{x}) = \frac{a}{\|\boldsymbol{x} - \boldsymbol{x}_{\mathrm{s}}\|_2},$$

où $\boldsymbol{x}_{\mathrm{s}}$ est la position de la source, et a est un coefficient dont le choix influe sur l'amplitude du signal.

Le véhicule, qui n'a pas de connaissances sur $f(\boldsymbol{x})$, a une vitesse constante $v = 0,1$ m/s, et le paramètre de commande est réglé à $k = 0,95$; son orientation initiale est choisie telle que $\theta_1(0) = \arctan\frac{x_2(0)}{x_1(0)}$ et $\theta_2(0) = \arccos\frac{x_3(0)}{\|\boldsymbol{x}(0)\|}$, et les vitesses angulaires initiales telles que $\dot{\theta}_1(0) = \dot{\theta}_2(0) = 0$. L'amplitude de la fonction de signal est $a = 25$.

La figure 12 A montre un exemple des trajectoires, pour le même point de départ et trois valeurs différentes de N.

Nous considérons maintenant le cas où chaque capteur donne une mesure du signal émis corrompu par le bruit. Nous pouvons voir sur la figure 12 B les trajectoires résultantes d'une simulation avec $N = 12$, $r = 1\,\mathrm{m}$ et quelques différentes valeurs de σ. Nous pouvons voir que, excepté l'oscillation due au bruit, les véhicules s'installent sur une petite boule centrée sur la source.

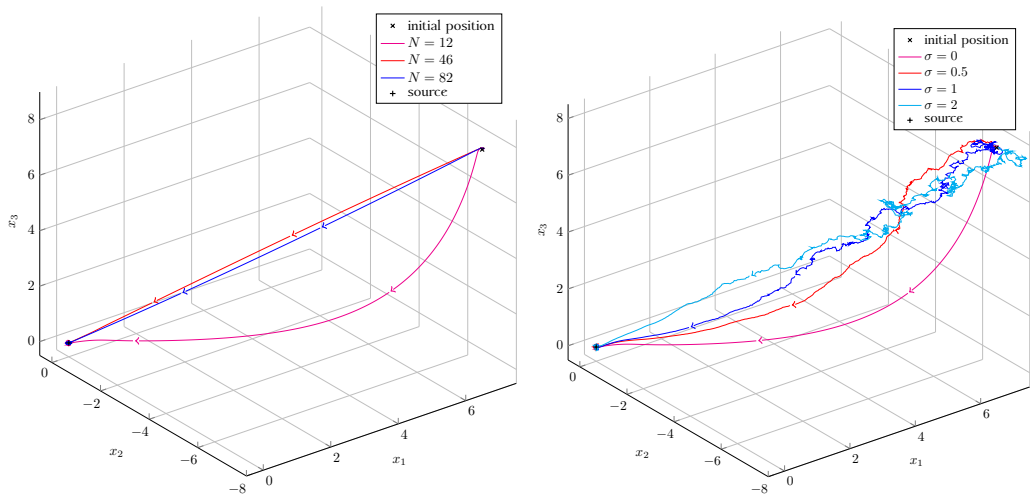

(A) N variants **(B)** $N = 12, \sigma$ variante

Figure 12. Trajectoires du véhicule de recherche de sources 3D pour nombres différents de capteurs et valeurs différentes de l'écart type du bruit.

Recherche de sources distribuée

Nous présentons ici une loi de contrôle distribuée pour diriger un groupe de capteurs communicants autonomes vers la source d'un processus de diffusion, sur la base des mêmes hypothèses définies précédemment. Nous supposons avoir un ensemble de capteurs (tous les capteurs sont autonomes en mouvement, et ils ne sont pas organisés de façon fixe comme dans les sections précédentes), et supposons que chaque capteur est capable de mesurer, en plus de la quantité de diffusion d'intérêt, seulement l'angle de gisement par rapport à son voisin, mais n'a pas d'informations de position absolue, et ne connaît pas la distance relative ; les capteurs peuvent communiquer les uns aux autres, et le graphique décrivant les liens de communication a une topologie en anneau invariant dans le temps.

Formulation du problème

Nous considérons un groupe de N capteurs autonomes communicants qui se déplacent dans une région $D \subset \mathbb{R}^2$ où un processus de diffusion se

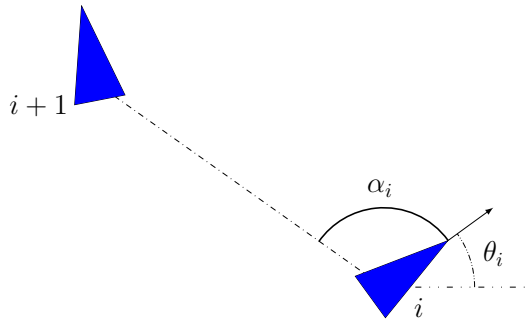

Figure 13. Représentation graphique de l'angle de gisement rélatif α_i.

déroule. La dynamique de chaque capteur est décrite par le modèle non linéaire monocycle

$$\begin{aligned} \dot{\boldsymbol{x}}_i(t) &= v_i(t) \begin{bmatrix} \cos\theta_i(t) \\ \sin\theta_i(t) \end{bmatrix} \\ \begin{bmatrix} v_i(t) \\ \dot{\theta}_i(t) \end{bmatrix} &= \boldsymbol{u}_i(t); \end{aligned} \tag{15}$$

où $\boldsymbol{x}_i$ représente la position du capteur dans le plan, et $\theta_i(t)$ est son angle de cap.

Les capteurs, qui peuvent prendre des mesures ponctuelles de la quantité émise, ne possèdent aucune information de position, mais connaissent la valeur de N et sont capables de mesurer l'angle de roulement par rapport à leur voisin suivant, c'est-à-dire l'angle entre l'orientation d'un agent et le vecteur liant sa position à celle de son voisin, comme expliqué dans la figure 13, défini par

$$\alpha_i(t) = \arg\left(\boldsymbol{x}_{i+1}(t) - \boldsymbol{x}_i(t)\right) - \theta_i(t). \tag{16}$$

Conception de la rétroaction

Nous devons développer un algorithme qui est capable à la fois d'orienter les capteurs vers la direction du gradient, et de les amener sur une

formation circulaire, de sorte que le gradient lui-même est estimé correctement.

Nous introduisons une loi de commande en supposant que chaque capteur i est capable de calculer la différence

$$\tilde{\theta}_i(t) = \theta^{\mathrm{r}}(t) - \theta_i(t),$$

où θ^{r} est une référence commune (nous discuterons après comment l'obtenir). Soient $v_{\mathrm{c}} > 0$ et $v_{\mathrm{r}} > v_{\mathrm{c}}$, avec $\tilde{v} = \frac{v_{\mathrm{c}}}{v_{\mathrm{r}}}$, des paramètres fixes ; nous proposons la loi de commande suivante :

$$\boldsymbol{u}_i(t) = \begin{bmatrix} v_i(t) \\ \dot{\theta}_i(t) \end{bmatrix} = \begin{bmatrix} v_{\mathrm{c}} \cos\tilde{\theta}_i(t) + \sqrt{v_{\mathrm{r}}^2 - v_{\mathrm{c}}^2 \sin^2\tilde{\theta}_i(t)} \\ b_i(t)\dot{\theta}^{\mathrm{r}}(t) + \big(1 - b_i(t)\big)\omega_i(t) \end{bmatrix}, \tag{17 A}$$

où

$$b_i(t) = \frac{v_{\mathrm{c}}}{v_i(t)} \cos\tilde{\theta}_i(t) \tag{17 B}$$

$$\omega_i(t) = k\Big(\alpha_i(t) + \arcsin\big(\tilde{v}\sin\tilde{\theta}_i(t)\big)\Big), \tag{17 C}$$

$k > 0$ est une constante de gain positive, et α_i est défini comme dans (16). Nous notons que cette loi de commande ne concerne que des variables locales, car elle est fonction seulement de l'angle de gisement mesuré et de l'angle $\tilde{\theta}_i$, qui est une différence d'angles et donc indépendant du système de coordonnées.

Nous donnons par la suite des propositions, que nous fournissons ici sans démontration, qui montrent comme cette loi de commande est effectivement capable d'amener les capteurs vers une formation circulaire qui bouge à sa fois vers la source en suivant le gradient du processus de diffusion.

Proposition 4. Le système en boucle fermée avec dynamique (15) et loi

de commande (17 A–17 B) est équivalent au système

$$\begin{aligned}\dot{\boldsymbol{x}}_i(t) &= v_{\mathrm{c}} \begin{bmatrix} \cos\theta^{\mathrm{r}}(t) \\ \sin\theta^{\mathrm{r}}(t) \end{bmatrix} + v_{\mathrm{r}} \begin{bmatrix} \cos\eta_i(t) \\ \sin\eta_i(t) \end{bmatrix} \\ \dot{\eta}_i(t) &= \omega_i(t). \qquad \bullet\end{aligned} \tag{18}$$

Convergence à la formation et mouvement de l'algorithme du gradient du centroïde de la formation

Prenons une flotte de véhicules sous-actionnés autonomes décrits par la dynamique (18). Par un changement adéquat de coordonnées, chaque sous-système peut être décrit par les nouvelles variables d'état

$$\begin{aligned} d_i(t) &= \|\boldsymbol{x}_{i+1}(t) - \boldsymbol{x}_i(t)\| \\ \tilde{\alpha}_i(t) &= \arg\big(\boldsymbol{x}_{i+1}(t) - \boldsymbol{x}_i(t)\big) - \eta_i(t) \\ \tilde{\beta}_i(t) &= \eta_i(t) - \eta_{i+1}(t) - \pi. \end{aligned} \tag{19}$$

Proposition 5. Pour le système (18), avec $\omega_i(t)$ comme dans (17 C), la dynamique dans les variables d'état (19) est

$$\begin{aligned} \dot{d}_i(t) &= -v_{\mathrm{r}}\Big(\cos\tilde{\alpha}_i(t) + \cos\big(\tilde{\alpha}_i(t) + \tilde{\beta}_i(t)\big)\Big) \\ \dot{\tilde{\alpha}}_i(t) &= \frac{v_{\mathrm{r}}\Big(\sin\tilde{\alpha}_i(t) + \sin\big(\tilde{\alpha}_i(t) + \tilde{\beta}_i(t)\big)\Big)}{d_i(t)} - k\tilde{\alpha}_i(t) \\ \dot{\tilde{\beta}}_i(t) &= k\big(\tilde{\alpha}_i(t) - \tilde{\alpha}_{i+1}(t)\big). \qquad \bullet \end{aligned} \tag{20}$$

Corollaire 2. Chaque système (19) a $2N-1$ points d'équilibre, parmi lesquels les deux localement asymptotiquement stables décrits par

$$\begin{aligned} \bar{d}_i &= \bar{d} = \frac{2v_{\mathrm{r}}}{k\bar{\alpha}}\sin\bar{\alpha} \\ \bar{\tilde{\alpha}}_i &= \bar{\alpha} = \pm\frac{\pi}{N} \\ \bar{\tilde{\beta}}_i &= \bar{\beta} = \pi - 2\bar{\alpha}. \qquad \bullet \end{aligned} \tag{21}$$

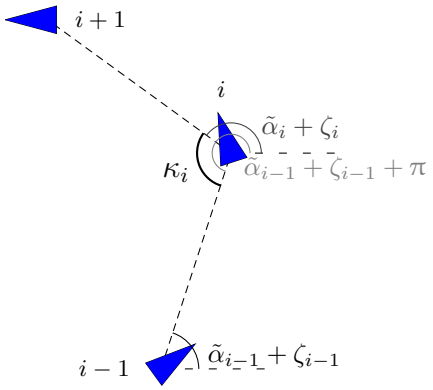

Figure 14. Représentation de l'angle interne κ_i entre capteurs consécutifs.

Proposition 6. Aux équilibres (21), les positions relatives $\boldsymbol{x}_{i+1}(t) - \boldsymbol{x}_i(t)$ dessinent un polygone régulier ordinaire (figure 14). •

Proposition 7. Si les conditions initiales des agents sont tels que le système correspondant (20) est dans le bassin attrayant de l'un des deux équilibres localement asymptotiquement stables (21), alors

$$\arg \dot{\boldsymbol{x}}^{\mathrm{c}}(t) - \theta^{\mathrm{r}}(t) \to 0. \qquad \bullet$$

Mise en œuvre distribuée

Nous discutons ici comment mettre en œuvre la loi de contrôle proposée précédemment.

L'algorithme est conçu pour utiliser les informations recueillies par chaque capteur et produire, de manière distribuée, une approximation discrète de la formule intégrale (8 B), c'est-à-dire pour calculer la somme de Riemann

$$\widehat{\nabla f}\big(\boldsymbol{x}^{\mathrm{c}}(t)\big) = \frac{2}{Nr^2} \sum_{i=1}^{N} f\big(\boldsymbol{x}_i(t)\big)\big(\boldsymbol{x}_i(t) - \boldsymbol{x}^{\mathrm{c}}(t)\big),$$

qui est équivalent à la (9 B), et puis obtenir la différence $\tilde{\theta}_i(t) = \theta^{\mathrm{r}}(t) - \theta_i(t)$, où idéalement $\theta^{\mathrm{r}}(t) = \arg \widehat{\nabla f}(\boldsymbol{x}^{\mathrm{c}}(t))$ (la difficulté réside dans le fait que le vecteur $\boldsymbol{x}_i(t) - \boldsymbol{x}^{\mathrm{c}}(t)$ n'est pas directement disponible, comme nous avons

supposé ne pas avoir toute information de position) ; nous proposons la technique suivante.

Au cours de chaque intervalle de temps $(t,\ t+\Delta t)$, avec Δt suffisamment long, chaque capteur i effectue $h = 1, 2, \ldots, N-1$ itérations qui impliquent un échange de messages avec ses voisins précédant et suivant : chaque capteur i reçoit la valeur actuelle calculée par ses prédécesseurs, la tourne d'un angle $\frac{2\pi}{N}$, ajoute sa propre mesure $f(\boldsymbol{x}_i)$ et l'envoie à son successeur. Les détails sont présentés dans l'algorithme ci-dessous.

Dans la suite nous supposerons par simplicité d'être dans la région attractive de l'équilibre avec $\bar{\alpha} > 0$, c'est-à-dire une rotation dans le sens antihoraire (cette hypothèse est justifiée par la propriété de stabilité locale des équilibres, ce qui justifie aussi le choix d'une topologie en anneau invariant dans le temps pour le graphique de la communication), par conséquent nous allons utiliser un angle de $\lambda = -\frac{2\pi}{N}$. De toute manière, une mise en œuvre générale serait d'avoir un angle de rotation en fonction de l'angle de gisement courant mesuré, c'est-à-dire $\lambda_i(t) = -\operatorname{sign}\big(\alpha_i(t)\big)\frac{2\pi}{N}$.

Algorithme Recherche de sources distribuée

$\boldsymbol{g}_i(0) = \begin{bmatrix} f(\boldsymbol{x}_i) \\ 0 \end{bmatrix}$ {initialisation}
for $h = 1, 2, \ldots, N-1$ **do**
  $\boldsymbol{g}_i(h) \leftarrow \boldsymbol{g}_{i-1}(h-1)$ {nœud i reçoit de $i-1$}
  $\boldsymbol{g}_i(h) \leftarrow \begin{bmatrix} \cos\lambda & \sin\lambda \\ -\sin\lambda & \cos\lambda \end{bmatrix} \boldsymbol{g}_i(h) + \begin{bmatrix} f(\boldsymbol{x}_i) \\ 0 \end{bmatrix}$ {mise à jour}
end for
$\theta_i^{\mathrm{r}} = \arg \boldsymbol{g}_i(N-1)$
$\delta_i = -\arctan \frac{v_{\mathrm{c}} \cos\theta_i^{\mathrm{r}}}{v_{\mathrm{r}} + v_{\mathrm{c}} \sin\theta_i^{\mathrm{r}}}$
$\tilde{\theta}_i = \theta_i^{\mathrm{r}} - \delta_i - \frac{\pi}{2}$

Nous allons montrer, dans la proposition suivante, l'efficacité de l'algorithme proposé si les capteurs sont déjà à l'équilibre.

Proposition 8. Si les N capteurs décrits par la dynamique (20) sont à l'équilibre (21) avec $\bar{\alpha} > 0$, alors $\tilde{\theta}_i$ calculé avec l'algorithme précédant

correspond à la différence

$$\tilde{\theta}_i(t) = \arg \widehat{\nabla f}(\boldsymbol{x}^{\mathrm{c}}(t)) - \theta_i(t). \qquad \bullet$$

Comme on peut le remarquer, cet algorithme ne donne l'argument de l'approximation de gradient correcte que lorsque les capteurs sont en formation ; autrement, non seulement θ_i^{r} n'est pas assuré d'être une bonne approximation de l'argument du gradient, mais il n'est même pas une référence commune, c'est-à-dire $\tilde{\theta}_i(t) + \theta_i(t)$ n'est pas le même pour tous les i. Cela contredit l'hypothèse que nous avons faite sur la référence θ^{r} identique pour tous les capteurs ; néanmoins, nous avons proposé cette mise en œuvre pour sa simplicité, car elle montre un bon comportement dans les simulations (et il est facile de fournir un autre algorithme pour assurer une référence commune θ^{r} pour chaque capteur i).

Simulations

Pour valider notre algorithme nous considérons la recherche d'une source de chaleur dans un espace à 2 dimensions 20×12 m de large ; les frontières sont considérées comme parfaitement isolantes, et nous supposons avoir une ouverture qu'impose une température extérieure de $f_{\mathrm{ex}} = 5$ °C, et un réchauffeur circulaire de $f_{\mathrm{s}} = 50$ °C au milieu.

Nous considérons un ensemble de $N = 5$ capteurs avec une dynamique (15) et la loi de contrôle décrite dans (5.3), partant de positions initiales aléatoires et avec des orientations initiales aléatoires, et des vitesses de $v_{\mathrm{r}} = 0,5$ et $v_{\mathrm{c}} = 0,1$ m/s ; la valeur de la constante de commande est choisie de telle sorte à avoir un rayon de formation de $r = 50$ cm, c'est-à-dire $k = \frac{Nv_{\mathrm{r}}}{\pi r} \approx 1,5915$.

La figure 15 montre le résultat de certaines simulations. Nous pouvons voir les trajectoires des capteurs ainsi que l'une de leurs centroïdes (en noir) ; les triangles bordés de blanc représentent les conditions initiales de chaque capteur, tandis que ceux bordés de noir montrent leur position et l'orientation lorsque la formation a atteint le réchauffeur (le cercle rouge

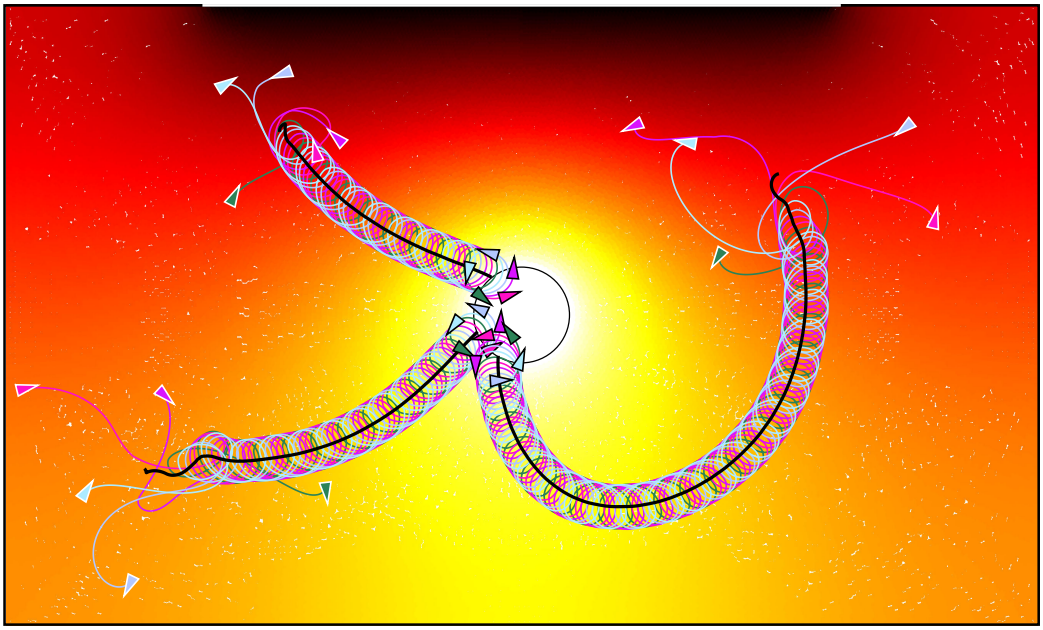

Figure 15. Résultats de simulations pour conditions initiales aléatoires ; les triangles bordées de blanc représentent les conditions initiales, ceux bordées de noir les conditions définitives.

au milieu). Les capteurs atteignent rapidement une configuration circulaire, puis continuent à se déplacer vers la source qui suit le gradient du champ. Les trajectoires des centroïdes des formations ne sont pas exactement alignées avec l'argument du gradient en raison de l'approximation discrète en arrière de la dérivée temporelle de la référence $\dot{\theta}^{\mathrm{r}}$. La figure 16 montre des simulations pour les mêmes conditions initiales, avec à la fois les mesures de température et de l'angle de roulement corrompues par un bruit blanc gaussien d'écart type $\sigma = 0,5$.

De l'analyse des résultats de simulations nous pouvons remarquer aussi que, même si la convergence théorique est locale, l'algorithme a démontré être efficace aussi pour des conditions initiales aléatoires ; en outre, malgré la demande théorique d'avoir la même référence commune pour chaque capteur, il n'y a pas de différence pratique entre les deux algorithmes : comme nous pouvons le voir, les centroïdes de la formation suivent le gradient (même avec l'écart introduit par l'approximation discrète et le bruit) même en utilisant l'algorithme qui ne satisfait pas cette hypothèse.

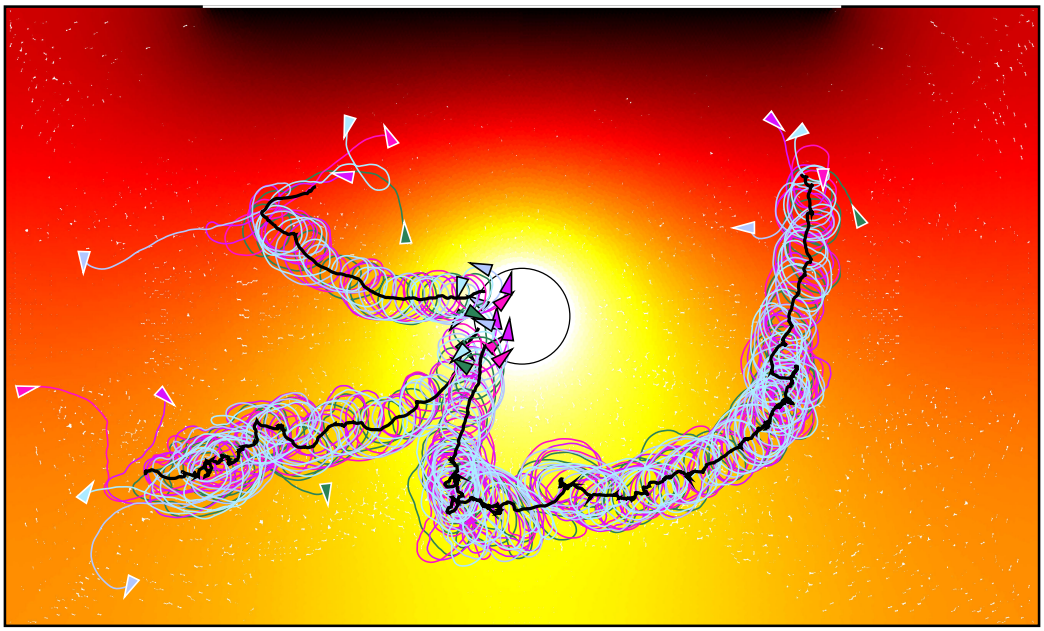

Figure 16. Résultats de simulations pour conditions initiales aléatoires et mesures bruitées ; les triangles bordées de blanc représentent les conditions initiales, ceux bordées de noir les conditions définitives.

Bibliography

[1] K. B. Ariyur and M. Krstić, *Real-Time Optimization by Extremum-Seeking Control*; Wiley-Interscience, John Wiley and Sons, 2003.

[2] K. J. Åstrom and B. Wittenmark, *Adaptive Control*; Addison Wesley, 1995.

[3] S. Axler, P. Bourdon and W. Ramey, *Harmonic Function Theory*; Springer-Verlag, New York (USA), 2001.

[4] R. Bachmayer and N. E. Leonard, "Vehicle Networks for Gradient Descent in a Sampled Environment", *Proceedings of the 41st IEEE Conference on Decision and Control (CDC)*, pp. 112–117; Las Vegas (USA), December 2002.

[5] H. Bai, M. Arcak and J. Wen, *Cooperative Control Design*; Springer, 2011.

[6] D. Baronov and J. Baillieul, "Autonomous Vehicle Control for Ascending/Descending along a Potential Field with Two Applications", *Proceedings of the 2008 American Control Conference (ACC)*, pp. 678–683; Seattle (USA), June 2008.

[7] D. P. Bertsekas and J. Tsitsiklis, *Parallel and Distributed Computation*; Upper Saddle River, 1989.

[8] E. Biyik and M. Arcak, "Gradient Climbing in Formation via Extremum Seeking and Passivity-Based Coordination Rules", *Asian Journal of Control, Special Issue on Collective Behavior and Control of Multi-Agent Systems*, vol. 10 Nº 2, pp. 201–211; March 2008.

[9] V. Borkar and P. Varaiya, "Asymptotic Agreement in Distributed Estimation", *IEEE Transactions on Automatic Control*, vol. 27 Nº 3, pp. 650–655; June 1982.

[10] M. Bowling and M. Veloso, "Multiagent Learning Using a Variable Learning Rate", *Artificial Intelligence*, vol. 136 Nº 2, pp. 215–250; April 2002.

[11] L. Briñón Arranz, *Cooperative Control Design for a Fleet of Autonomous Underwater Vehicles under Communication Constraints*; PhD thesis, Université de Grenoble, Grenoble (France), November 2011.

[12] L. Briñón Arranz, A. Seuret and C. Canudas de Wit, "Collaborative Estimation of Gradient Direction by a Formation of AUVs under Communication Constraints", *Proceedings of the 50th IEEE Conference on Decision and Control (CDC) and 11th EUCA European Control Conference (ECC)*, pp. 5583–5588; Orlando (USA), December 2011.

[13] F. Bullo, J. Cortés and S. Martinez, *Distributed Control of Robotic Networks*; Princeton University Press, 2009.

[14] E. Burian, D. Yoerger, A. Bradley and H. Singh, "Gradient Search with Autonomous Underwater Vehicles Using Scalar Measurements", *Proceedings of the 1996 Symposium on Autonomous Underwater Vehicle Technology*, pp. 86–98; Monterey (USA), June 1996.

[15] D. Chang, W. Wu, D. R. Webster, M. J. Weissburg and F. Zhang, "A Bio-Inspired Plume-Tracking Algorithm for Mobile Sensing Swarms in Tubulent Flow", *Proceedings of the 2013 IEEE International Conference on Robotics and Automation (ICRA)*, pp. 921–926; Karlsruhe (Germany), May 2013.

[16] Y. Q. Chen and Z. Wang, "Formation Control: a Review and a New Consideration.", *Proceedings of the 2005 IEEE/RSJ International Conference on Intelligent Robots and Systems*, pp. 3181–3186; Edmonton (Canada), August 2005.

[17] J. Cochran, N. Ghods and M. Krstić, "3D Nonholonomic Source-Seeking without Position Measurement", *Proceedings of the 2008 American Control Conference (ACC)*, pp. 3518–3523; Seattle (USA), June 2008.

[18] J. Cochran and M. Krstić, "Nonholonomic Source Seeking with Tuning of Angular Velocity", *IEEE Transactions on Automatic Control*, vol. 54 Nº 4, pp. 717–731; April 2009.

[19] J. Cochran and M. Krstić, "Source Seeking with a Nonholonomic Unicyle without Position Measurements and with Tuning of Angular Velocity. Part I: Stability Analysis", *Proceedings of the 46th IEEE Conference on Decision and Control (CDC)*, pp. 6009–6016; New Orleans (USA), December 2007.

[20] J. Cochran, A. A. Siranosian, N. Ghods and M. Krstić, "3-D Source Seeking for Underactuated Vehicles without Position Measurement", *IEEE Transactions on Robotics*, vol. 25 Nº 1, pp. 117–129; February 2009.

[21] J. Cochran, A. A. Siranosian, N. Ghods and M. Krstić, "GPS Denied Source-Seeking for Underactuated Autonomous Vehicles in 3D", *Proceedings of the 2008 IEEE International Conference on Robotics and Automation (ICRA)*, pp. 2228–2233; Pasadena (USA), May 2008.

[22] J. Cochran, A. A. Siranosian, N. Ghods and M. Krstić, "Source Seeking with a Nonholonomic Unicyle without Position Measurements and with Tuning of Angular Velocity. Part II: Applications", *Proceedings of the 46th IEEE Conference on Decision and Control (CDC)*, pp. 1951–1956; New Orleans (USA), December 2007.

[23] J. Cortés, "Achieving Coordination Tasks in Finite Time via Nonsmooth Gradient Flows", *Proceedings of the 44th IEEE Conference on Decision and Control (CDC) and 8th EUCA European Control Conference (ECC)*, pp. 6376–6381; Seville (Spain), December 2005.

[24] X. Cui, C. T. Hardin, R. K. Ragade and A. S. Elmaghraby, "A Swarm Approach for Emission Sources Localization", *Proceedings of the 16th IEEE International Conference on Tools with Artificial Intelligence (ICTAI)*, pp. 424–430; Boca Raton (USA), November 2004.

[25] T. B. Curtin, J. G. Bellingham, J. Catipovic and D. Webb, "Autonomous Oceanographic Sampling Networks", *Oceanography*, vol. 6 Nº 3, pp. 86–94; 1993.

[26] P. Davidsson, "Agent Based Social Simulation: a Computer Science View", *Journal of Artificial Societies and Social Simulation*, vol. 5 Nº 1, January 2002.

[27] P. M. Dower, P. M. Farrell and D. Nešić, "Extremum-Seeking Control of Cascaded Raman Optical Amplifiers", *IEEE Transactions on Control Systems Technology*, vol. 16 Nº 3, pp. 396–407; May 2008.

[28] R. Fabbiano, C. Canudas de Wit and F. Garin, "Distributed Source Localisation with no Position Information", *Proceedings of the 13th EUCA European Control Conference (ECC)*, pp. 569–574; Strasbourg (France), June 2014.

[29] J. Ferber, *Multi-Agent Systems: an Introduction to Distributed Artificial Intelligence*; Addison Wesley Longman, 1999.

[30] E. Fiorelli, P. Bhatta, N. E. Leonard and I. Shulman, "Adaptive Sampling Using Feedback Control of an Autonomous Underwater Glider fleet", *Proceedings of the 13th International Symposium on Unmanned Untethered Submersible Technology*, pp. 1-16; Durham (USA), August 2003.

[31] G. B. Folland, *Introduction to Partial Differential Equations*; Princeton Academic Press, 2nd edition, 1995.

[32] B. Francis, *Distributed Control of Autonomous Mobile Robots* (course notes); September 2011.

[33] Y. Gaudfrin, *Source seeking via Poisson integrals — Practical implementation of a source-localisation set-up*; Master's thesis, University of Bristol, Bristol (England, UK), September 2013.

[34] N. Ghods, P. Frihauf and M. Krstić, "Multi-Agent Deployment in the Plane Using Stochastic Extremum Seeking", *Proceedings of the 49th IEEE Conference on Decision and Control (CDC)*, pp. 5505-5510; Atlanta (USA), December 2010.

[35] N. Ghods and M. Krstić, "Multi-Agent Deployment Around a Source in One Dimension by Extremum Seeking", *Proceedings of the 2010 American Control Conference (ACC)*, pp. 4794-4799; Baltimore (USA), July 2010.

[36] N. Ghods and M. Krstić, "Speed Regulation in Steering-Based Source Seeking", *Automatica*, vol. 46 Nº 2, pp. 452-459; February 2010.

[37] A. T. Hayes, A. Martinoli and R. M. Goodman, "Distributed Odor Source Localization", *IEEE Sensors Journal*, vol. 2 Nº 3, pp. 260-271; June 2002.

[38] F. Hecht, O. Pironneau and A. Le Hyaric, *FreeFem++*, 2004; URL: http://www.freefem.org/ff++/ftp/freefem++doc.pdf.

[39] A. Khapalov, "Source Localization and Sensor Placement in Environmental Monitoring", *International Journal of Applied Mathematics and Computer Science*, vol. 20 Nº 3, pp. 445-458; 2010.

[40] S. Z. Khong, Y. Tan, C. Manzie and D. Nešić, "Multi-Agent Source Seeking via Discrete-Time Extremum Seeking Control", *Automatica*, vol. 50 Nº 9, pp. 2312-2320; September 2014.

[41] M. Krstić and H.-H. Wang, "Stability of Extremum-Seeking Feedback for General Nonlinear Dynamic Systems", *Automatica*, vol. 36 Nº 4, pp. 595-601; April 2000.

[42] N. E. Leonard, D. A. Paley, F. Lekien, R. Sepulchre, D. M. Frantatoni and R. E. Davis, "Collective Motion, Sensor Networks, and Ocean Sampling", *Proceedings of the IEEE*, vol. 95 Nº 1, pp. 48-74; January 2007.

[43] P. Leopardi, "A Partition of the Unit Sphere into Regions of Equal Area and Small Diameter", *Electronic Transactions on Numerical Analysis (ETNA)*, vol. 25, pp. 309-327; 2006.

[44] S.-J. Liu and M. Krstić, "Stochastic Source Seeking for Nonholonomic Unicycle", *Automatica*, vol. 46 Nº 9, pp. 1443-1453; September 2010.

[45] J. A. Marshall, M. E. Broucke and B. A. Francis, "A Pursuit Strategy for Wheeled-Vehicle Formations", *Proceedings of the 42nd IEEE Conference on Decision and Control (CDC)*, pp. 2555-2560; Maui (USA), December 2003.

[46] J. A. Marshall, M. E. Broucke and B. A. Francis, "Formations of Vehicles in Cyclic Pursuit", *IEEE Transactions on Automatic Control*, vol. 49 Nº 11, pp. 1963-1974; November 2004.

[47] J. A. Marshall, M. E. Broucke and B. A. Francis, "Unicycles in Cyclic Pursuit", *Proceedings of the 2004 American Control Conference (ACC)*, pp. 5344-5349; Boston (USA), July 2004.

[48] M. Masbahi and M. Egerstedt, *Graph Theoretic Methods in Multiagent Networks*; Princeton University Press, 2010.

[49] J. Matthes, L. Gröll and H. B. Keller, "Source Localization Based on Pointwise Concentration Measurements", *Sensors and Actuators A: Physical*, vol. 115 Nº 1, pp. 32-37; September 2004.

[50] A. S. Matveev, H. Teimoori and A. V. Savkin, "Navigation of a Unicycle-Like Mobile Robot for Environmental Extremum Seeking", *Automatica*, vol. 47 Nº 1, pp. 85-91; January 2011.

[51] C. G. Mayhew, R. G. Sanfelice and A. R. Teel, "Robust Hybrid Source-Seeking Algorithms Based on Directional Derivatives and Their Approximations", *Proceedings of the 47th IEEE Conference on Decision and Control (CDC)*, pp. 1735-1740; Cancún (Mexico), December 2008.

[52] C. G. Mayhew, R. G. Sanfelice and A. R. Teel, "Robust Source-Seeking Hybrid Controllers for Autonomous Vehicles", *Proceedings of the 2007 American Control Conference (ACC)*, pp. 1185–1190; New York (USA), July 2007.

[53] P. P. Menon and D. Ghose, "Simultaneous Source Localization and Boundary Mapping for Contaminants", *Proceedings of the 2012 American Control Conference (ACC)*, pp. 4174–4179; Montréal (Canada), June 2012.

[54] A. R. Mesquita, J. P. Hespanha and K. Åström, "Optimotaxis: a Stochastic Multi-Agent Optimization Procedure with Point Measurements", *Proceedings of the 11th International Workshop on Hybrid Systems: Computation and Control*, pp. 358–371; Springer, Saint Louis (USA), April 2008.

[55] B. J. Moore and C. Canudas de Wit, "Source Seeking via Collaborative Measurements by a Circular Formation of Agents", *Proceedings of the 2010 American Control Conference (ACC)*, pp. 6417–6422; Baltimore (USA), July 2010.

[56] L. Moreau, R. Bachmayer and N. E. Leonard, "Coordinated Gradient Descent: a Case Study of Lagrangian Dynamics with Projected Gradient Information", *Proceedings of the 2nd IFAC Workshop on Lagrangian and Hamiltonian Methods in Nonlinear Control*, pp. 57–62; Seville (Spain), April 2003.

[57] N. Moshtagh, N. Michael, A. Jadbabaie and K. Daniilidis, "Bearing-Only Control Laws for Balanced Circular Formations of Ground Robots", *Robotics: Science and Systems IV*, pp. 119–126; Zürich (Switzerland), June 2008.

[58] D. Nešić, "Extremum Seeking Control: Convergence Analysis", *European Journal of Control*, vol. 15 Nº 3-4, pp. 331–347; April 2009.

[59] P. Ögren, E. Fiorelli and N. E. Leonard, "Cooperative Control of Mobile Sensor Networks: Adaptive Gradient Climbing in a Distributed Environment", *IEEE Transaction on Automatic Control*, vol. 49 Nº 8, pp. 1292–1302; August 2004.

[60] B. Porat and A. Nehorai, "Localizing Vapor-Emitting Sources by Moving Sensors", *IEEE Transactions on Signal Processing*, vol. 44 Nº 4, pp. 1018–1021; April 1996.

[61] P. Pyk, S. Bermúdez i Badia, U. Bernardet, P. Knüsel, M. Carlsson, J. Gu, E. Chanie, B. S. Hansson, T. C. Pearce and P. F. M. J. Verschure, "An Artificial Moth: Chemical Source Localization Using a Robot-Based Neuronal Model of Moth Optomotor Anemotactic Search", *Autonomous Robots*, vol. 20, pp. 197–213; 8 June 2006.

[62] M. Rabbat and R. Nowak, "Distributed Optimization in Sensor Networks", *Proceedings of the 3rd International Symposium on Information Processing on Sensor Networks*, pp. 20–27; Berkeley (USA), April 2004.

[63] W. Ren and Y. Cao, *Distributed Coordination of Multi-Agent Systems*; Springer, 2011.

[64] E. B. Saffet and A. B. J. Kuijlaars, "Distributing Many Points on a Sphere", *The Mathematical Intelligencer*, vol. 19 Nº 1, pp. 5–11; 1997.

[65] S. S. Sahyoun, S. M. Djouadi and H. Qi, "Dynamic Plume Tracking Using Mobile Sensors", *Proceedings of the 2010 American Control Conference (ACC)*, pp. 2915–2920; Baltimore (USA), June 2010.

[66] M. Stanković and D. Stipanović, "Extremum Seeking under Stochastic Noise and Applications to Mobile Sensors", *Automatica*, vol. 46 Nº 8, pp. 1243–1251; August 2010.

[67] S. H. Strogatz, *Sync: the Emerging Science of Spontaneous Order*; Hachette Books, 2003.

[68] Y. Tan, W. H. Moase, C. Manzie, D. Nešić and I. M. Y. Mareels, "Extremum Seeking from 1922 to 2010", *Proceedings of the 29th Chinese Control Conference (CCC)*, pp. 14–26; Beijing (China), July 2010.

[69] Y. Tan, D. Nešić and I. M. Y. Mareels, "On non-Local Stability Properties of Extremum Seeking Control", *Proceedings of the 16th IFAC World Congress*, pp. 746–760; Prague (Czech Republic), July 2005.

[70] Y. Tan, D. Nešić and I. M. Y. Mareels, "On Stability Properties of a Simple Extremum Seeking Scheme", *Proceedings of the 45th IEEE Conference on Decision and Control (CDC)*, pp. 2807–2812; San Diego (USA), December 2006.

[71] Y. Tan, D. Nešić, I. M. Y. Mareels and A. Astolfi, "On Global Extremum Seeking in the Presence of Local Extrema", *Automatica*, vol. 45 Nº 1, pp. 245–251; January 2009.

[72] W. Truszkowski, H. L. Hallock, C. Rouff, J. Karlin, J. Rash, M. Hinchey and R. Sterritt, *Autonomous and Autonomic Systems: with Applications to Nasa Intelligent Spacecraft Operations and Exploration Systems*, chapter "Swarms in Space Missions", pp. 207–221; Nasa Monographs in Systems and Software Engineering, 2009.

[73] J. N. Tsitsiklis, D. P. Bertsekas and M. Athans, "Distributed Asynchronous Deterministic and Stochastic Gradient Optimization Algorithms", *IEEE Transactions on Automatic Control*, vol. 31 Nº 9, pp. 803–812; September 1986.

[74] H.-H. Wang, S. Yeaung and M. Krstić, "Experimental Application of Extremum Seeking on an Axial-Flow Compressor", *IEEE Transactions on Control Systems Technology*, vol. 8 Nº 2, pp. 300–309; 2000.

[75] D. R. Webster, K. Y. Volyanskyy and M. J. Weissburg, "Bioinspired Algorithm for Autonomous Sensor-Driven Guidance in Turbulent Chemical Plumes", *Bioinspiration & Biomimetics*, vol. 7 Nº 3, pp. 23–36; June 2012.

[76] W. Wu, D. Chang and F. Zhang, "A Bio-Inspired Robust 3D Plume-Tracking Strategy Using Mobile Sensor Networks", *Proceedings of the 52nd IEEE Conference on Decision and Control (CDC)*, pp. 4571–4578; Florence (Italy), December 2013.

[77] W. Wu, I. D. Couzin and F. Zhang, "Bio-Inspired Source Seeking with no Explicit Gradient Estimation", *Proceedings of the 3rd Ieac Workshop on Distributed Estimation and Control in Networked Systems (Necsys)*, pp. 240–245; Santa Barbara (USA), September 2012.

[78] D. Zarzhitsky, D. F. Spears and W. Spears, "Swarms for Chemical Plume Tracing", *Proceedings of the 2005 IEEE Swarm Intelligence Symposium*, pp. 249–256; Pasadena (USA), June 2005.

[79] C. Zhang, D. Arnold, N. Ghods, A. A. Siranosian and M. Krstić, "Source Seeking with Nonholonomic Unicycle without Position Measurement and with Tuning of Forward Velocity", *Systems & Control Letters*, vol. 56 Nº 3, pp. 245–252; March 2007.

[80] C. Zhang, D. Florêncio, D. E. Ba and Z. Zhang, "Maximum Likelihood Sound Source Localization and Beamforming for Directional Microphone Arrays in Distributed Meetings", *IEEE Transactions on Multimedia*, vol. 10 Nº 3, pp. 538–548; April 2008.

[81] C. Zhang and R. Ordóñez, "Numerical Optimization-Based Extremum Seeking Control with Application to ABS Design", *IEEE Transactions on Automatic Control*, vol. 52 Nº 3, pp. 454–467; March 2007.

[82] F. Zhang and N. E. Leonard, "Cooperative Filters and Control for Cooperative Exploration", *IEEE Transactions on Automatic Control*, vol. 5 Nº 3, pp. 650–663; January 2010.

[83] B. Zuo, W.-A. Hu and J. Li, "PID Controller Tuning by Using Extremum Seeking Algorithm Based on Annealing Recurrent Neural Network", *3rd Annual Symposium on Knowledge Acquisition and Modeling (KAM)*, pp. 132–135; Wuhan (China), October 2010.